Jagiellonian University

Faculty of Biochemistry, Biophysics and Biotechnology

Anna Mistarz, M.Sc.

Reprogramming the Tumor Microenvironment in Ovarian Cancer by Oncolytic Virotherapy Targeting CXCL12 Chemokine/CXCR4 Receptor Signaling Pathway

PhD thesis prepared in the Department of Immunology of Roswell Park Comprehensive Cancer Center, Buffalo, United States under supervision of Dr. Danuta Kozbor, Prof. of Oncology and Prof. Dr. Hanna Rokita from the Jagiellonian University, Faculty of Biochemistry, Biophysics and Biotechnology

Kraków 2023

TABLE OF CONTENTS

ACKNOWLEDGEMENTS

I would like to express my deepest gratitude to this PhD thesis supervisors, Dr. Danuta Kozbor and Prof. Dr. Hanna Rokita, for unwavering support, guidance, and encouragement. Your expertise, patience, and dedication have been invaluable to me, and I could not have completed this thesis without your constant mentorship.

I would also like to extend my thanks to the Genomics Shared Resource and Biostatistics and Bioinformatics Group from Roswell Park Comprehensive Cancer Center, in particular Dr. Prashant Singh and Dr. Jianmin Wang, for their expertise, bioinformatics analysis of scRNAseq, constructive feedback and technical support.

I would like to thank the Roswell Park Comprehensive Cancer Center's Flow Cytometry Core and Laboratory Animal Resources for their services and technical support.

I am grateful to the faculty, staff, and students of the Department of Immunology of Roswell Park Comprehensive Cancer Center for providing a supportive academic community and for creating an environment that fosters learning and growth.

Finally, I would like to thank my family for their unconditional love and support. Your help and encouragement have sustained me throughout this journey.

Thank you all for your support and for making this endeavor possible.

This work was supported by the NCI-funded U01 CA233085, the NCI-funded Ovarian Cancer SPORE 2P50CA159981-07A1, Ovarian Cancer Immunotherapy Research, the Roswell Park Alliance Foundation, and the NCI funded Immuno-oncology Translation Network U24CA232979.

LIST OF ABBREVIATIONS

AC - *adenylyl cyclase*

ACKRs - *atypical chemokine receptors*

ACT - *adoptive cell transfer*

ASR - *age-standardized rate*

BiTE - *bispecific T-cell engager*

BSA - *bovine serum albumin*

CAF - *cancer-associated fibroblasts*

cCKRs - *conventional chemokine receptors*

CEV - *cell-associated enveloped virions*

CLP - *common lymphoid progenitor*

CMP - *common myeloid progenitor*

CTL - *cytotoxic T lymphocyte*

DAG - *diacylglycerol*

DAMPs - *damage-associated molecular pattern molecules*

DCs - *dendritic cells*

DGE - *differential gene expression*

DMEM - *Dulbecco's modified Eagle's medium*

DPBS - *Dulbecco's phosphate-buffered saline*

ECM - *extracellular matrix*

EEV - *extracellular enveloped virions*

EGF - *epidermal growth factor*

EGFP - *enhanced green fluorescent protein*

EGFR - *epidermal growth factor receptor*

EOC - *epithelial ovarian cancer*

FAP - *fibroblast-activation protein*

FDR - *false discovery rate*

FIGO - *International Federation of Gynecology and Obstetrics*

FSC-A - *forward scatter-area*

FSC-H - *forward scatter-height*

GDP - *guanosine-5'-diphosphate*

G-MDSCs - *granulocytic myeloid-derived suppressor cells*

GPCRs - *G protein-coupled receptors*

GSEA - *gene set enrichment analysis*

GTP - *guanosine-5'-triphosphate*

HSC - *hematopoietic stem cells*

IEV - *intracellular enveloped virions*

ILC - *innate lymphoid cells*

IMV - *intracellular mature virions*

IP3 - *inositol (1,4,5)- trisphosphate*

KLH - *keyhole limpet hemocyanin*

MAPK - *mitogen-activated protein kinase*

MDR - *multi-drug resistance*

MHCII - *major histocompatibility complex class II*

M-MDSCs - *monocytic myeloid-derived suppressor cells*

MMPs - *matrix metalloproteinases*

MOI - *multiplicity of infection*

MSigDB - *molecular signatures database*

mTOR - *mammalian target of rapamycin*

NES - *normalized enrichment score*

NF-κB - *nuclear factor kappa light chain enhancer of activated B cells*

NGS - *next generation sequencing*

OC - *ovarian cancer*

OS - *overall survival*

OVV - *oncolytic vaccinia virus*

PAMPs - *pathogen-associated molecular pattern molecules*

PBS - *phosphate buffered saline*

PCA - *principal component analysis*

PD-1 - *programmed cell death protein 1*

PDGF-α - *platelet-derived growth factor alpha*

PDPN - *podoplanin*

PFS - *progression-free survival*

PFU - *plaque-forming units*

PI3K - *phosphoinositide-3 kinase*

PID - *pathway interaction database*

PIP2 - *phosphatidylinositol (4,5)-bisphosphate*

PKA - *protein kinase A*

PKB - *protein kinase B (also known as* **AKT***)*

PKC - *protein kinase C*

PLC - *phospholipase C*

PP2A - *protein phosphatase 2A*

Rb - *retinoblastoma protein*

RPMI - *Roswell Park Memorial Institute medium*

SDF-1 - *stromal cell-derived factor 1*

SNN - *shared nearest neighbor*

STR - *short tandem repeat*

TAg - *Simian Virus 40 large T antigen*

TALs - *tumor-associated lymphocytes*

TAMs - *tumor-associated macrophages*

TCR - *T cell antigen receptor*

TK - *thymidine kinase*

TME - *tumor microenvironment*

Treg - *T regulatory cells*

tSNE - *t-distributed stochastic neighbor embedding*

UMAP - *uniform manifold approximation and projection*

UMI - *unique molecular identifier*

VEGF - *vasculature endothelial growth factor*

VGF - *vaccinia growth factor*

VIM - *vimentin*

VV - *vaccinia virus*

α-SMA - *alpha-smooth muscle actin*

LIST OF FIGURES AND TABLES

ABSTRACT

Ovarian cancer is one of the most common gynecologic cancers, with the highest mortality rate. It is often diagnosed at an advanced stage when patients already present with metastatic disease. In that case, first-line therapies such as debulking surgery and primary chemotherapy are often not curative. Poor prognosis and high mortality rate for patients at an advanced stage, can be related to extensive intraperitoneal metastasis and chemotherapy resistance. Available therapies can prolong progression-free survival but not overall survival, indicating that novel, improved therapeutic strategies are needed. It has been shown that treatment effectiveness after immunotherapy is directly impacted by tumor antigen-driven responses to weakly immunogenic self- and neoantigens. In this study, I have examined the effects of CXCR4-antagonist-armed oncolytic virotherapy on innate and adaptive immune responses which lead to tumor control and tumor growth, using orthotopically grown ovarian cancer cells expressing SV40 T antigen in wild-type and tolerogenic murine models. Mouse models such as antigen-naïve wild-type and Tg*MISIIR-TAg-Low* transgenic mice expressing TAg protein in epithelial cells lining fallopian tubes under the transcriptional control of the Müllerian inhibiting substance type II receptor gene promoter as a self-antigen are a suitable tool for studies aiming to improve understanding of T cell biology in the context of the tolerogenic tumor microenvironment.

Using immunostaining and single-cell RNA sequencing analyses, I have compared phenotypic and transcriptomic changes in the peritoneal tumor microenvironment of untreated tumors in tolerogenic Tg*MISIIR-TAg-Low* mice and syngeneic wild-type mice with SV40 T antigen serving as a neoantigen. The study revealed distinctions in the tumorigenicity of TAg-expressing MOVCAR 5009 ovarian cancer cells between mouse models. Transgenic Tg*MISIIR-TAg-Low* mice had poor immune activation, polarized M2 tumor-associated macrophages, and immunosuppressive cancer-associated fibroblasts. On the other hand, performed analyses in untreated wild-type mice showed the presence of SV40 T antigen-specific $CD8^+$ T cells, a balanced M1/M2 transcriptomic signature of tumor-associated macrophages, and immunostimulatory cancer-associated fibroblasts.

Additionally, I have demonstrated that intraperitoneal injection of CXCR4-antagonist-armed oncolytic vaccinia virus resulted in induction of SV40 T antigen-specific $CD8^+$ T cells in both murine models, but their therapeutic efficacy and activation states differed. In tumor

microenvironment of OV-CXCR4-A-treated wild-type mice $CD8^+$ T cells had elevated expression of genes important in regulating T cell development, differentiation, survival, regulation of T cell homeostasis, activation and maintenance of effector cells, and effector function of cytotoxic T lymphocytes. However, $CD8^+$ T cells in Tg*MISIIR-TAg-Low* mice despite maintaining some of the effector cell gene expression patterns, they expressed genes characteristic of dysfunctional tumor-specific T cells. They had an increased expression of genes associated with tumor-induced exhaustion and a reduced level of the $TCR_{Tag\text{-}I}$ tetramer binding compared to $CD8^+$ T cells from wild-type mice. Moreover, changes in the transcriptomic signature of $CD8^+$ T cells correlated with their functional activities. Functional assays showed that $CD8^+$ T cells were less effective in managing tumor growth in transgenic Tg*MISIIR-TAg-Low* mice and exhibited reduced cytotoxic activity after OV-CXCR4-A treatment compared with their counterparts in non-tolerogenic wild-type mice. Further studies on cell depletion demonstrated that $CD8^+$ cells were predominantly responsible for the therapeutic impact of armed oncolytic virotherapy. OV-CXCR4-A-induced epitope spreading, and TAg-specific antigen activation can reprogram unresponsive tumor-specific $CD8^+$ T cells in MOVCAR 5009-challenged transgenic mice. Moreover, administered viral treatment led to nearly total elimination of cancer-associated fibroblasts and M1 polarization of macrophages in transgenic mice.

My observations emphasize the potential of Tg*MISIIR-TAg-Low* murine model in preclinical evaluation of ovarian cancer therapeutic agents. The findings showed that, in an immunocompetent ovarian cancer model, CXCR4-A-armed oncolytic virotherapy, by targeting the immunosuppressive interaction between tumor-associated macrophages and cancer-associated fibroblasts, induces tumor/self-specific $CD8^+$ T cell responses that participate in controlling ovarian tumor growth. This approach significantly increases therapeutic efficacy and may hold great potential to improve the outcome of cancer treatment when rationally combined with other treatment approaches.

Keywords: ovarian cancer, immunotherapy, tumor microenvironment, immunological tolerance, CXCR4 antagonist, oncolytic vaccinia virus

STRESZCZENIE

Przeprogramowanie mikrośrodowiska guza raka jajnika przy wykorzystaniu wirusoterapii onkolitycznej wycelowanej w oś sygnałową CXCL12/CXCR4

Rak jajnika jest jednym z najczęstszych nowotworów ginekologicznych i charakteryzuje się najwyższym wskaźnikiem śmiertelności. Często diagnozuje się go w zaawansowanym stopniu, gdy u pacjentów pojawiają się już przerzuty. W takich przypadkach terapie pierwszej linii leczenia, takie jak operacyjne usunięcie guza i chemioterapia często są nieskuteczne. Niepomyślne rokowanie i wysoki wskaźnik śmiertelności u pacjentów w zaawansowanym etapie nowotworzenia mogą być związane z rozległymi przerzutami wewnątrzotrzewnowymi i opornością na chemioterapię. Dostępne obecnie leczenie może wydłużyć przeżycie wolne od progresji, ale nie wpływa na ogólną przeżywalność, co wskazuje, że są potrzebne nowe, ulepszone strategie terapeutyczne. Skuteczność leczenia metodą immunoterapii jest bezpośrednio uzależniona od odpowiedzi immunologicznej na słabo immunogenne antygeny nowotworowe, zarówno własne jak i neoantygeny. W tej pracy zbadałam wpływ onkolitycznej wirusoterapii, z wykorzystaniem rekombinowanego wirusa krowianki wykazującego ekspresję antagonisty receptora CXCR4, na nabytą i wrodzoną odpowiedź układu odpornościowego, co w efekcie doprowadziło do kontroli wzrostu guza. Badania przeprowadziłam używając ortotopowo rosnące komórki raka jajnika wykazujące ekspresję dużego antygenu T SV40 w tolerogennych i dzikich myszach. Mysie modele, takie jak antygenowo-naiwne myszy dzikiego typu i transgeniczne myszy Tg*MISIIR-TAg-Low* wykazujące ekspresję antygenu T SV40 w komórkach nabłonka wyścielającego jajowody pod kontrolą promotora genu receptora typu II czynnika hamującego rozwój przewodów Müllera jako własny, są odpowiednie do badań mających na celu zwiększenie zrozumienia biologii limfocytów T w kontekście tolerogennego mikrośrodowiska nowotworowego.

Przy użyciu techniki barwienia immunologicznego oraz sekwencjonowania RNA na poziomie pojedynczej komórki porównałam zmiany fenotypowe i transkryptomiczne w otrzewnowym mikrośrodowisku nowotworowym nieleczonych guzów u tolerogennych myszy Tg*MISIIR-TAg-Low*. Równolegle te same analizy zostały wykonane u myszy dzikiego typu dla których antygen T SV40 pełnił funkcję neoantygenu. Badania wykazały różnice w tumorogenności komórek raka jajnika MOVCAR 5009, które wykazują ekspresję antygenu

T SV40, pomiędzy dwoma modelami myszy. Myszy transgeniczne Tg*MISIIR-TAg-Low* charakteryzowały się słabą aktywacją immunologiczną i obecnością związanych z nowotworem makrofagów (TAM) spolaryzowanych w kierunku typu M2 oraz fibroblastów związanych z nowotworem (CAF) wykazujących właściwości immunosupresyjne. Natomiast analizy przeprowadzone na myszach dzikiego typu, niepoddanych żadnej terapii, wykazały obecność limfocytów T $CD8^+$ skierowanych przeciwko antygenowi T SV40, zrównoważoną M1/M2 transkryptomiczną sygnaturę makrofagów oraz obecność fibroblastów o właściwościach immunostymulujących.

Dodatkowo wykazałam, że dootrzewnowe podanie rekombinowanego wirusa krowianki wykazującego ekspresję antagonisty receptora CXCR4 prowadzi do indukcji limfocytów T $CD8^+$ skierowanych przeciwko antygenowi T SV40 w obu modelach myszy, ale ich skuteczność terapeutyczna i stan aktywacji jest odmienny. W mikrośrodowisku guza u myszy dzikiego typu poddanych wirusoterapii OV-CXCR4-A, limfocyty T $CD8^+$ wykazywały podwyższoną ekspresję genów ważnych dla regulacji rozwoju, różnicowania i przeżycia limfocytów T, regulacji ich homeostazy, aktywacji i utrzymania komórek efektorowych oraz funkcji efektorowych limfocytów T cytotoksycznych. Jednakże limfocyty T $CD8^+$ u myszy Tg*MISIIR-TAg-Low*, mimo że zachowały częściowo ekspresję genów komórek efektorowych, wykazywały cechy dysfunkcyjnych limfocytów skierowanych przeciwko komórkom nowotworowym. Miały one zwiększoną ekspresję genów związanych z „wyczerpaniem" indukowanym przez guza oraz mniejsze wiązanie tetrameru $TCR_{Tag\text{-}I}$ w porównaniu z limfocytami T $CD8^+$ pochodzącymi od myszy typu dzikiego. Ponadto zmiany w sygnaturze transkryptomicznej limfocytów T $CD8^+$ odpowiadały ich zmienionym właściwościom funkcjonalnym. Testy funkcjonalne wykazały, że limfocyty T $CD8^+$ były mniej skuteczne w hamowaniu wzrostu guza u myszy Tg*MISIIR-TAg-Low* i wykazywały zmniejszoną aktywność cytotoksyczną po terapii OV-CXCR4-A w porównaniu z ich odpowiednikami u myszy typu dzikiego. Dalsze badania polegające na usunięciu limfocytów T $CD8^+$ lub $CD4^+$ wykazały, że to limfocyty T $CD8^+$ były głównie odpowiedzialne za terapeutyczny wpływ zastosowanej wirusowej terapii onkologicznej. Rozprzestrzenianie się antygenów powodowane wirusoterpią OV-CXCR4-A oraz aktywacja antygenu T SV40 mogą przeprogramować niewrażliwe limfocyty T $CD8^+$ skierowane przeciwko komórkom nowotworowym u myszy Tg*MISIIR-TAg-Low*. Ponadto zastosowana terapia wirusowa doprowadziła do niemal

całkowitej eliminacji fibroblastów oraz polaryzacji makrofagów w kierunku typu M1 u myszy transgenicznych.

Moje obserwacje podkreślają potencjał modelu mysiego Tg*MISIIR-TAg-Low* w przedklinicznej ocenie leków w terapii onkologicznej raka jajnika. Uzyskane wyniki pokazały, że u immunokompetentnych myszy obarczonych rakiem jajnika, terapia oparta na rekombinowanym wirusie krowianki wykazującym ekspresję antagonisty receptora CXCR4, poprzez celowanie w immunosupresyjne interakcje pomiędzy makrofagami a fibroblastami, wywołuje odpowiedzi $CD8^+$ limfocytów T, które uczestniczą w kontroli wzrostu guza jajnika. Ta metoda znacznie zwiększa skuteczność terapeutyczną i może prowadzić do nowych, skutecznych interwencji immunoterapeutycznych.

Słowa kluczowe: rak jajnika, immunoterapia, mikrośrodowisko guza, tolerancja immunologiczna, antagonista receptora CXCR4, onkolityczny wirus krowianki

1. INTRODUCTION

1.1 Ovarian cancer

Ovarian cancer (OC) is classified in epithelial and non-epithelial subtypes. They vary not only in their origin, but also in risk factors, molecular profile, pathogenesis, and medical prognosis. Ovarian cancer may occur at any age, but it is infrequent in women under 40 years. In this age group non-epithelial germ cell tumors are the most common. Above that age, more than 90% are epithelial ovarian cancer (EOC). This is the most common type of ovarian cancer and the leading cause of death in gynecological malignancies. Incidence of ovarian cancer can differ significantly by race and ethnicity [1,2]. The highest incidence of OC is reported in high-income level countries in Central and Eastern Europe, followed by Northern Europe, Polynesia, and North America, whereas the lowest incidence is found in Central Africa. In 2020 313,959 new cases of OC were reported, with a global incidence rate 6.6 per 100,000. That year age-standardized rate (ASR) mortality reached 4.2 per 100,000 [3].

The International Federation of Gynecology and Obstetrics (FIGO) staging system defines four ovarian cancer stages: Stage I when tumors are confined to ovaries or fallopian tubes, Stage II when tumors involve one or both ovaries with pelvic extension or primary peritoneal cancer, Stage III where tumor involves one or both ovaries with intraperitoneal metastases outside the pelvis and/or metastasis to the retroperitoneal lymph nodes. Finally, Stage IV includes distant metastasis out of peritoneal implants [2]. Ovarian cancer is often diagnosed at an advanced stage when patients already present with metastatic disease. In that case, first-line therapies such as debulking surgery and primary chemotherapy are often not curative. Poor prognosis and high mortality rate for patients at an advanced stage, with a 5-year survival rate of only 17%, can be related to extensive intraperitoneal metastasis and chemotherapy resistance [4,5].

1.1.1 Treatment strategies

Surgery in conjunction with platinum-based chemotherapy is the primary treatment for ovarian cancer patients. They effectively induce remission, however for most women the disease is recurrent and therapy-resistant. Surgical debulking is performed to remove all visible sites of disease but recurrence rates are very high and may vary by the stage. Probability of recurrence within two years of diagnosis for Stages III and IV reaches 70-75%. Platinum sensitive patients

are defined when the disease recur after 6 months from the last platinum dose, and they usually respond to platinum-based doublet retreatment. Platinum resistant patients recur within 6 months from the last dose and the treatment for these patients typically requires second-line cytotoxic chemotherapies, including pegylated liposomal doxorubicin, topotecan, gemcitabine, paclitaxel, or experimental therapy. Aforementioned therapies can be administered alone or in combination with bevacizumab, humanized monoclonal antibody that inhibits VEGF-A. A median overall survival (OS) for platinum-resistant ovarian cancer patients is less than 16 months [6,7]. Available therapies can prolong progression-free survival (PFS) but not overall survival, indicating that novel, improved therapeutic strategies are needed.

1.2 Vaccinia virus

Vaccinia virus (VV) is a large, enveloped member of the poxvirus family, closely related to cowpox virus. It has linear, double-stranded DNA genome with harpin loop at each end, encoding approximately 200 genes. It replicates within the cytoplasm of the infected cell, outside of the nucleus. Large genome is crucial for encoding all agents, such as DNA-dependent RNA polymerase, transcription factors, poly(A) polymerase and various enzymes involved in viral replication and gene transcription, so VV can synthesize translatable mRNAs independently from the host cell. Vaccinia virus produces four types of infectious particles, and majority of them are of the intracellular form. Particles differ mainly in their outer membranes. Intracellular mature virions (IMV) and the intracellular enveloped virions (IEV) have a single lipid bilayer envelope and are mostly located inside the infected cell until its lysis. Two other forms are cell-associated enveloped virions (CEV) and the extracellular enveloped virions (EEV) with an extra lipid bilayer and perform budding from the host cell without lysis. Large transgenes can be efficiently inserted into VV genome using standard techniques to manipulate genetic material. Moreover, VV can be easily produced to high titers and its particles are stable without infectivity loss for prolonged periods of time. Therefore, vaccinia virus is a very attractive research tool and is used for the treatment of many diseases, especially cancer. Its highly immunogenic nature, which produces a strong cytotoxic T lymphocyte (CTL) response is crucial for its continued use in immunotherapy [8,9].

Vaccinia virus can be used for cancer therapy in different ways. It can serve as a gene delivery vector, because of its high infectivity, efficient gene expression and can hold up to

25 kb of foreign DNA. VV has been shown to efficiently infect tumor cells directly lysing them, therefore it is a safe and effective agent in ovarian cancer treatment. Lastly, VV can be used as a cancer vaccine to induce anticancer immunity. Furthermore, cytoplasmic replication of the virus lowers the chance of recombination or integration of viral DNA into recipient cells, positively impacting its safety. There are many vaccinia virus strains that induce different immune responses *in vivo*. They were given different names, reflecting the locality or health agency in which the virus was propagated [10].

1.2.1 Oncolytic vaccinia virus

Oncolytic potential depends on the vaccinia virus strain. Western Reserve strain, derived from Wyeth strain through passaging in mice, has the strongest oncolytic effect and high tumor selectivity. The antitumor effect can be achieved through different mechanisms of action. One of them is rapid, direct lysis of infected tumor cells, caused by viral replication process. The first viral particles are secreted from cells within 8 hours and infected cells are destroyed 48 to 72 hours after infection, releasing 10,000 new virions. The other mechanism is immune-mediated cell death induction. Because of the highly destructive nature of this virus, after cell destruction, cellular agents are released at the site of infection, such as damage-associated molecular pattern molecules (DAMPs), viral danger signals (pathogen-associated molecular pattern molecules, PAMPs) as well as tumor-associated antigens. Lastly, oncolytic vaccinia virus (OVV) has been shown to induce vascular collapse within tumors. VV strains are capable of infecting tumor vascular endothelial cells, after intravenous delivery [11].

High tumor selectivity is based on the natural biology of the viruses. What is important, viral biology, genetic engineering and modifications can be utilized to further enhance tumor selectivity. It has been shown that oncolytic viruses naturally target cancers overexpressing molecules such as DNA repair enzymes or anti-apoptotic proteins, that tend to make tumor cells therapy resistant. Different genetic engineering approaches have been used not only to increase cancer tissue specific replication of the viruses, but also to augment the therapeutic effects by arming them with therapeutic transgenes. The products of these transgenes can include cytokines to help overcome immunosuppressive tumor microenvironment, anti-angiogenic agents targeting the vasculature endothelial growth factor (VEGF) to lower blood vessel densities within the tumor tissue, or enzymes for gene-directed enzyme prodrug therapy to

selectively activate prodrugs within the tumor [12]. Schematic representation of tumor-selective viral replication and oncolysis is presented in Figure 1.

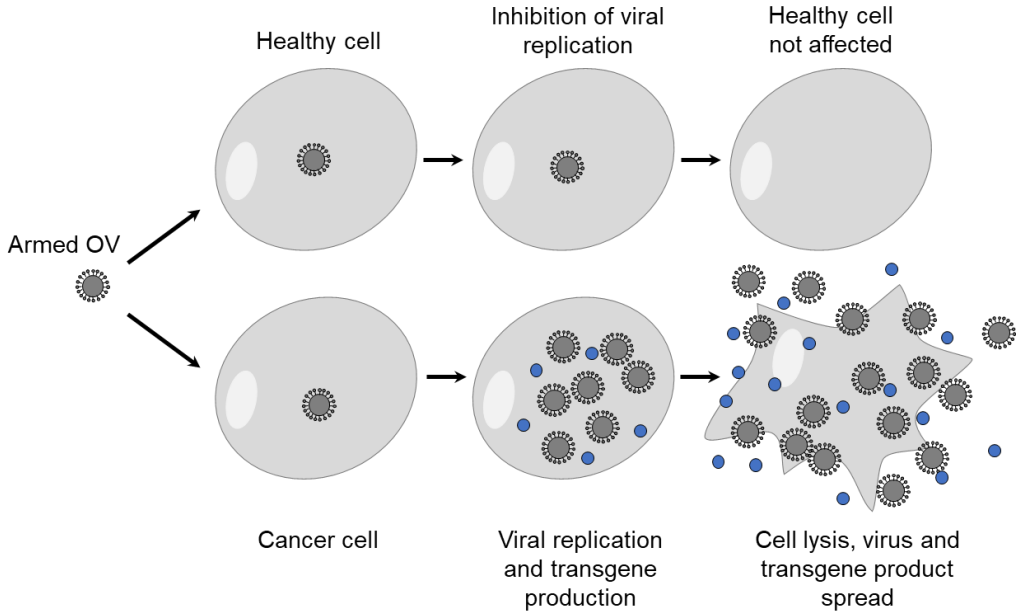

Figure 1. *Schematic representation of armed oncolytic virus's mechanism of action. Presented steps: infection, viral replication and transgene production (marked in blue), cell lysis, transgene product and virus release and spread within tumor tissue but not normal cells. Reproduced from [13].*

Increased tumor selectivity can be achieved, among others, through the deletion of the thymidine kinase (TK) gene, which is involved in deoxyribonucleotides synthesis. Cellular thymidine kinase, regulated by the E2F transcription factors, is only induced during DNA replication in normal cells and low level of TK protein in the cytoplasm is not sufficient to support viral replication. Nonetheless, TK is constitutively expressed at high levels in most cancers regardless of proliferation status. Because normal cells have generally low nucleotide content, deletion of TK in VV genome leads to dependence of the virus on cellular thymidine kinase expression and limits viral replication to nucleotide rich cancer cells. Another approach to strengthen tumor selectivity is to remove vaccinia growth factor (VGF) from its genome. Vaccinia virus encodes two copies of VGF, an EGF homologue functioning as mitogen by binding epidermal growth factor receptor (EGFR) on both infected and surrounding non-infected cells, inducing proliferation. VGF is produced and secreted at early phase of viral infection and deletion of the this gene dramatically diminishes viral replication in resting cells [14]. Moreover, it was reported that the effect of deleting TK and VGF genes was synergistic [15].

1.3 Chemokine receptors as therapeutic targets

Chemokines (or chemotactic cytokines) are a large family of small (8-10 kDa) cytokines or signaling proteins. Most chemokines have four cysteine residues, which stabilize the tertiary structure of the protein. Based on the number and spacing of their N-terminal cysteine residues, chemokines are classified into four subfamilies: CXC, CC, CX3C and C. In the largest groups, CXC and CC, the first two cysteines are separated by one amino acid (aa) residue (CXC motif) or are adjacent (CC motif). CX3C motif has three intervening aa between the first two cysteine residues, whereas C chemokines have only one N-terminal cysteine. Chemokines regulate various biological processes, such as migration of different cell types, regulate leukocyte trafficking, maturation, cytoskeletal rearrangement, and angiogenesis [16].

Chemokine receptors belong to a class A (also known as rhodopsin-like receptors) of G protein-coupled receptors (GPCRs) superfamily characterized by seven transmembrane α-helix domains. To date, 19 conventional chemokine receptors (cCKRs) and four atypical chemokine receptors (ACKRs) have been characterized in humans. Chemokine receptors are classified based on the type of their ligands, for example, CXC receptors bind only CXC ligands, etc. Intracellular signaling by chemokine receptors is dependent on neighboring G-proteins, which exist as heterotrimer composed of α, β and γ distinct subunits. G-protein is in the inactivated state when bound to guanosine-5'-diphosphate (GDP). Following interaction with their specific chemokine ligand, the activation signal allows the exchange of GDP for another molecule guanosine-5'-triphosphate (GTP) at the Gα subunit, leading to dissociation from the Gβγ dimer. Different G protein subunits transduce downstream signaling contributing to cell survival, cell proliferation, chemotaxis and gene transcription [17].

Chemokine system plays a significant role in various biological functions and pathology, therefore the chemokine ligand-receptor interactions have been the focus of targeted therapy.

1.3.1 CXCL12 ligand

CXCL12, also known as stromal cell-derived factor 1 (SDF-1), is a homeostatic chemokine protein ubiquitously expressed in many cell types and organs such as liver, thymus, lung, brain, kidney, lymph nodes, heart, colon, and bone marrow by stromal fibroblasts, vascular endothelial cells, and osteoblasts. CXCL12 is produced in two forms, CXCL12a and CXCL12b,

by alternative splicing. It is essential during development and critical for the homeostatic regulation of leukocyte trafficking and tissue regeneration. CXCL12 directs the migration of hematopoietic cells from fetal liver to bone marrow and the formation of large blood vessels. It is expressed in hypoxic and pro-angiogenic conditions and intratumoral hypoxia induces CXCL12 secretion by cancer-associated fibroblasts (CAFs) [18].

1.3.2 CXCR4 receptor

The chemokine system is highly promiscuous as several chemokines can bind to the same receptor and some chemokine receptors can interact with multiple ligands. The chemokine receptor 4 (CXCR4) is unique in that as it exclusively interacts with the endogenous ligand CXCL12. CXCR4, also known as fusin and CD184, is a G-protein coupled receptor widely expressed by most cells, including endothelial mature and precursor cell, pericytes, neuron and stem cells. Its downstream signaling pathways lead to altered gene expression, migration, survival, and proliferation. During the metastatic process of tumorigenesis, aforementioned pathways are utilized, where tumor cells expressing CXCR4 are chemotactically attracted to organs that have high levels of CXCL12 [19]. There is an evidence that CXCR4 overexpression is present in many human tumor types, such as ovarian and breast cancer [20-23]. Additionally, there is a correlation between CXCR4 overexpression, increased tumor aggressiveness, and a higher likelihood of recurrence [24-26].

1.3.3 CXCL12/CXCR4 signaling pathway

It has been shown that CXCL12-CXCR4 interaction activates several signaling pathways, including mammalian target of rapamycin (mTOR), phosphoinositide-3 kinase/protein kinase B (PI3K/AKT) and nuclear factor kappa light chain enhancer of activated B cells (NF-κB). Initiation of those pathways can lead to diverse responses such as chemotaxis, cell survival, proliferation, an increase in intracellular calcium levels, and transcription of different genes [27]. After binding of CXCL12 chemokine to CXCR4, GDP is exchanged for GTP, and the heterotrimeric G protein ($G\alpha\beta\gamma$) dissociates into $G\alpha_i$ subunit and $G\beta/G\gamma$ dimer. The dissociated $G\beta/G\gamma$ subunit activates phospholipase C (PLC). PLC catalyzes the hydrolysis of phosphatidylinositol (4,5)-bisphosphate (PIP2) into diacylglycerol (DAG) and inositol (1,4,5)-trisphosphate (IP3), which increases intracellular calcium. DAG activates protein kinase C (PKC), which together with intracellular free calcium activates mitogen-activated

protein kinase (MAPK) pathway contributing to chemotaxis. Either the Gβ/Gγ dimer or the $G\alpha_i$ subunit can activate PI3K, which can activate serine-threonine kinase AKT, thus stimulating the downstream transcription nuclear factor NF-κB and mTOR pathways, which play key roles in tumor cell survival and proliferation. The $G\alpha_i$ subunit also decreases cyclic adenosine monophosphate (cAMP) by inhibiting adenylate cyclase (AC) [28]. Adenylyl cyclase when activated elevates cAMP levels and triggers the downstream cAMP-dependent protein kinase A (PKA). Under most circumstances increased cAMP inhibits proliferation and can also stimulate apoptosis [29,30]. In result, cAMP suppression is a critical growth-promoting event downstream of CXCR4 activation [31]. Aforementioned pathways are shown schematically in Figure 2.

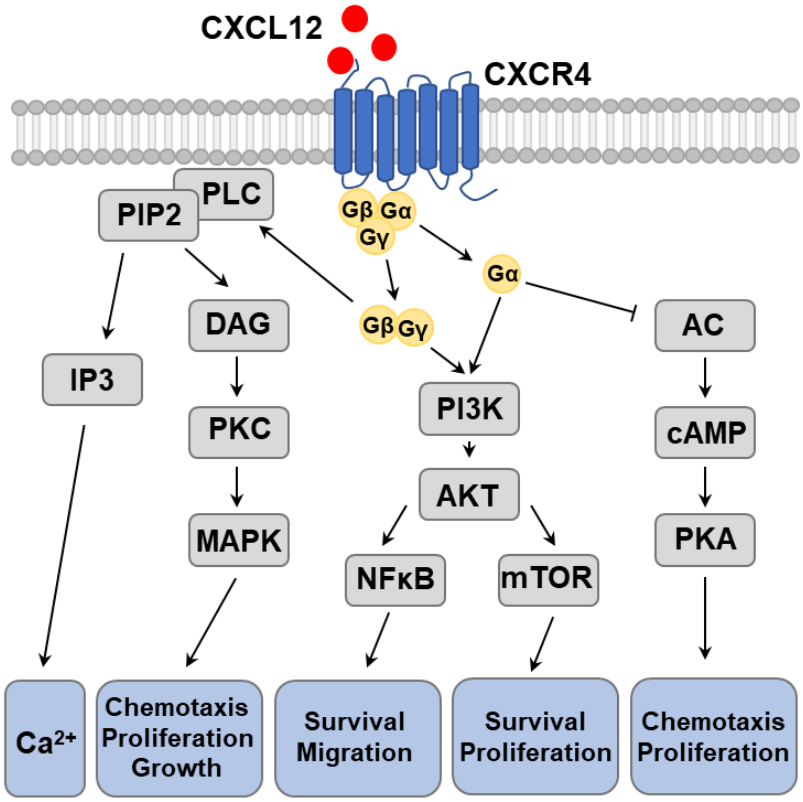

***Figure 2**. Selected pathways involved in CXCL12-CXCR4 signaling. Binding of CXCL12 chemokine to chemokine receptor CXCR4, activates downstream signaling through G proteins. Dissociation of the* Gαβγ *protein complex activates PI3K-AKT-NFκB/mTOR and MAPK signaling pathways, thereby promoting cell survival, proliferation, migration and metastasis in tumors. CXCL12 binding to CXCR4 results in inhibition of AC.*

CXCL12/CXCR4 signaling pathway plays a crucial role in promoting metastasis by many solid tumor types. Activation of this pathway upregulates VEGF expression, a critical mediator of angiogenesis and tumor proliferation, at both mRNA and protein level via PI3K/AKT pathway activation [32]. Induction of migration of ovarian cancer cells and invasion through the extracellular matrix, plays a central role in the progression of epithelial ovarian cancer. CXCL12/CXCR4 expression can be correlated with prognosis and survival rates. High expression of CXCR4 and CXCL12 was shown to be significantly associated with liver and

lymphatic metastasis [33] and low overall and disease-free survival rates [34,35]. Therefore, CXCL12/CXCR4 has the potential to serve as an independent predictor of poor survival outcomes in cancer patients [24,36].

1.4 Tumor microenvironment

Within the tumor microenvironment we can distinguish cellular and non-cellular parts. Stromal cells that form cellular part can include pericytes, cancer cells, cancer stem cells, cancer-associated fibroblasts (CAFs), endothelial cells (ECs) and immune cells. On the other hand, extracellular matrix (ECM) creates non-cellular part and consists of chemokines, inflammatory cytokines, integrins, matrix metalloproteinases (MMPs) and other secreted molecules. The interaction between cancer cells and their microenvironment is extremely dynamic and can be influenced by the release of extracellular paracrine signals such as cytokines, chemokines or DAMPs promoting for example peripheral immune tolerance or tumor angiogenesis [37]. The consequence of such an intensive crosstalks is often reflected in tumor maintenance, poor response to therapy and multi-drug resistance (MDR). The tumor microenvironment within the peritoneal cavity is a major component determining peritoneal metastasis and plays a pivotal role in prognosis and progression of ovarian cancer. Several specific types of immune cells have been identified to play crucial roles in tumor microenvironment.

1.4.1 Myeloid cells

Myeloid cells are the main cell branches generated during hematopoiesis from hematopoietic stem cells (HSC) in bone marrow. HSCs have both self-renewal potential and multipotency to generate all the blood cells, that be categorized into myeloid or lymphoid lineage. These two lineages can be distinguished at the oligopotent progenitor level: common myeloid progenitor (CMP) and common lymphoid progenitor (CLP). CMPs can give rise to different myeloid cell types such as erythrocytes, megakaryocytes, mast cells, granulocytes and monoblasts, which serve as progenitors for macrophages and monocytes. Dendritic cells (DCs) are not clearly grouped either in lymphoid or myeloid lineage, as they can be derived from either CMPs or CLPs [38]. Myeloid cells are key players of the innate immune system. Among many of their functions we can distinguish first response to inflammation by neutrophils, maintenance and defense of host tissues by macrophages, processing and presenting antigens by dendritic

cells, homeostasis and wound healing by platelets. Myeloid cells play an important role in cancer-cell recognition, initiation of inflammation and antitumor responses. However, they can also lead to chronic cancer-associated inflammation by promoting local inflammation [39,40]. Myeloid cells are the most abundant cell population infiltrating the tumor microenvironment, therefore, are important modulators of anticancer therapies, hence functional activities of those cells in tumors are raising increasing interest.

Heterogeneous group of immature myeloid cells, that was found in pathological settings with Gr-1^{+}CD11b^{+} signature, have immunosuppressive potential and is characterized as pro-tumorigenic [41]. In 2007 Gabrilovich *et al*. [42] proposed the term myeloid-derived suppressor cells (MDSCs) to describe them. This term has been subdivided to distinguish the differences between granulocyte-like MDSCs (G-MDSCs) versus monocyte-like MDSCs (M-MDSCs). Predominantly, mouse G-MDSCs have been described as CD11b^{+} Ly6G^{+} Ly6C^{low} and M-MDSCs as CD11b^{+} Ly6G^{-} Ly6C^{+}. Immune suppression of both the innate and adaptive responses distinguish MDSCs from other myeloid cell populations, despite their morphological and phenotypical similarities to neutrophils and monocytes. MDSCs lower antitumor immune responses by inhibition of T cell proliferation, cytokine secretion and regulatory T cells recruitment. In the context of cancer, MDSCs are produced abnormally, recruited to tumor microenvironment and contribute to tumor angiogenesis and metastasis. Elevated levels of MDSCs correlate with poor prognosis, shortened relapse-free and overall survival [43].

1.4.2 Tumor-associated macrophages

Macrophages are myeloid cells that are essential members of the innate immune response and play important role in the tissue development, homeostasis, immune surveillance and the tumor microenvironment. Macrophages are highly heterogeneous and have different biological functions such as phagocytosis, exogenous antigen presentation and immunomodulation through cytokine and growth factor secretion. Multiple populations of macrophages are known to be present within the same microenvironment and each phenotype has a distinctive combination of expressing receptors, secreting chemokines and cytokines. In response to variety of microenvironmental stimuli, such as different cytokines, macrophages may present reversible changes in their functional phenotypes and distribution. Macrophages infiltration can be

mediated by the cytokines colony-stimulating factor 1, vascular endothelial growth factor and selected chemokines [44].

Tumor-associated macrophages (TAMs) can be derived from resident macrophages or peripheral blood monocytes that infiltrates into solid tumor tissues. It is proposed to classify TAMs into anti-tumor M1 (classically activated) and pro-tumor M2 (alternatively activated) types. Those two major phenotypes can be activated under different conditions. When stimulated with interferon-gamma (IFN-γ), bacterial lipopolysaccharide (LPS) or granulocyte-macrophage-colony-stimulating factor (GM-CSF), monocytes differentiate into M1 macrophages [45]. M1 macrophages promote antitumor immune responses secreting proinflammatory cytokines and chemokines. However, stimulation with cytokines, including IL-4, IL-10, and IL-13 differentiates monocytes into M2 macrophages that mainly promote tumor progression [46]. TAMs can be defined as $CD45^+$, $CD11b^+$ and $F4/80^+$ cells [47]. However, expression of major histocompatibility complex class II (MHCII) antigen can be used to distinguish M1-like from M2-like macrophages, as lack of MHCII is often associated with M2 immunosuppressive phenotype [48].

TAMs are abundant in the ovarian cancer microenvironment and are usually associated with tumor invasion, metastasis and angiogenesis, therefore, can affect the prognosis of patients. TAMs secrete epidermal growth factor (EGF) in large amounts, which activate EGFR on ovarian cancer cells. This results in upregulated integrin, ICAM-1 and VEGF/VEGFR signaling pathways, creating a positive autocrine feedback loop that promotes aforementioned invasion, proliferation and migration [49]. M1 infiltration in tumors is associated with a good prognosis in some cancers [50]. Compared with patients with benign OC, the proportion of M2 macrophage infiltration is significantly increased in peritoneal metastases. M2 TAMs can inhibit the proliferation of T cells, take part in tissue repair, ECM remodeling and angiogenesis, which are strictly involved in tumor progression. In addition to regulating the metastasis of ovarian cancer, TAMs are involved in chemoresistance. By secretion of a variety of cytokines, chemokines, enzymes, and exosomes containing microRNAs that can, for example, upregulate and activate different signal transducers, they trigger in tumor cells pro-survival signaling pathways [51]. Recognition of TAMs' involvement in tumor progression and chemoresistance has provided opportunity to develop many successful therapies for ovarian cancer.

1.4.3 Lymphocytes

Lymphocytes are the major component of the tumor microenvironment, include B lymphocytes and T lymphocytes and mediate innate and adaptive immune response, respectively. T cells originate from bone marrow hematopoietic stem cells and migrate for maturation to thymus. T lymphocytes are important in the process of tumor cells elimination. Mature T cells, due to exclusive expression of CD4 and CD8 markers, are categorized into three main cellular subtypes: $CD3^+CD8^+$ effector cells, $CD3^+CD4^+$ helper cells and $CD4^+$ Treg cells [52]. Through T-cell receptors naïve $CD8^+$ T cells interact with antigen-presenting cells, and followed by a specific co-stimulatory signals, activated $CD8^+$ T cells differentiate into IL-2 dependent and highly cytotoxic effector $CD8^+$ T cells. Cytotoxic $CD8^+$ T cells have long been recognized as important mediators of tumor protection, because of their cytotoxic functions and ability to clonally expand. However, their presence is not sufficient for tumor rejection [53]. Enhancements in the cytotoxic activity of tumor antigen-specific cytotoxic T cells in the tumor microenvironment are crucial for the development of cancer immunotherapy. $CD4^+$ T helper cells are very important regulators in TME, mainly through the activation of $CD8^+$ T cells and macrophages [54]. Upon recognition of an antigen and receiving appropriate co-stimulation, naïve T helper cells become activated and undergo clonal expansion. The differentiation of subtypes of effector T helper cells is determined by the specific cytokines release. These subtypes have different functions, as they can mediate both anti- and pro-tumorigenic responses. $CD4^+$ T_H1 helper cells producing interferon gamma and $CD8^+$ cytotoxic cells are the key players against tumor cells. Other subtypes of $CD4^+$ cells in conjunction with different cell types, including MDSCs or TAMs, can have pro-tumorigenic properties that together with secreted factors inhibit anti-tumor innate and adaptive immune responses, promoting tumor growth and progression [55].

The balance between antitumor effector T cells and Tregs may be critical in determining the outcome of immune responses within tumors. A high CD8/CD4 ratio in tumor microenvironment correlates with improved outcome in ovarian cancer patients, while higher infiltration of highly suppressive $CD4^+CD25^+FOXP3^+$ Tregs is associated with worse clinical outcomes and reduced long-term survival. The infiltration of Tregs into a tumor can reduce the amount or response of cytotoxic cells in the tumor microenvironment and allow cancerous cells to escape destruction by the immune system [56,57].

1.4.4 Cancer-associated fibroblasts

Cancer associated fibroblasts (CAFs) originate from activated fibroblasts with a mesenchymal cell lineage in local tissues. They are one of the key components of the tumor microenvironment influencing tumor cell growth and invasion, by secretion of cytokines promoting the epithelial-mesenchymal transition of tumor cells. They participate, among others, in immune regulation, angiogenesis, ECM remodeling and metabolic responses. CAFs as well as activated fibroblasts are known to be very heterogeneous, displaying different expression patterns. They have an elongated spindle morphology but lack markers that are exclusively expressed on their surface. To distinguish CAFs populations, a combination of different morphological features and biomarkers is required [58,59]. Many biomarkers have been proposed to isolate CAFs, including mesenchymal biomarkers such as fibroblast activation protein (FAP), Thy1 (CD90), integrin alpha 5 (CD49e), podoplanin (PDPN), alpha-smooth muscle actin (α-SMA), vimentin (VIM) and platelet-derived growth factor alpha (PDGF-α), but they lack non-mesenchymal biomarkers [60,61]. Abundance and phenotype of CAFs may vary in different tumors. It has been shown that pre-existing CAFs are associated with immunotherapy outcome in melanoma. $Thy1^{+}$CAFs and FAP^{+}CAFs were significantly positively correlated with progression-free survival and overall survival, whereas that of SMA^{+}CAFs was negatively correlated with the prognosis of patients receiving programmed cell death protein 1 (PD-1) immunotherapy [62]. Cancer-associated fibroblasts can affect tumor initiation, progression and therapeutic resistance. Transformation of peritoneal fibroblasts into CAFs is one of the important causes of peritoneal metastasis of ovarian cancer. With the rapid development of personalized medicine and immunology, CAFs have become a promising target in tumor immunotherapy and targeted therapy [63].

The cross-talk between CAFs and TAMs is a dynamic state capable of altering each other's functions. In addition, both CAFs and TAMs are in a reciprocal communication with the nearby tumor cells and the interplay between cancer cells, immune cells, CAFs and TAMs is very complex. CAFs may increase monocyte recruitment and differentiation into TAMs. Also, $podoplanin^{+}$ CAFs were reported to be associated with $CD204^{+}$ TAM infiltration in lung squamous cell carcinoma and lung adenocarcinoma. Different studies showed that CAFs isolated from human invasive breast cancer facilitated the differentiation of monocytes into M2 pro-tumoral macrophages, in contrast to normal breast-derived fibroblasts. Interestingly, M2

type TAMs can activate CAFs and reciprocally, CAFs can play its part in M1 to M2 macrophage switch in the tumor microenvironment and thus help in tumor progression. CAFs produce high amounts of CXCL12 and CXCL14, which can promote monocyte recruitment and polarization into M2 macrophages [64-66]. Those finding stress the pivotal role of CXCL12/CXCR4 axis in the progression of many cancers.

1.5 Immunological tolerance

A state of unresponsiveness in which immunocompetent host cannot exert effector functions and fails to respond to a specific antigen is called immunological tolerance. It is an active antigen-dependent process and applies to many layers of protection provided by the immune system to prevent attack against its own tissues and components. Active tolerance also prevents inflammatory reactions to many innocuous airborne and food antigens at mucosal surfaces. Mechanisms that protect an individual from anti-self immune attacks are collectively termed self-tolerance and a failure of the host's immune system to distinguish self from non-self results in autoimmunity, causing destruction of self-cells and organs. Establishing self-tolerance is a complicated process and involves both the elimination of immune cells that can react against self-antigens and active inhibition of immune responses against self-proteins. While the most important form of tolerance is non-reactivity to self-antigens, it is possible to induce tolerance to non-self-antigens. In this case form, time and location is important, as depending on how and where the same compound is presented to the immune system, it can act as immunogen or tolerogen [67,68].

There are two types of immunological tolerance: central and peripheral. The first type, central tolerance, occurs in the primary lymphoid organs – for T cells in the thymus and for B cells in the bone marrow. The mechanism of this process is based on clonal deletion, where T or B cell clones that have expressed receptors that recognize self-antigens with high affinity, are removed through apoptosis before the cells are allowed to mature. Because some low affinity self-reactive lymphocytes find their way into the periphery and secondary lymphoid tissues, a second type of tolerance is necessary. Peripheral tolerance ensures that self-reactive T cells are deleted or become anergic and can occur through three mechanisms: anergy, cell death or immune deviation to a less harmful response by regulatory processes. Anergy occurs when T cells are functionally unresponsive to an antigen and it happens when an antigen is presented

to T cells without appropriate co-stimulation. A third mechanism for maintaining tolerance, in addition to T cell anergy and apoptosis, is through the activity of regulatory T cells (Tregs). They can be generated by intermediate affinity to self-antigens encountered in the thymus or after induction by antigen in the peripheral tissues. Generation of Tregs requires up-regulation of transcription factor Foxp3. Tregs recognize specific self-antigens, and sometimes foreign antigens, via TCR interactions and down-regulate immune processes when they engage with these antigens in the periphery [69,70].

1.5.1 Immune responses to neoantigens

Tumor neoantigens are immunogenic molecules that are found on the tumor cell surface and can be specifically recognized by TCRs in the context of MHC molecules. In recent years, emerging evidence has suggested that neoantigens play a pivotal role in tumor-specific T cell-mediated antitumor immunity. Treatment effectiveness after immunotherapy is directly impacted by tumor antigen-driven responses to weakly immunogenic self- and neoantigens. Neoantigens are recognized as non-self and activate an immune response that is not subject to central and peripheral tolerance. Previous studies showed the importance of tumor-specific neoantigens as critical targets of antitumor immune responses [71]. Immune recognition of neoantigens has the potential to destroy developing cancers or, when manipulated in the appropriate therapeutic manner, promote the immune elimination of growing tumors. It can occur via specific T cell responses to neoantigens in tumors with high mutational loads, where the immune system recognizes foreign epitopes due to sufficient amount of DNA damage. Moreover, neoantigen vaccines are an effective approach for stimulating, enhancing and diversifying anti-tumor T cell responses. They are characterized by general safety and are easy to manufacture. Many forms of neoantigen-based vaccines are being evaluated in clinical trials, including peptide, nucleic acid and dendritic cell vaccines. In addition, neoantigen-based adoptive cell therapies have promising clinical outcomes. Highly immunogenic neoantigens are excellent targets for therapies that employ genetically engineered tumor-infiltrating lymphocytes. Other cancer therapies that use the potential of immune responses to neoantigens are antibody-based therapies, checkpoint inhibitor-based immunotherapies such as anti-PD1/PD-L1/CTLA4 and combinational therapies that integrate therapies with different mechanisms of action to overcome the resistance induced by tumor heterogeneity [72].

1.6 Single-cell RNA sequencing

Ribonucleic acid (RNA) is involved in many biological processes such as cell to cell communication, embryonal development, tissue homeostasis and tumor formation, progression or metastasis. There are various types of RNA that are essential for cell growth and differentiation. Studying the full range of RNA molecules would help in understanding development and disease, as well as interpreting the functional elements of the genome. It is known that mRNA processing is crucial for gene expression and is constantly altered in cancer. Various gene expression profiles may indicate different cancer subtypes, the stage of cancer development or tumor microenvironment [73].

Because of RNA's pivotal role in various biological processes, RNA sequencing (RNAseq) is a powerful tool for studying molecular mechanisms in tumorigenesis, cancer prevention and treatment development. RNAseq, which often refers to a bulk RNAseq, is a technique that examines constantly changing cellular complete set of coding and non-coding RNA transcripts, known as transcriptome, using next generation sequencing (NGS) to determine the presence and the amount of RNA in any biological sample. This sequencing approach relies on an average gene expression from a cell population during the time of measurement. Therefore, this technique can determine differences between sample conditions. This method allows to study the differential gene expression and can reveal any gene fusions, mutations or splicing variants. The introduction of high-throughput NGS technologies transformed transcriptomics where RNA analysis through cDNA sequencing is possible at the massive scale.

Single cell RNA sequencing (scRNAseq) has evolved from classic bulk RNA sequencing and in 2013 was titled as one of the most anticipated technologies of the year in Nature Methods [74] with a follow up nomination in 2019. The introduction of this method has revolutionized genomic research and made significant progress since its beginning. scRNAseq research began in 2009 with the characterization of cells in their early developmental phases [75]. This tremendous progress was driven by the rapid development of computational analysis methods, modern technologies and broadening our biological knowledge about cellular heterogeneity and its implications for cell functions. ScRNAseq method enables researchers to conduct genome-wide profiling at the level of individual cell. By studying the fluctuations of gene expression at the single-cell level, this technology has given transcriptomics a new life and provided insight

into intricate biological processes like cancer and embryogenesis. In the recent years, several scRNAseq technologies have been created, such as plate-, microfluidic-, valve- and droplet-based [76], but all of them have similar basic steps conducting scRNAseq: sample preparation, single-cell capture, cell lysis with mRNA preservation, transcription and amplification, library preparation, sequencing and analysis.

The 10X Genomics Chromium single cell RNAseq technology is a rapid droplet-based encapsulation of single cells using gel beads in emulsion (GEM) approach. The first step in this process is the effective isolation of viable, single cells from the tissue of interest. Next, sample multiplexing is performed and each sample is labeled with unique sample tag and then pooled together. Next step involves GEM generation. Each functional GEM is formed on a microfluidic chip using partitioning oil and contains a single cell, a single Gel Bead with barcoded oligonucleotides and reverse transcription reagents. Immediately following GEM generation, the Gel Bead is dissolved releasing reaction reagents and lysis of a single cell and barcoded reverse transcription of polyadenylated mRNA is performed within each GEM reaction vesicle. As a result, all cDNA from a single cell are labeled with the same barcode, allowing to analyze and track back the sequencing results to their original single cell. In the next step after incubation, GEMs are broken and barcoded cDNA is pooled and separated from post GEM-RT reaction mixture. Preparation of NGS libraries is carried out in a highly efficient bulk reaction [77]. Described process is shown schematically in Figure 3.

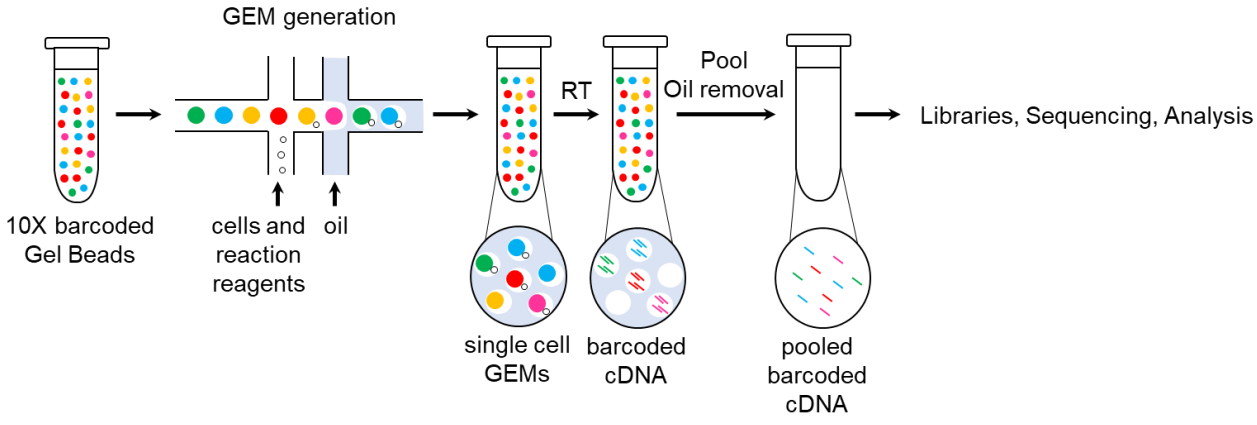

***Figure 3**. 10X Genomics Chromium single cell RNAseq. Schematical representation of workflow of scRNAseq technology including GEMs and libraries generation, sequencing and analysis steps. Reproduced from the current version of the 10x Genomics User Guide (Chromium Single Cell 3' Reagent Kits User Guide (v3.1 Chemistry)).*

2. METHODOLOGY

2.1 Mice and Ovarian Carcinoma Cell Line

In this study, six week old female wild-type C57BL/6 mice were purchased from Charles River Laboratories (Wilmington, MA, USA). The C57BL/6 Tg*MISIIR-TAg-Low* transgenic mice were obtained from Dr. Denise Connolly (Fox Chase Cancer Center, Philadelphia, PA, USA) and bred in the Laboratory Animal Resources at Roswell Park Comprehensive Cancer Center (Buffalo, NY, USA). To generate these mice, SV40 large T antigen (TAg)-positive male transgenic founders were crossed with wild type C57BL/6 mice to produce female offspring with low TAg transgene expression without obvious pathology. The C57BL/6 Tg*MISIIR-TAg-Low* mice express the TAg protein in epithelial cells lining fallopian tubes under the transcriptional control of the Müllerian inhibiting substance type II receptor gene promoter and have little or no susceptibility to spontaneous tumor development [78]. All animal studies were performed following guidelines established by the Institutional Animal Care and Use Committee (IACUC) under an approved protocol.

MOVCAR 5009 is one of the MOVCAR cell lines derived from ascites of C57BL/6 Tg*MISIIR-TAg* mice expressing a high level of TAg, that recapitulate crucial features of serous ovarian carcinoma such as metastatic potential. MOVCAR 5009 murine ovarian carcinoma cell line expressing TAg, transduced with a retroviral construct encoding luciferase gene (pWZL-Luc) for *in vivo* imagining [78,79], was provided by Dr. Denise Connolly (Fox Chase Cancer Center, Philadelphia, PA, USA). This cell line was established from ascites of the spontaneous ovarian tumors developed in Tg*MISIIR-TAg* mice, characterized by rapid tumor growth and production of voluminous ascites associated with expression of VEGF and selected based on tumorigenicity in both syngeneic Tg*MISIIR-TAg-Low* and wild type C57BL/6 mice [80]. Scheme of Tg*MISIIR-TAg-Low* mice and MOVCAR 5009 cell line generation is shown in Figure 4.

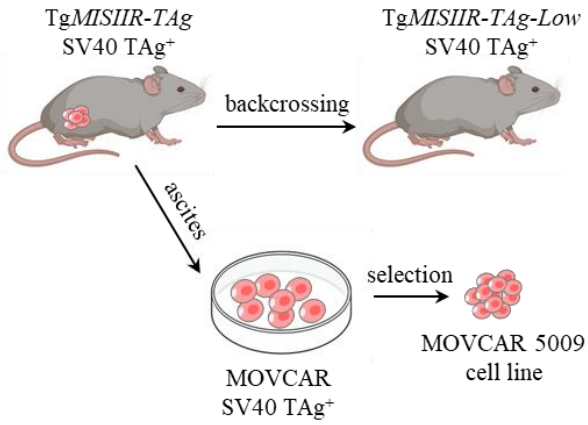

Figure 4. *Development of C57BL/6 TgMISIIR-TAg-Low mice and MOVCAR 5009 cell line.*

MOVCAR 5009 cells were cultured in Dulbecco's Modified Eagle's Medium (DMEM, 10-017-CV, Corning, NY, USA) supplemented with 10% fetal bovine serum (FBS, 35-011-CV, Corning, NY, USA), 5 µg/ml gentamicin sulfate (30-005-CR, Corning, NY, USA) and maintained at 37°C, 5% CO_2 in Thermo Fisher Scientific (Waltham, MA, USA) incubator using 75 cm^2 sterile culture flasks (TL32, Alkali Scientific, Fort Lauderdale, FL, USA). Confluency of cells did not exceed 80%. MOVCAR 5009 cells grow as adherent cells, therefore Dulbecco's Phosphate-Buffered Saline (DPBS, 20-031-CV, Corning, NY, USA) and 0.25% trypsin solution (25-053-CI, Corning, NY, USA) were used. Aforementioned cell line was authenticated by short tandem repeat (STR) profiling in ATCC (Gaithersburg, MA, USA).

2.2 Vaccinia viruses

Vaccinia viruses used in this study are of Western Reserve stain with disrupted TK and VGF genes for enhanced cancer cell specificity. The generation and characterization of oncolytic vaccinia viruses expressing enhanced green fluorescent protein (OV-EGFP) and the CXCR4 antagonist in the context of the Fc portion of murine IgG2a (OV-CXCR4-A) have been described by Gil *et al*. [81]. Briefly, vaccinia viruses used in this study were created by homologous recombination of EGFP or the CXCR4-A-Fc fusion protein into the *TK* gene of VSC20, VGF deleted vaccinia virus. VSC20, used as a background virus, has the *lacZ* gene inserted into its VGF sites. The expression of EGFP in OV-EGFP infected NXS2 cells was confirmed by immunofluorescence microscopy [82,83]. For OV-CXCR4-A generation, mouse IgG2a Fc fragments were cloned in-frame with the annealed oligonucleotides AAGGGAGTCAGCCTGAGCTACAGA corresponding to the CTCE-9908 peptide, which is an analog of CXCL12 that competitively binds to CXCR4. As a result, first eight amino acids (KGVSLSYR) of CTCE-9908 were expressed in the context of the IgG2a Fc portion with disulfide bonds in a hinge region for preservation of its dimeric structure (Figure 5).

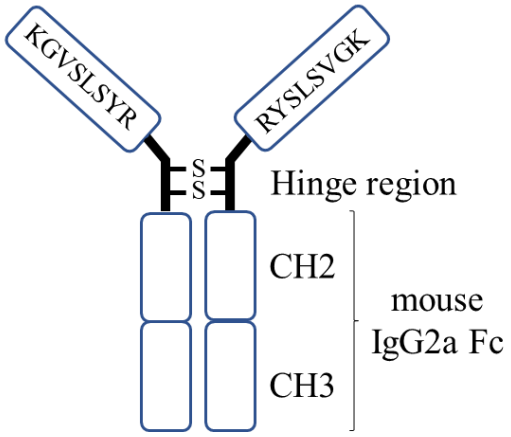

Figure 5. *CXCR4-A-Fc fusion protein construct. First eight amino acids of CTCE-9908 expressed in the context of the Fc portion of murine IgG2a with disulfide bonds in a hinge region. Adapted from [81].*

2.2.1 Vaccinia virus amplification

Vaccinia viruses were amplified from viral stocks by infection of successively larger number of 293 LTV cells. For continuous culture 293 LTV cells were seeded to 75 cm^2 sterile culture flasks (TL32, Alkali Scientific, Fort Lauderdale, FL, USA) at approximately 2,5 x 10^6 cells in 30 ml DMEM (10-017-CV, Corning, NY, USA) supplemented with 5% fetal bovine serum (FBS, 35-011-CV, Corning, NY, USA), 50 µg/ml gentamicin sulfate (30-005-CR, Corning, NY, USA) and maintained at 37°C, 5% CO_2. Cells were passaged after the culture reached 90-95% confluency. Monolayer of 293 LTV cells was infected with multiplicity of infection (MOI) = 1 in 10 ml of DMEM (10-017-CV, Corning, NY, USA) supplemented with 2% fetal bovine serum (FBS, 35-011-CV, Corning, NY, USA) and 50 µg/ml gentamicin sulfate (30-005-CR, Corning, NY, USA) using original vaccinia virus stock. Cells were incubated at 37°C, 5% CO_2 for 2 hours, with gentle agitation at approximately 15 minutes intervals to achieve an evenly spread infection. Infected cells were cultured for 48 hours in a fresh 30 ml DMEM (10-017-CV, Corning, NY, USA) supplemented with 2% fetal bovine serum (FBS, 35-011-CV, Corning, NY, USA) and 50 µg/ml gentamicin sulfate (30-005-CR, Corning, NY, USA). After this incubation time cells were scraped, centrifuged and vaccinia-infected cell pellet was stored at -80ºC. For subsequent rounds of infections, infected cell pellets were used instead of viral stocks. Freeze-thaw cycling were carried out to release the recombinant virus from the cells. Total of 100 viral pellets were collected for purification.

2.2.2 Vaccinia virus purification

Vaccinia viruses were purified by zonal sucrose (84097-1KG, Sigma-Aldrich, Saint Louis, MO, USA) gradient centrifugation. This method allowed to reduce infected-cell proteins contamination and increase the virus titer. Previously collected viral pellets were subject to freeze-thaw cycling and homogenized in 10 mM Tris-Cl pH 9.0 using a tight fitting glass Dounce homogenizer. Obtained suspension was centrifuged for 5 minutes at 300 x g for nuclei removal. Supernatant was sonicated and gently layered on 36% sucrose in 10 mM Tris-Cl pH 9.0 and centrifuged at 32 900 x g at 4ºC for 80 minutes. Virus pellet was collected, sonicated on ice and gently layered on previously prepared continuous sucrose gradient 40%, 36%, 32%, 28%, 24%. After centrifugation at 26 000 x g for 50 minutes at 4ºC, milky bands containing the virus were collected. Aggregated virus that appeared as a pellet at the bottom was sonicated and

rebanded. Virus bands were centrifuged again in 1 mM Tris-Cl pH 9.0 at 32 900 x g for 60 minutes at 4ºC. Purified virus pellet thus obtained was resuspended in pure DMEM (10-017-CV, Corning, NY, USA) and used as viral stocks for all experiments.

2.2.3 Vaccinia virus plaque assay titration

Plaque assays remain one of the most accurate methods for the direct quantification of infectious virions through the counting of discrete plaques in cell culture. A confluent monolayer of CV-1 host cells was infected with a serially diluted, to a countable range, purified vaccinia virus stock of an unknown concentration. CV-1 cell line exhibits fibroblast morphology that was isolated from the kidney of a male adult African green monkey. Cells were seeded at 5 x 10^5 in 3 ml Roswell Park Memorial Institute Medium (RPMI, 10-040-CV, Corning, NY, USA) on 6-well plates (92006, TPP, Switzerland) and maintained for 24 hours at 37°C, 5% CO_2. Culture medium was discarded and vaccinia virus serial dilutions in RMPI (10-040-CV, Corning, NY, USA) supplemented with 2% fetal bovine serum (FBS, 35-011-CV, Corning, NY, USA) were added to wells. Visible plaques were formed within three days. Cellular monolayers were counterstained by crystal violent in order to readily identify plaques. Crystal violet provided a rapid and distinct counter stain which allowed for the identification of very small plaques. A log drop was noted between serial dilutions, distinct plaques counted and concentration was calculated.

2.3 *In Vivo* Studies

Mice were injected intraperitoneally with 5 x 10^6 MOVCAR 5009 cells resuspended in sterile 300 µl of Phosphate Buffered Saline (PBS, 20-040-CM, Corning, NY, USA). Ten days after tumor challenge, mice were treated intraperitoneally with 5 x 10^7 plaque-forming units (PFU) of OV-EGFP or OV-CXCR4-A and control mice were injected with PBS (20-040-CM, Corning, NY, USA). Tumor growth was monitored by bioluminescence imaging. Each mouse received 150 mg D-Luciferin (LUCK-1G, GoldBio, St Louis, MO, USA) per kilogram body weight. The quantification of bioluminescence signal was determined using IVIS Spectrum In Vivo Imaging System (PerkinElmer, Waltham, MA, USA). Average radiance (photons/sec/cm2/sr) in the standard region of interest (ROI) was determined using the Living Image 4.7.3 Software for IVIS Spectrum.

2.4 Flow Cytometry

10 days after OV treatment single-cell suspensions were obtained from peritoneal fluids of MOVCAR 5009-bearing mice for flow cytometry analysis. ACK Lysing Buffer (118-156-101, Quality Biological, Gaithersburg, MD, USA) was used for red blood cells lysis prior to incubation with anti-mouse CD16/CD32 Fc blocker (553142, BD Biosciences, San Jose, CA, USA) for 20 min at 4°C. Next, cells were stained with selected cell surface markers. For intracellular assays, the Transcription Factor Buffer Set (562574, BD Biosciences, San Jose, CA, USA) was used according to the manufacturer's recommendation. All fluorochrome-conjugated antibodies were purchased from BD Biosciences (San Jose, CA, USA), BioLegend (San Diego, CA, USA), Thermo Fisher Scientific (Waltham, MA, USA) or Sigma-Aldrich (Saint Louis, MO, USA), as detailed in Table 1. The TAg-D^b/SAINNYAQKL tetramer conjugated to PE was obtained from MBL International Corporation (Woburn, MA, USA) and B8R-K^b/TSYKFESV tetramer conjugated to PE was purchased from Baylor College of Medicine (Houston, TX, USA). All samples were analyzed on the LSR Fortessa flow cytometer (BD Biosciences, San Jose, CA, USA) and data analysis was performed using WinList 3D 9.0.1 (Verity Software House, Topsham, ME, USA). During the analysis doublets were excluded using forward scatter-height (FSC-H) vs forward scatter-area (FSC-A), followed by exclusion of dead cells stained with LIVE/DEAD Fixable Aqua Dead Cell Stain (L34957, Invitrogen, Waltham, MA, USA).

Table 1. *Antibodies used in flow cytometry analysis.*

Antibody	Clone	Catalog Number	Source
Extracellular staining			
CD8α-V450	53-6.7	560471	BD Biosciences
CD3-Alexa Fluor 700	17A2	561388	BD Biosciences
CD38-FITC	Ab90	558813	BD Biosciences
CD101-Ax647	307707	564473	BD Biosciences
CD45-PerCP-Cy5.5	30-F11	550994	BD Biosciences
CD45-V450	30-F11	560501	BD Biosciences
CD11b-BV786	M1/70	740861	BD Biosciences
Ly6G-PE	1A8	561104	BD Biosciences

Ly6C-FITC	AL-21	561085	BD Biosciences
I-A\I-E-BV605	M5/114.15.2	107639	BioLegend
F4/80-FITC	BM8	123107	BioLegend
CD25-FITC	3C7	101908	BioLegend
CD4-PE	GK1.5	553730	BD Biosciences
TAg-Db/SAINNYAQKL-PE	-	TB-M539-1	MBL International
B8R-Kb/TSYKFESV-PE	-	-	Baylor College of Medicine
CD45-APC/Fire750	30-F11	103154	BioLegend
CD31-FITC	390	102405	BioLegend
CD90.2-PE/Cy7	30-H12	105325	BioLegend
CD49e-BV786	5H10-27	740863	BD Biosciences
PDPN-BV421	8.1.1	127423	BioLegend
FAP	73.3	MABC1145	Sigma-Aldrich
Mouse IgG1-APC	A85-1	560089	BD Biosciences
CD4-APC	RM4-4	116013	BioLegend
CD8α-FITC	CT-CD8α	MA5-17597	Thermo Fisher Scientific
Intracellular staining			
Foxp3-Alexa Fluor 647	MF23	560401	BD Biosciences

2.5 T cell depletion study

The following antibodies from Bio X Cell (Lebanon, NH, USA) were used for T cell depletion study: anti-CD4 (rat IgG2b, clone YTS 191), anti-CD8 (rat IgG2b, clone YTS 169.4) and isotype control (anti-KLH, rat IgG2b, clone LTF-2) antibodies. For sufficient T cell depletion in mice, beginning one day before MOVCAR 5009 tumor challenge, mice were injected intraperitoneally with 100 µg per injection of anti-CD4 or anti-CD8α in 300 µl PBS (20-040-CM, Corning, NY, USA), followed by the same dosing on days 2, 6, 10, and 14. Control mice received an equal dose of anti-keyhole limpet hemocyanin (KLH) as an isotype control. Mice were treated intraperitoneally ten days post-inoculation with 5 x 10^7 PFU of OV-EGFP or OV-CXCR4-A. An experimental scheme is presented in Figure 6. To confirm reductions of the respective T cell subsets, flow cytometry staining of peripheral blood CD8 and CD4 lymphocytes with noncompetitive anti-CD8 (clone CT-CD8, Thermo Fisher Scientific,

Waltham, MA, USA) and anti-CD4 (clone RM4-4, BioLegend, San Diego, CA, USA) monoclonal antibodies was performed one day after the last antibody treatment. Tumor growth was monitored by bioluminescence imaging.

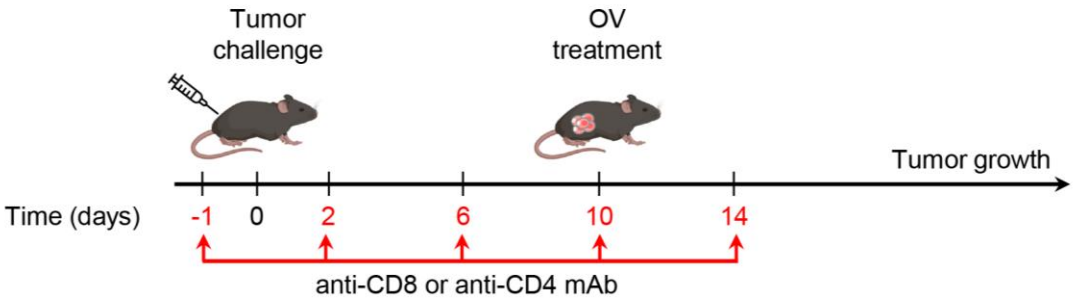

Figure 6. *T cell depletion study - an experimental scheme. WT or TgMISIIR-TAg-Low mice (n = 5 per group) were injected intraperitoneally with 5 x 10^6 MOVCAR 5009 cells 10 days before treatments with OV-EGFP or OV-CXCR4-A. Control mice were treated with PBS. Anti-CD8 or anti-CD4 antibodies (100 µg/injection) were injected intraperitoneally 1 day before and on days 2, 6, 10, and 14 after the tumor inoculation.*

2.6 Adoptive cell transfer

Donor mice, WT or Tg*MISIIR-TAg-Low*, were injected intraperitoneally with 5 x 10^6 MOVCAR 5009 cells. Peritoneal fluids were collected 20 days after tumor inoculation for TAMs or CAFs isolation for adoptive cell transfer (ACT) to the recipient MOVCAR 5009-challenged WT mice.

2.6.1 TAMs adoptive cell transfer

For the adoptive transfer of TAMs, $CD45^+CD11b^+F4/80^+$ cells were sorted from single-cell suspensions obtained from peritoneal fluids of WT or Tg*MISIIR-TAg-Low* tumor-bearing mice using BD FACS Aria Cell Sorter under sterile conditions. 1 x 10^6 isolated cells, that were >95% $CD11b^+F480^+$, were injected intraperitoneally to MOVCAR 5009-challenged WT mice 10 days after tumor inoculation. Subsequently, mice were treated intraperitoneally with 300 µl of either OV-CXCR4-A (5 x 10^7 PFU) or PBS (20-040-CM, Corning, NY, USA) twelve hours after the transfer. Tumor growth was monitored by bioluminescence imaging.

2.6.2 CAFs adoptive cell transfer

For the adoptive transfer of CAFs, $CD45^-$ cells were isolated by negative selection from single-cell suspensions obtained from peritoneal fluids of control WT or Tg*MISIIR-TAg-Low* tumor-bearing mice (*n* = 10) using CD45 MicroBeads (130-052-301, Miltenyi Biotec, Baltimore, MD, USA) and LS columns (130-042-401, Miltenyi Biotec, Baltimore, MD, USA) following the manufacturer's instructions. The CD49e-enriched CAF populations (>90% $CD49e^+$, <5% $CD31^+$, and <3% $CD45^+$) were resuspended in PBS (20-040-CM, Corning, NY, USA) and injected intraperitoneally to MOVCAR 5009-bearing WT mice (1 x 10^6 cells) one day after tumor inoculation. Subsequently, mice were treated intraperitoneally with 300 µl of OV-CXCR4-A (5 x 10^7 PFU) or PBS (20-040-CM, Corning, NY, USA) nine days after CAFs transfer. Tumor growth was monitored by bioluminescence imaging.

2.7 Cytotoxic assay

Effector $CD8^+$ T cells were obtained from single-cell suspensions of peritoneal fluids collected from MOVCAR 5009-challenged mice 10 days after the OV-CXCR4-A treatment using the $CD8^+$ T Cell Isolation Kit (130-104-075, Miltenyi Biotec, Baltimore, MD, USA) and LS columns (130-042-401, Miltenyi Biotec, Baltimore, MD, USA) following the manufacturer's instructions. MOVCAR 5009 target cells were labeled with CellTracker Blue CMF_2HC (C12881, Thermo Fisher Scientific, Waltham, MA, USA) for 45 minutes in serum free DMEM medium (10-017-CV, Corning, NY, USA) at 37ºC. Labeled MOVCAR 5009 target cells were mixed with isolated effector $CD8^+$ T cells at a 1:1 ratio in 500 µl of DMEM medium (10-017-CV, Corning, NY, USA) supplemented with 10% FBS (35-011-CV, Corning, NY, USA) and incubated in triplicates on 24-well plates (92012, TPP, Switzerland) at 37 °C for 17 hours. Cell cultures containing CellTracker Blue CMF_2HC-labeled MOVCAR 5009 cells only were included as controls. After the incubation time, cultures were collected and analyzed on an LSR Fortessa flow cytometer (BD Biosciences, San Jose, CA, USA). Cell killing was calculated using the following formula:

$$\%\ Lysis = 100\% - \left(\frac{\%\ labeled\ cells\ in\ experimental\ group}{\%\ labeled\ target\ cells}\ x\ 100\%\right)$$

2.8 Single-cell RNA sequencing

2.8.1 Sample preparation

For scRNAseq experiments WT and Tg*MISIIR-TAg-Low* mice were treated as shown in Figure 7. Peritoneal fluid of MOVCAR 5009-bearing mice was isolated 10 days after OV-CXCR4-A treatment and single-cell suspensions were prepared using cell strainers (22-363-548, Thermo Fisher Scientific, Waltham, MA, USA). Untreated tumor-bearing mice served as controls.

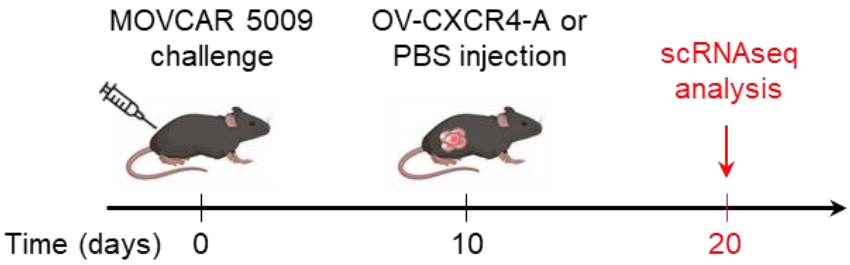

Figure 7. *Schematic representation of experimental design and samples for scRNAseq.*

After red blood cell lysis with ACK Lysing Buffer (118-156-101, Quality Biological, Gaithersburg, MD, USA), cells were washed in 0.04% BSA (A9418-5G, Sigma-Aldrich, Saint Louis, MO, USA) in DPBS (20-031-CV, Corning, NY, USA), stained with Cell Multiplexing Oligos from a 3' CellPlex Kit Set (PN-1000268, 10x Genomics, Pleasanton, CA, USA) for 5 min at room temperature and washed three times with 1% BSA (A9418-5G, Sigma-Aldrich, Saint Louis, MO, USA) in DPBS (20-031-CV, Corning, NY, USA). For single-cell gene expression libraries generation, the Chromium Next GEM Single Cell 3′ GEM, Library & Gel Bead Kit v3.1 (PN-1000121, 10x Genomics, Pleasanton, CA, USA) was used. To determine the concentration, viability, and absence of clumps and debris that could interfere with single-cell capture, cells previously tagged with CellPlex oligos were first analyzed with Trypan Blue (15250061, Thermo Fisher Scientific, Waltham, MA, USA), using a Countess II FL Automated Cell Counter (Thermo Fisher Scientific, Waltham, MA, USA). Before loading into the Chromium Controller (10x Genomics, Pleasanton, CA, USA) two samples with different CellPlex tags were pooled together in equal amounts for multiplexing. Reverse transcription was performed, and the resulting cDNA was amplified following the manufacturer's instructions. Amplified cDNA was separated into full-length transcript and CellPlex Barcode fractions using SPRISelect beads (Beckman Coulter, Brea, CA, USA). The transcriptome libraries were generated by enzymatic fragmentation, end-repair, a-tailing, and adapter ligation

using the full-length amplified cDNA. CellPlex barcode-derived cDNA was PCR amplified to incorporate Illumina adapter sequences and unique sample indexes. The resulting libraries were evaluated on D1000 screen tape using a TapeStation 4200 (Agilent Technologies, Santa Clara, CA, USA) and quantitated using the Kapa Biosystems qPCR quantification kit for Illumina platform. Final libraries were then pooled, denatured, and diluted to 300 pM (picomolar) with 1% PhiX control library added. The PhiX control is a reliable, adapter-ligated library derived from the small, well-characterized bacteriophage genome with an average size of 500 bp. The obtained pool was then loaded into the NovaSeq Reagent cartridge and sequenced on a NovaSeq6000 (Illumina Inc., San Diego, CA, USA) following the manufacturer's recommended protocol.

2.8.2 Single-cell RNAseq analyses

The Cell Ranger output was used for detailed data analysis. The raw sequencing data from the 10x Genomics libraries, mapping results (BAM files), and quantification matrices were processed and generated using Cellranger version 6.0.0 [84] software with mouse mm10 genome and GENCODE annotation database. CellPlex barcodes were used to identify different samples in the pool and data was separated for individual samples with Cellranger multi-function. For further analysis, the filtered gene-barcode matrices which contain barcodes with the unique molecular identifier (UMI) counts that passed the cell detection algorithm were used. The downstream analyses were performed primarily using Seurat single cell data analysis R package [85]. First, cells with unique RNA feature counts over 7500 or less than 500, or cells that have >15% mitochondrial RNA contents were filtered out from the analysis to remove dead cells and doublets. Then, the normalized and scaled UMI counts were calculated using the SCTransform method. Dimension reductions including principal component analysis (PCA), uniform manifold approximation and projection (UMAP), and t-distributed stochastic neighbor embedding (tSNE) were performed using the highly variable genes. Cell clusters were identified using the shared nearest neighbor (SNN)-based clustering on the first 12 principal components. The cell clusters were annotated by SingleR packages [86] using the ImmGen reference database of the celldex R package [86]. Seurat's AddModuleScore function was used to calculate M1 and M2 macrophage scores with M1 and M2 macrophage signature genes. Differentially expressed genes between clusters and samples were identified using

the FindMarkers function with the Wilcoxon rank sum test from Seurat. Fgsea R package [87] was carried out for pathway analysis with gene list ranked by average log2 fold change. The volcano plots were generated with EnhancedVolcano R package [88] and the heatmaps were prepared using heatmap R package [89].

2.8.3 Pathway analyses

Gene set enrichment analysis (GSEA) of selected differential expression profiles identified between groups or clusters was done using enrichR and clusterProfiler in R. AUCell [90] was used for single-cell functional enrichment analysis, which applies an area under the curve method to query cell-to-cell pathway activity that is robust to noise typical of scRNAseq datasets. Six pathway databases (Hallmark Pathways, GO biological processes, BioCarta, KEGG, Reactome, and the Pathway Interaction Database (PID)) were compiled from the Molecular Signatures Database (MSigDB) [91] and used as reference sets for functional enrichments. For GSEA, only gene sets with $p < 0.05$ and false discovery rate (FDR) $q < 0.25$ were considered significantly enriched. Also, I generated heat maps of normalized enrichment scores (NES) of relevant biological pathways, to visualize selected functional enrichments.

2.8.4 scRNA sequencing data availability

The raw data and quantification matrices of scRNA sequencing have been deposited in the database of Gene Expression Omnibus (GEO) under the accession number GSE199880.

2.9 Statistical analysis

GraphPad Prism 6 (GraphPad Software Inc., San Diego, CA, USA) was used to conduct all statistical analyses. Unless otherwise noted, data are presented as mean ± SD. All quantitative results were assessed by an unpaired Student's *t*-test. The Student *t*-test assumed two-tailed distributions to calculate statistical significance between groups. Animal survival impact was determined by the Kaplan-Meier analysis, and median survival times were determined for tumor-challenged groups of mice. Sample size estimation was done taking into consideration previous experience with animal strains, assay sensitivity and tissue collection methodology used. Statistical differences in the survival across groups were assessed using the log-rank Mantel-Cox method. The threshold for statistical significance was set to $p < 0.05$.

3. RESULTS

3.1 OV-CXCR4-A exhibits reduced antitumor efficacy in Tg*MISIIR-TAg-Low* mice compared to their wild type counterparts

For the analysis of tumor and self-antigen expression in the host and its effect on efficacy of OV-CXCR4-A treatment, I have compared the progression of TAg^+ MOVCAR 5009 tumor in syngeneic WT (TAg^-) and Tg*MISIIR-TAg-Low* (TAg^+) mice. Murine ovarian carcinoma MOVCAR 5009 cells (5 x 10^6/mouse) were injected intraperitoneally into both groups of mice (n = 5 - 6 mice per group) and 10 days later treated intratumorally with 5 x 10^7 PFU/mouse of OV-EGFP or OV-CXCR4-A, while control mice received PBS, as summarized in Figure 8. Tumor growth was quantified by bioluminescence imaging and representative photos are shown in Figure 9.

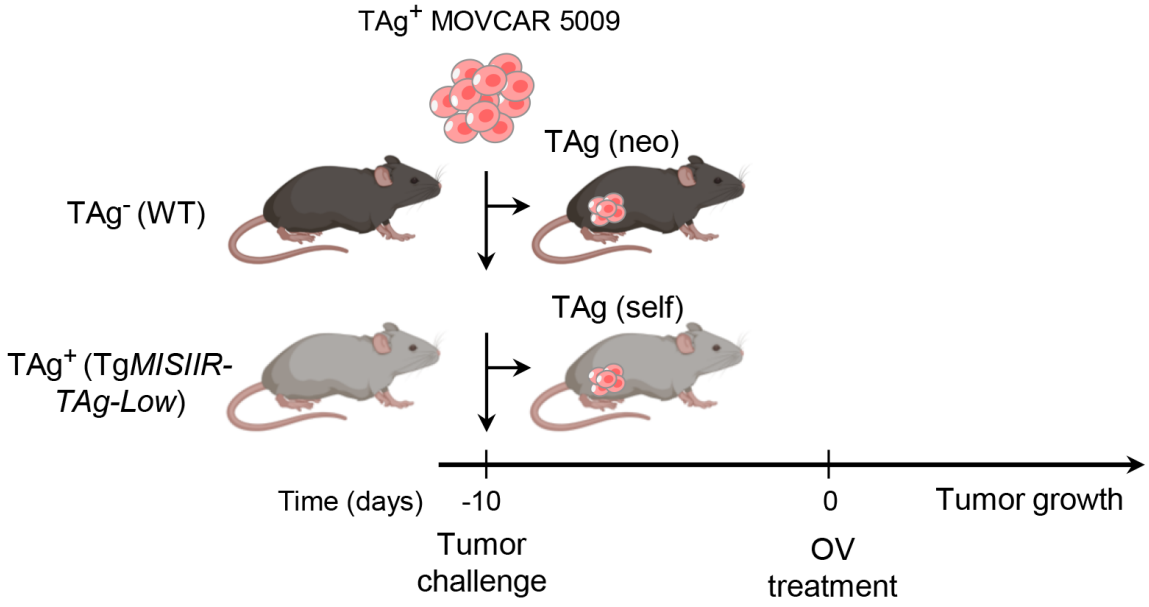

Figure 8. *Analysis of tumor/self-antigen expression effect on efficacy of OV treatment - an experimental scheme. TAg antigen in syngeneic WT mice is marked as neoantigen, whereas in TgMISIIR-TAg-Low mice as self-antigen.*

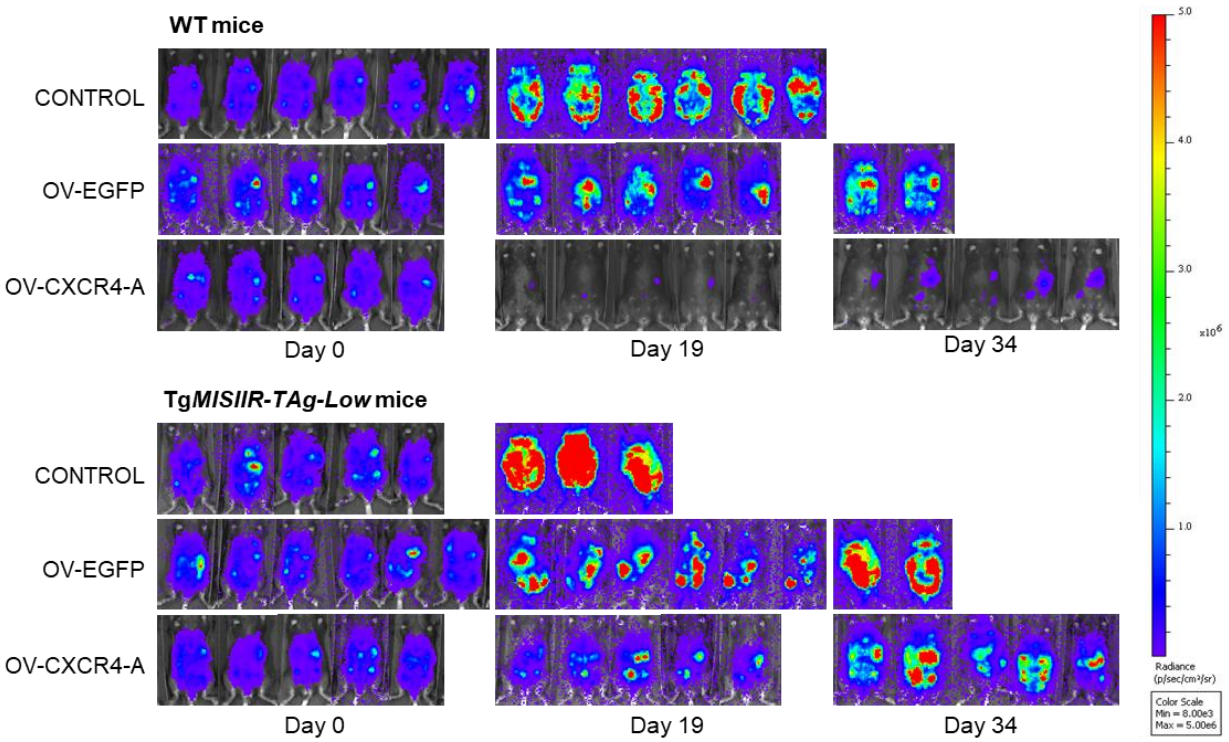

Figure 9. *Bioluminescence images of mice treated with OV-EGFP or OV-CXCR4-A. Presented signals were measured on day 0, 19 and 34.*

In this study, treatment with OV-EGFP served as a control of parental vaccinia virus and was used to delineate the effects of the OV over PBS control and armed OV-CXCR4-A over the virus itself. In both WT and Tg*MISIIR-TAg-Low* mice, kinetic tumor study showed that OV-CXCR4-A treatment exhibited significant therapeutic efficacy compared to the OV-EGFP virus (Figure 10A; *left panel* $p = 0.02$ and *right panel* $p = 0.04$). Comparing to the untreated tumors in both WT and Tg*MISIIR-TAg-Low* mice, OV-EGFP therapy reduced tumor volume (Figure 10B) and extended survival in WT mice for approximately 10 days and in transgenic group of mice for 4 days (Figure 10), however those differences did not reach statistically significant levels. Those findings are consistent with previous studies conducted by Gil *et al.* [92] using oncolytic virotherapy to target mouse ID8-T ovarian epithelial cells and human CAOV2 ovarian cancer cells in syngeneic (C57BL/6) and xenograft (SCID) murine models, respectively. Furthermore, I found that the tumor growth in WT mice after OV-CXCR4-A treatment was noticeably slower than in Tg*MISIIR-TAg-Low* mice (Figure 10A, *left panel* $p = 0.02$ and *right panel* $p = 0.04$) compared to control group. Tumor remained dormant for over 20 days in WT mice after OV-CXCR4-A treatment in contrast to approximately a 10-day dormancy

period in Tg*MISIIR-TAg-Low* mice. That difference in tumor growth rate was also reflected in longer survival. Median survival for OV-CXCR4-A treated WT mice was 69 days, whereas in transgenic mice survival period was 41 days (Figure 10B). Based on these data, and since both the tumor cancer cells and treatment were identical, I have reasoned that the differences in observed treatment efficacy were likely due to microenvironment impact on the ability to generate OV-induced antitumor immunity through immune modulation.

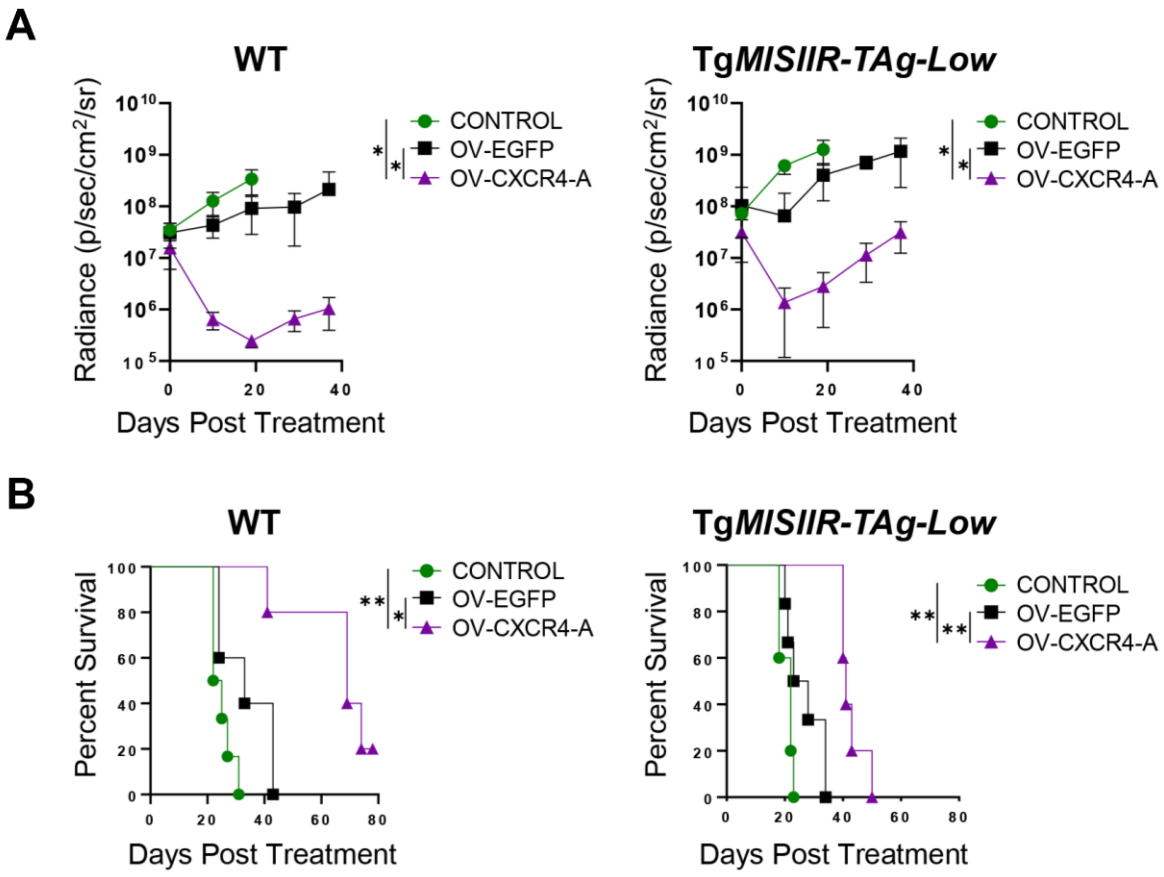

Figure 10. *Tumor growth and survival of mice treated with OV-EGFP or OV-CXCR4-A. (A) Tumor volume curves in WT (left panel) and TgMISIIR-TAg-Low (right panel) mice after different treatments. Individual data points represent mean ± SD. *p < 0.05. (B) Kaplan-Meier survival plots. Survival was defined as the point at which mice were euthanized due to the development of abdominal distention. Significance was calculated using the log-rank method. *p < 0.05, **p < 0.01.*

3.2 Immunosuppressive myeloid cells accumulate in MOVCAR 5009-challenged Tg*MISIIR-TAg-Low* mice.

To further investigate the potential of OV-treatment to induce antitumor immune responses and the heterogeneity of the tumor microenvironment, I have performed flow cytometry analysis of single-cell suspensions isolated from peritoneal fluids of untreated and OV-treated mice 10 days post-virotherapy. It revealed robust, more than 70% accumulation of $CD11b^+$ myeloid cells in control tumors both in WT and Tg*MISIIR-TAg-Low* mice, with lower numbers after viral therapy ($p < 0.05$). Differences between OV-EGFP and OV-CXCR4-A did not reach statistically significant levels (Figure 11A). The frequency of $Ly6G^{high}Ly6C^{low}$ granulocytic myeloid-derived suppressor cells (G-MDSCs) among the $CD11b^+$ myeloid populations was visibly higher in untreated Tg*MISIIR-TAg-Low* mice (10.9%) than in their WT (7.3%) counterparts (Figure 11B, *left panel* $p = 0.02$). OV-EGFP treatment in WT mice increased percentages of G-MDSCs almost two times compared to the untreated control, whereas this increase in tumor-bearing transgenic mice was not that prominent, but still statistically significant (Figure 11B, *left panel*, in WT mice $p = 0.006$, in Tg*MISIIR-TAg-Low* mice $p = 0.04$). The accumulation of G-MDSCs after OV-CXCR4-A treatment was significantly reduced compared to their untreated (in WT mice from 7.3% to 3.5%, $p = 0.02$ and in Tg*MISIIR-TAg-Low* mice from 10.9% to 7.1%, $p = 0.02$) and OV-EGFP-treated (in WT mice from 12.5% to 3.5%, $p = 0.0005$, in Tg*MISIIR-TAg-Low* mice from 15.2% to 7.1%, $p = 0.005$) counterparts in both groups of mice (Figure 11B, *left panel*). $CD11b^+Ly6G^-Ly6C^+$ monocytic myeloid-derived suppressor cells (M-MDSCs) comprised less than 10% of the $CD45^+$ leukocytes and no changes were detected between treatment groups (Figure 11B, *right panel*).

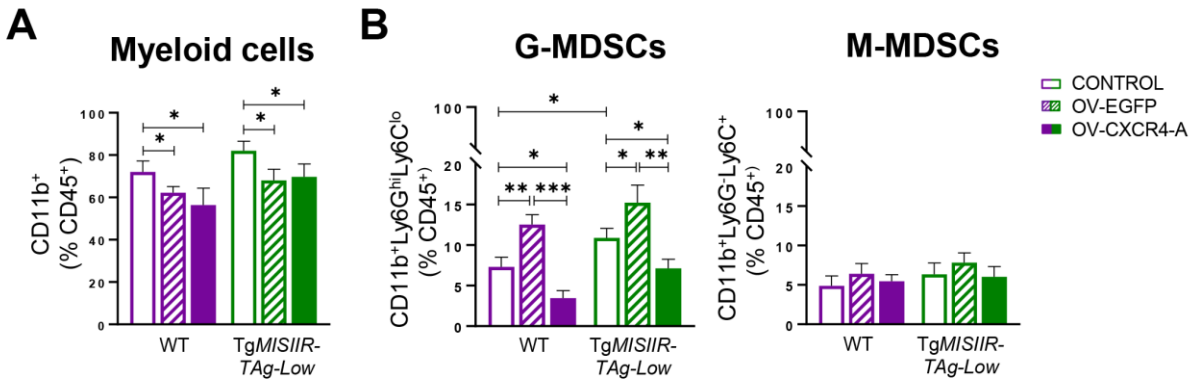

Figure 11. *Accumulation of peritoneal myeloid cells in MOVCAR 5009 tumor-bearing mice. Cells were analyzed by flow cytometry for the percentages of (A) CD11b$^+$ myeloid cells, (B) CD11b$^+$Ly6G^{hi}Ly6C^{lo} G-MDSCs (left panel) and CD11b$^+$Ly6G$^-$Ly6C$^+$ M-MDSCs (right panel) among CD45$^+$ leukocytes. *p < 0.05, **p < 0.01, ***p < 0.001.*

Next, I have examined accumulation of CD11b$^+$F4/80$^+$ tumor-associated macrophages (TAMs) in both untreated and OV-treated WT and Tg*MISIIR-TAg-Low* mice. Gating strategy used to subset TAMs population in peritoneal tumor microenvironment by flow cytometry is presented in Figure 12.

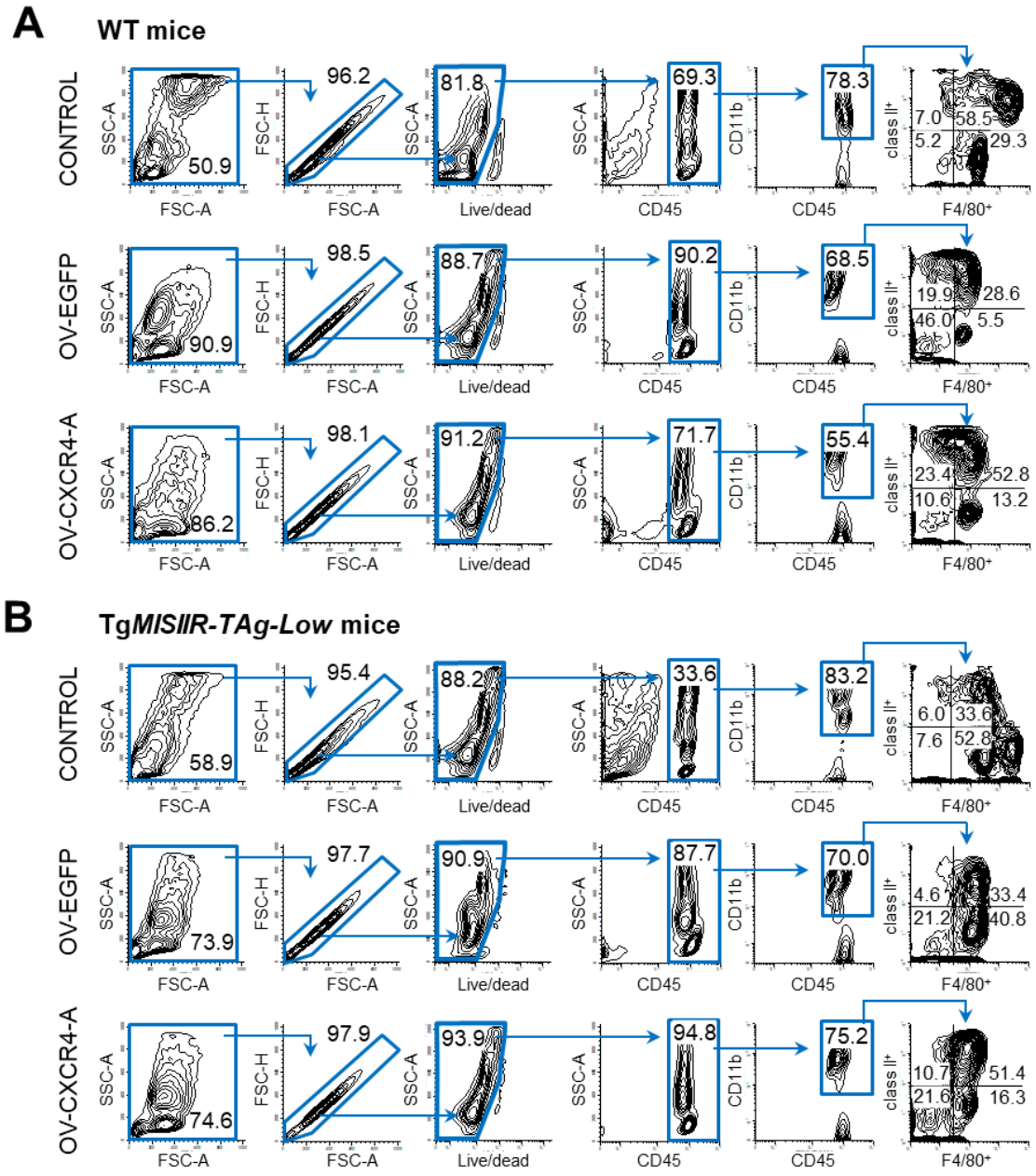

Figure 12. *TAMs gating strategy. Representative flow cytometric plots showing differences in MHC class II expression among F4/80$^+$ TAMs in control, OV-EGFP- and OV-CXCR4-A-treated tumors in (A) WT and (B) TgMISIIR-TAg-Low mice.*

After choosing cells of interest, first step in gating TAM populations was doublets elimination. Doublet and clump exclusion were performed by plotting height against the area for forward scatter. Doublets had approximately the same height, but area was doubled, so any disproportion between height and area was used to identify doublets. Next, to remove dead cells from the analysis LIVE/DEAD Aqua viability dye was used. In cells with compromised membranes, the dye reacts with free amines both on the cell surface and in the cell interior, resulting in intense fluorescent staining. For viable cells, fluorescence is less intense because dye's reactivity is restricted to the cell-surface amines only. After choosing viable population, CD45$^+$ (lymphocyte common antigen positive) cells were selected to exclude nonimmune cells. To pick myeloid-lineage populations, all CD11b$^+$ cells were then gated. In this particular analysis I gated also F4/80 which is a specific marker for murine macrophages, and MHC class II marker. Figure 13 shows that the frequency of CD11b$^+$F4/80$^+$ TAMs in the CD45$^+$ leukocyte population decreased after OV-EGFP and OV-CXCR4-A treatment compared to untreated WT mice ($p = 0.004$ and $p = 0.005$, respectively) and Tg*MISIIR-TAg-Low* mice ($p = 0.03$ and $p = 0.009$, respectively).

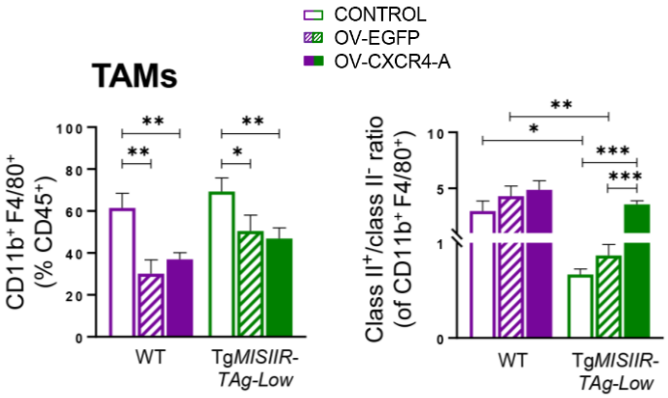

Figure 13. *TAMs population in peritoneal TME after virotherapy. The left panel shows the percentages of CD11b$^+$F4/80$^+$ TAMs among CD45$^+$ leukocytes. The right panel shows the ratios of class II$^+$ to class II$^-$ TAMs in WT and transgenic mice. Data points represent the mean of 5 mice per group ± SD. *p < 0.05, **p < 0.01, ***p < 0.001.*

A lack of MHC II expression on TAMs can be associated with their immunosuppressive phenotype, and it was previously shown that MHC class II^{low} TAMs inhibit T cell activation and promote tumor growth and invasion of tumor cells [48]. Hence, I investigated MHC class II expression on TAMs. I observed strong differences in MHC II expression between untreated

tumor-bearing WT and Tg*MISIIR-TAg-Low* mice (Figures 12 and 13 *right panel*). The ratios of MHC class II^+ to MHC class II^- $CD11b^+F4/80^+$ TAMs in the untreated tumors of WT mice ranged between 2.0 to 3.8 (mean 2.9 ± 0.9) and showed small increases after OV-EGFP (mean 4.3 ± 0.9) and OV-CXCR4-A treatments (mean 4.9 ± 0.8). The ratios of MHC class II^+/MHC class II^- TAMs in both untreated (mean 0.7 ± 0.06) and OV-EGFP-treated (mean 0.8 ± 0.11) tumors of Tg*MISIIR-TAg-Low* mice were reversed and significantly lower compared to their counterparts in WT mice ($p = 0.01$ and $p = 0.003$, respectively). The ratios of MHC class II^+/MHC class II^- TAMs in transgenic mice after OV-CXCR4-A (mean 3.6 ± 0.3) treatment were similar to those measured in OV-CXCR4-A-treated WT tumors and significantly higher compared to untreated and OV-EGFP-treated tumors ($p = 0.0001$ and 0.0002, respectively).

3.3 Accumulation of CAFs in the ovarian TME is reduced by OV-CXCR4-A treatment

Recent studies show that CAFs can be a key component of the tumor microenvironment of all solid tumors, including ovarian cancer, and have important effects on tumor behavior such as cancer cell proliferation, rate of cancer progression, promotion of cancer cell migration and invasion [93]. The relationship between M2 macrophages and CAFs is reciprocal [65], so I have next examined whether the qualitative differences within TAM subsets between tumors of WT and transgenic mice also reflect changes in the CAFs subsets. Representative phenotypic analysis of single-cell suspensions isolated from the peritoneal fluids of tumor-bearing WT and transgenic mice is presented in Figure 14A-B. Single-cell suspensions prepared from peritoneal fluids of tumor-bearing mice were stained with monoclonal antibodies specific for CD45 and CD31, to exclude hematopoietic and endothelial cells, respectively. Cells negative for both antigens were analyzed for expression of CAF markers CD49e and CD90.2. This analysis revealed higher frequencies of CAFs in the untreated MOVCAR 5009 tumors in Tg*MISIIR-TAg-Low* than in WT mice (Figure 14C, $p = 0.02$). The $CD49e^+CD90.2^+$ cells were then gated and analyzed for expression of fibroblast-activation protein (FAP) and podoplanin (PDPN). FAP is upregulated in many cancers [94], and both FAP and podoplanin were reported to restrain the proliferation of activated T cells in a nitric oxide-dependent manner [95]. The accumulation of double positive cells is visible in untreated tumors in both groups of mice (Figure 14D). The numbers of CAFs decreased after OV-treatment, which was consistent with previous findings that proliferating CAFs show higher sensitivity to oncolytic viruses compared with regular

fibroblasts [96,97]. Although the treatment with OV-EGFP decreased numbers of CAFs compared to untreated tumors in both mice groups, the differences did not reach statistical significance. OV-CXCR4-A treatment boosted the impact of OV on reducing numbers of CAFs, resulting in a significant drop in the percentage of CAFs compared to untreated tumors in both WT (from 14.9% to 4.7%) and transgenic mice (from 23.7% to 4.8%) (Figure 14C, $p = 0.014$ and $p = 0.0003$, respectively). It is worth noting that OV-CXCR4-A treatment visibly ablated the FAP^+PDPN^+ CAF subsets in both groups of mice (Figure 14D, $p < 0.01$).

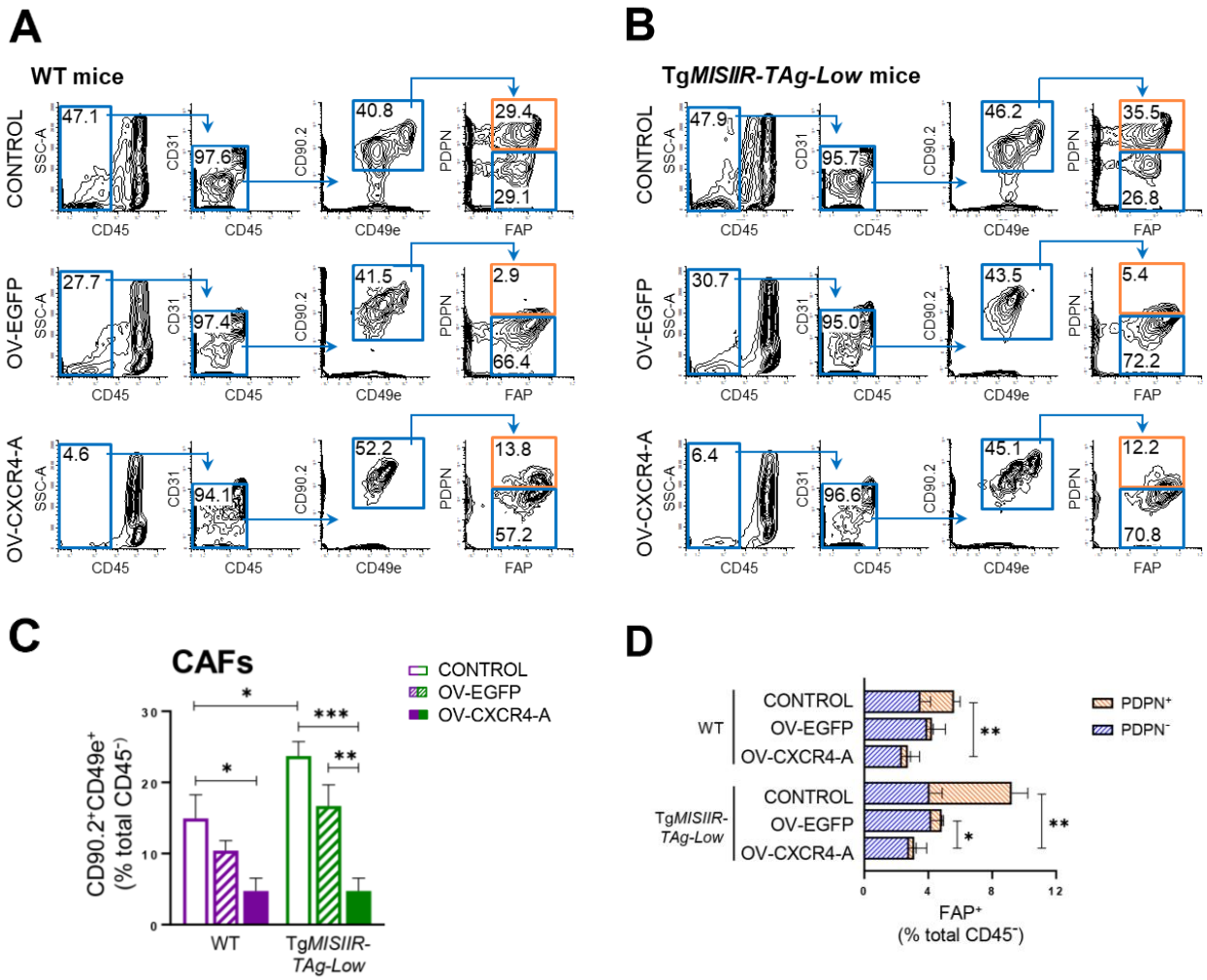

Figure 14. *CAFs in peritoneal TME of WT and TgMISIIR-TAg-Low mice. Representative staining of CAFs in MOVCAR 5009-challenged control, OV-EGFP- and OV-CXCR4-treated (A) WT and (B) TgMISIIR-TAg-Low mice. (C) Relative proportions of tumor-infiltrating $CD90.2^+CD49e^+$ CAFs are presented as a percentage of total $CD45^-$ cells. (D) FAP^+ CAFs were depicted as PDNP-positive or PDNP-negative. Results are presented as mean ± SD. *p < 0.05, **p < 0.01, ***p < 0.001.*

3.4 OV-CXCR4-A treatment induces antigen-specific CD8$^+$ T cell responses

Due to the discovery that immune suppression by the FAP-positive CAFs is mediated by CXCL12/CXCR4 interaction and inhibition of CXCR4 leads to the elimination of tumor cells through accumulation of cytotoxic CD8$^+$ T cells [98], I have investigated the effect of OV-CXCR4-A treatment on tumor-associated lymphocytes (TALs) in the peritoneal tumor microenvironment of the WT and Tg*MISIIR-TAg-Low* mice. Tumor microenvironment was poorly infiltrated by CD4$^+$ TALs in control mice, that comprised 7.5% in WT and 5.1% in transgenic mice of CD45$^+$ leukocytes (Figure 15A). OV-treatment slightly increased the percentages of CD4$^+$ TALs within each group of mice compared to their respective controls. A significant difference was detected only in the Tg*MISIIR-TAg-Low* mice after OV-CXCR4-A treatment (8.8%, p = 0.01).

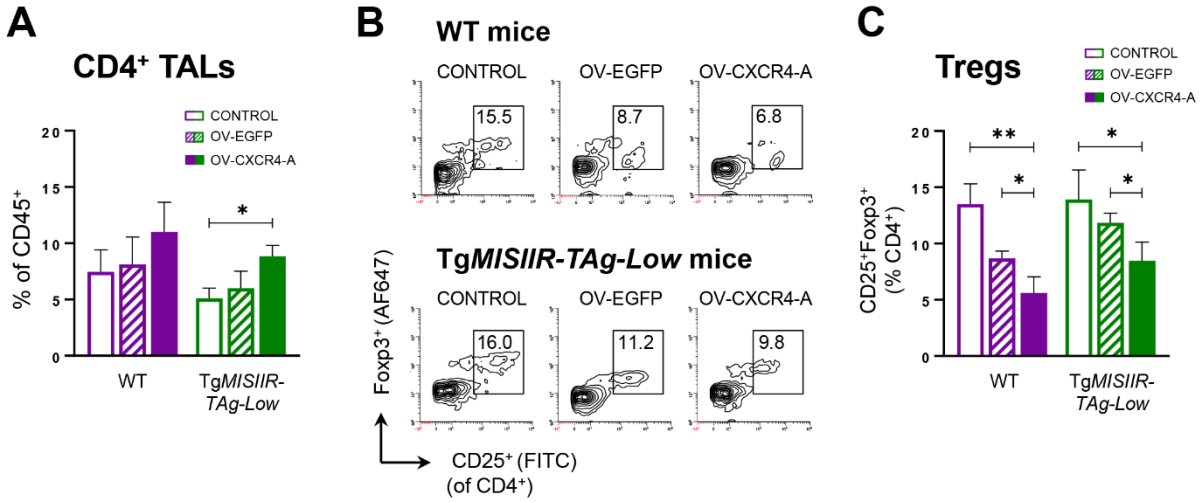

Figure 15. *The changes in the intraperitoneal accumulation of CD4$^+$ TALs after OV-treatment. (A) The percentages of CD4$^+$ TALs of total CD45$^+$ leukocytes in the peritoneal TME of untreated, OV-EGFP- and OV-CXCR4-A-treated mice presented as mean ± SD. *p < 0.05. (B) Flow cytometry plots demonstrating the accumulation of CD4$^+$CD25$^+$Foxp3$^+$ T lymphocytes in peritoneal TME of untreated, OV-EGFP-, OV-CXCR4-A-treated mice and (C) percentages of Tregs of CD4$^+$ TALs (n = 5). *p < 0.05, **p < 0.01.*

In the untreated tumor microenvironment, I have found approximately 15% of T regulatory (Treg) cells, CD4$^+$ T cells that express CD25 and Foxp3 antigens (Figure 15B and 15C). Treatment with OV-CXCR4-A, that inhibits the CXCL12/CXCR4 signaling pathway, reduced percentages of Tregs infiltrating the peritoneal tumor microenvironment compared to control

(from 13.5% to 5.6%, p = 0.004) and OV-EGFP-treated (from 8.7% to 5.6%, p = 0.03) tumors in WT mice. Similarly, Treg frequencies in the peritoneal tumor microenvironment of Tg*MISIIR-TAg-Low* mice decreased after OV-CXCR4-A treatment compared to untreated (from 13.9% to 8.5%, p = 0.03) and OV-EGFP-treated counterparts (from 11.8% to 8.5%, p = 0.04), though differences between respective treatment groups in WT and Tg*MISIIR-TAg-Low* mice did not reach significance (Figure 15C). Those results were consistent with the finding that CXCR4 antagonism selectively reduces intratumoral $CD4^+CD25^+$Foxp3 Tregs infiltration in ovarian cancer [99].

Figure 16 shows the intraperitoneal accumulation of $CD8^+$ TALs. After OV-CXCR4-A treatment in WT mice percentages of $CD8^+$ TALs were increased compared to their $CD4^+$ counterparts to 27.7% of $CD45^+$ leukocytes. They were also significantly elevated compared to untreated (8.4%) and OV-EGFP-treated (17%) tumors (Figure 16; p = 0.007 and p = 0.049, respectively). The percentages of $CD8^+$ TALs in the untreated Tg*MISIIR-TAg-Low* mice were lower (4.5%) than those in the WT mice (p = 0.03), but their numbers increased after OV-CXCR4-A treatment (16%) compared to untreated and OV-EGFP-treated (10%) tumors (Figure 16; p = 0.005 and p = 0.04, respectively).

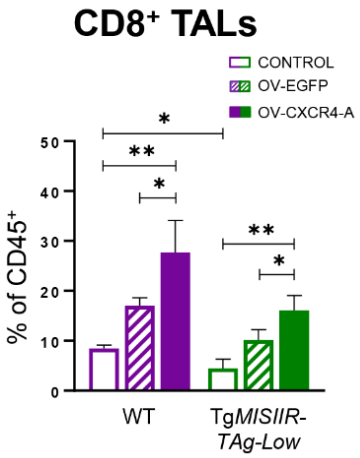

Figure 16. *Intraperitoneal accumulation of $CD8^+$ TALs. The differences in percentages of $CD8^+$ TALs between different groups of mice and treatments were analyzed and presented as mean ± SD. *p < 0.05, **p < 0.01.*

Because my data showed an increased accumulation of $CD8^+$ TALs, I have decided to check by flow cytometry how tumor microenvironment influences induction of antigen-specific $CD8^+$ T cell responses to both the vaccinia virus B8R protein and the SV40 TAg antigen. For staining I used B8R-K^b/TSYKFESV tetramer for vaccinia virus responses study and TAg-D^b/SAINNYAQKL ($TCR_{Tag\text{-}I}$) tetramer for SV40 TAg antigen-specific $CD8^+$ TALs. As shown in Figures 17A (*upper panel*) and 17B, no B8R-specific responses were detected in the untreated mice. In WT mice approximately 13% of $CD8^+$ TALs were vaccinia-specific after OV-EGFP treatment and this was further increased to 16% in OV-CXCR4-A-treated mice (Figures 17B; p = 0.02), probably due to reduction of immunosuppressive elements in the microenvironment

after the armed-virotherapy treatment [100]. Approximately 3% of $CD8^+$ TALs were SV40 TAg-specific in untreated tumor-bearing WT mice and their percentages increased to 5.3% after OV-EGFP treatment, though the differences were not significant. After OV-CXCR4-A treatment in WT mice we observed an increase to 8% of TAg-specific $CD8^+$ T cell responses compared to control and OV-EGFP-treated tumors (Figures 17A, *lower panel* and 17B, p = 0.007 and p = 0.03, respectively).

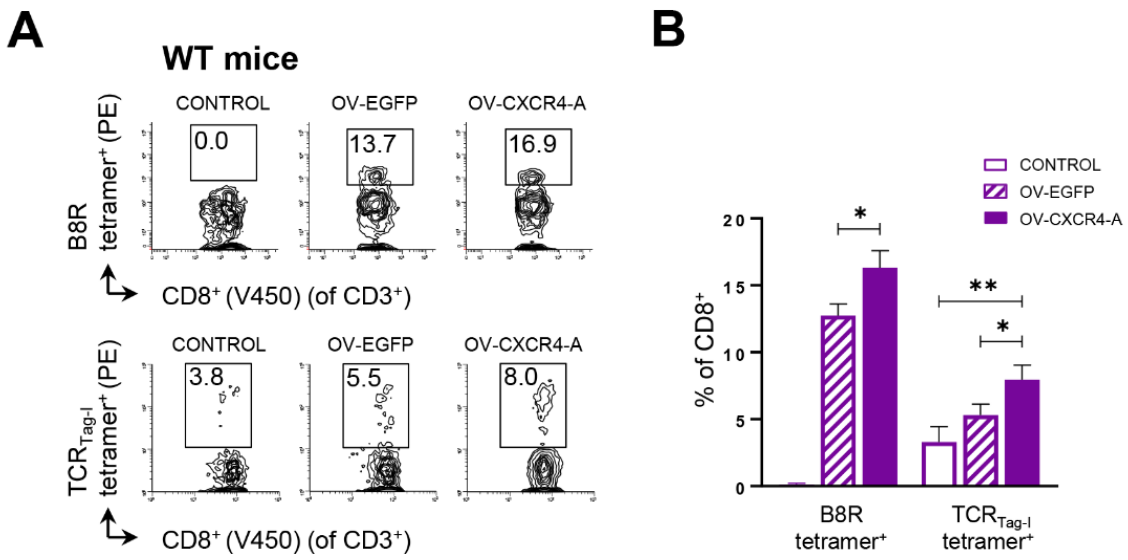

Figure 17. *Antigenic specificity of $CD8^+$ TALs in WT mice. (A) Representative flow cytometry plots demonstrating specific binding of B8R tetramer$^+$ and $TCR_{Tag\text{-}I}$ tetramer$^+$ to $CD8^+$ TALs (upper and lower panels, respectively) and (B) percentages of tetramer-positive $CD8^+$ TALs of total $CD45^+$ leukocytes in peritoneal TME of WT mice. *p < 0.05, **p < 0.01.*

The same analysis was performed for Tg*MISIIR-TAg-Low* mice. As shown in Figures 18A (*upper panel*) and 18B, B8R-specific responses generated by OV-EGFP or OV-CXCR4-A were over 2-fold lower compared to those detected in their WT counterparts and did not exceed 7% of $CD8^+$ TALs. OV-CXCR4-A treatment resulted in higher numbers of vaccinia specific $CD8^+$ TALs (6%) compared to those detected in OV-EGFP-treated tumors (3%, p = 0.02). $CD8^+$ $TCR_{Tag\text{-}I}{}^+$ TALs were not detected in the untreated or OV-EGFP-treated tumors of Tg*MISIIR-TAg-Low* mice, and the TAg-specific $CD8^+$ T cell responses reached 5% only in OV-CXCR4-A-treated mice (Figures 18A, *lower panel* and 18B).

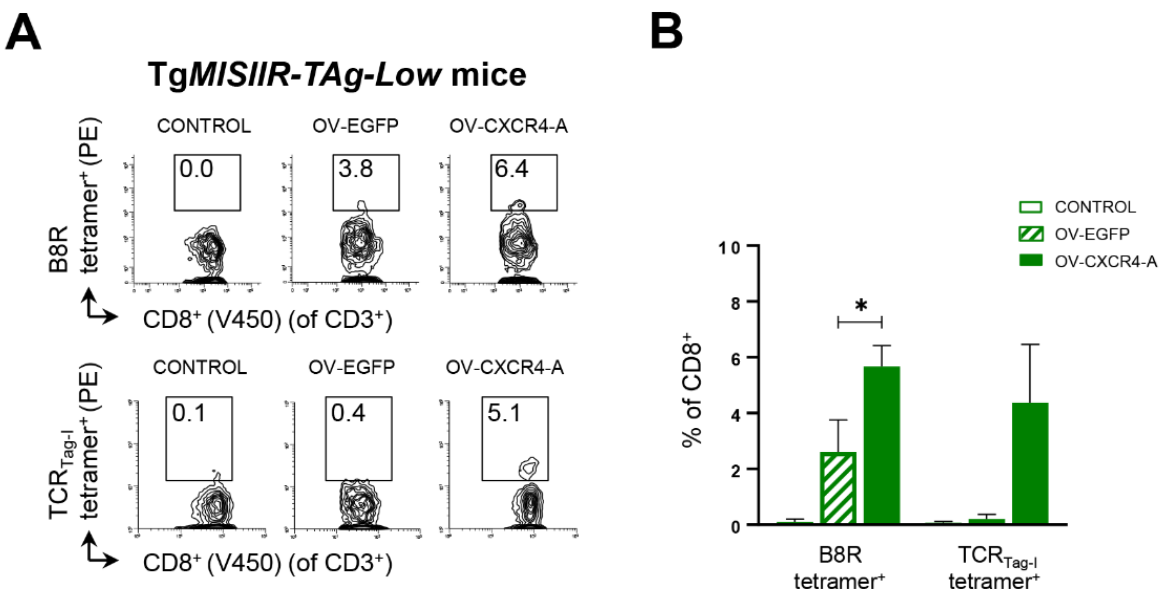

Figure 18. *Antigenic specificity of CD8⁺ TALs in TgMISIIR-TAg-Low mice. (A) Representative flow cytometry plots demonstrating specific binding of B8R tetramer⁺ and TCR_{Tag-I} tetramer⁺ to CD8⁺ TALs (upper and lower panels, respectively) and (B) percentages of tetramer-positive CD8⁺ TALs of total CD45⁺ leukocytes in peritoneal TME of TgMISIIR-TAg-Low mice (n = 3 - 5). *p < 0.05.*

Moreover, SV40 TAg antigen-specific tetramer biding was measured as median fluorescence intensity (MFI) and was 4-fold higher in WT mice than in Tg*MISIIR-TAg-Low* mice (Figure 17A and 18A *lower panels*; MFI = 93.3 ± 7.5 vs MFI = 22.3 ± 2.5, p = 0.001). This difference could be indicative of changes in activation status for tolerant self-reactive CD8⁺ T cells to ovalbumin (Ova) in iFABP-Ova mice producing Ova in the small intestine [101].

3.5 CD8⁺ T cells depletion nullifies the therapeutic effect of OV-CXCR4-A treatment

To investigate the role of CD4⁺ and CD8⁺ T responses in OV-CXCR4-A therapy effectiveness, I performed a depletion study. WT and transgenic mice were treated intraperitoneally with rat IgG2b anti-CD4 and anti-CD8 monoclonal antibodies before and after MOVCAR 5009 inoculation. Keyhole limpet hemocyanin is not expressed by mammals, which makes it an ideal isotype-matched control for rat IgG2b antibodies. Therefore, an equal dose of anti-KLH antibodies was used as an isotype control [102]. Ten days after tumor injection OV-EGFP or OV-CXCR4-A treatment was performed. Depletion efficiency was determined by flow cytometric analysis and revealed that administration of anti-CD4 and anti-CD8 antibodies depleted more than 92% of both CD4⁺ and CD8⁺ T cell subsets as demonstrated in Figure 19.

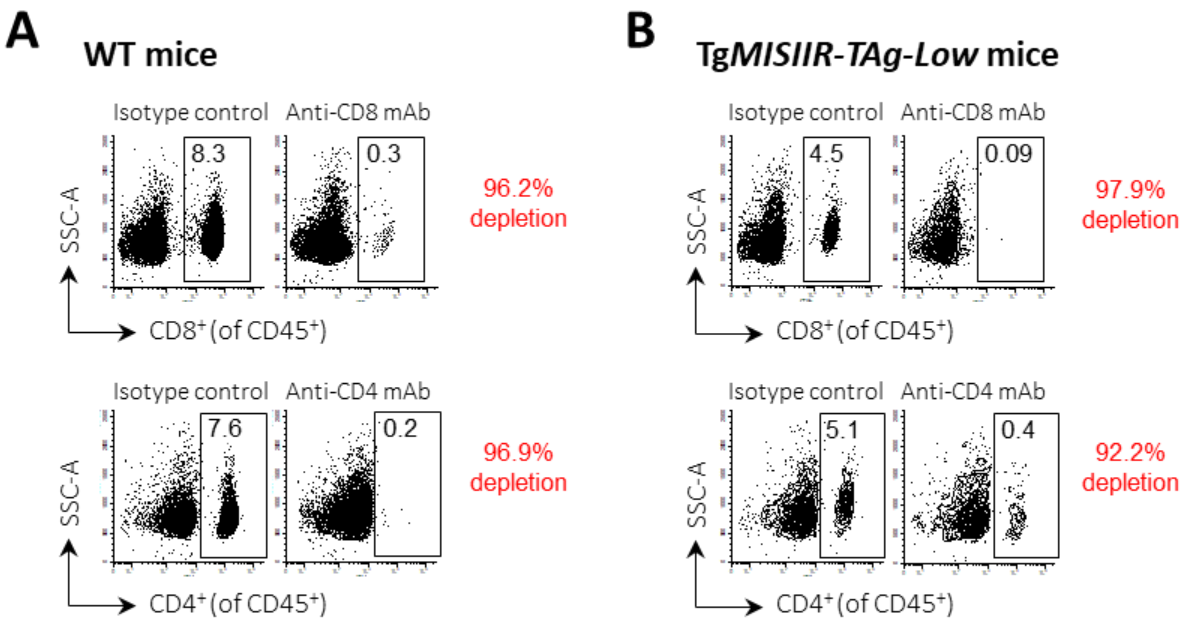

Figure 19. *Depletion study efficiency check by flow cytometry analysis. Peripheral blood was isolated and stained for CD4 and CD8 lymphocytes in control mice, one day after the last depleting antibody treatment. Representative flow cytometry plots for WT mice (A) and TgMISIIR-TAg-Low mice (B) after different antibody treatments are shown.*

Next, tumor growth after each treatment was measured in time and results are shown in Figure 20. CD8 depletion effect in MOVCAR 5009 tumor-bearing WT untreated or OV-EGFP-treated mice (Figure 20, *upper panel*) was modest and did not reach significant values compared to their respective isotype controls. Due to cytolytic effect of the virus, temporary inhibition of tumor growth was observed within the first ten days after OV-EGFP treatment. Interestingly, CD8 depletion in WT mice abrogated OV-CXCR4-A treatment effect compared to its isotype control ($p = 0.03$) and this reduction was more pronounced compared to $CD4^+$ T cells depletion. The same analysis was performed for transgenic mice. Consistent with the absence of TAg-specific $CD8^+$ TALs in peritoneal cavities in Tg*MISIIR-TAg-Low* mice (Figure 18B), depletion of either $CD4^+$ or $CD8^+$ T cells in control and OV-EGFP-treated tumors had minimal antitumor effect (Figure 20, *lower panel*). On the other hand, the depletion of $CD8^+$ T cells abrogated the OV-CXCR4 treatment effect on tumor growth compared to anti-KLH treated mice ($p = 0.007$). Similarly to WT mice, this effect was more pronounced compared to $CD4^+$ T cells depletion.

Presented data shows that OV-CXCR4-A therapy-induced $CD8^+$ T cell responses cause the reduced growth rate of MOVCAR 5009 tumors in mice. This treatment is associated with robust immune changes in tumor microenvironment and can induce TAg-specific $CD8^+$ TALs. Interestingly, OV-EGFP treatment induced only medium changes in tumor environment and was insufficient to break self-tolerance.

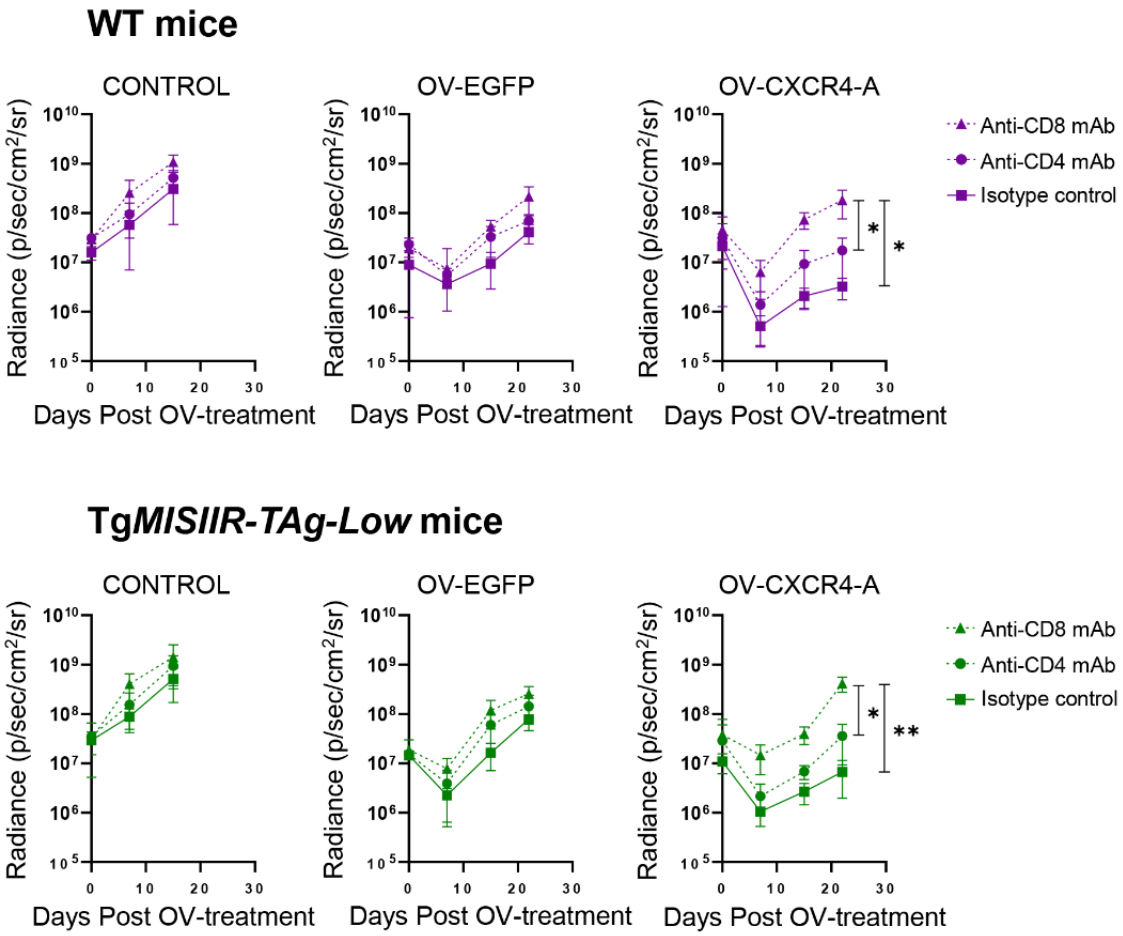

Figure 20. *Tumor growth curves in T cell depletion study. Tumor volume curves in WT (upper panel) and TgMISIIR-TAg-Low (lower panel) mice after different treatments are indicated. Individual data points represent mean ± SD. *p < 0.05.*

3.6 OV-CXCR4-A treatment overcomes the immunosuppressive landscape of TAMs in tumor-bearing Tg*MISIIR-TAg-Low* mice

Based on the observed differences in tumor microenvironment between WT and the transgenic mice and the impact of OV-CXCR4-A on a single cellular phenotype, to further define local changes I have reasoned that a global analysis of the cellular landscape of the tumor microenvironment would allow me to better assess key differences between the treatment groups. The scRNAseq profiling of the peritoneal TME in WT and Tg*MISIIR-TAg-Low* mice before and after OV-CXCR4-A treatment, confirmed the myeloid-driven phenotype of MOVCAR 5009 tumors in both groups of mice (Figures 21A-C). I have performed the clustering analysis shown in Figure 21A, followed by cell-type annotation (Figure 21B) and the fraction graph (Figure 21C). Cell types on UMAP plots in Figures 21B and 21D are highlighted by matching colors on the data panel in Figure 21C. Thirteen clusters were identified

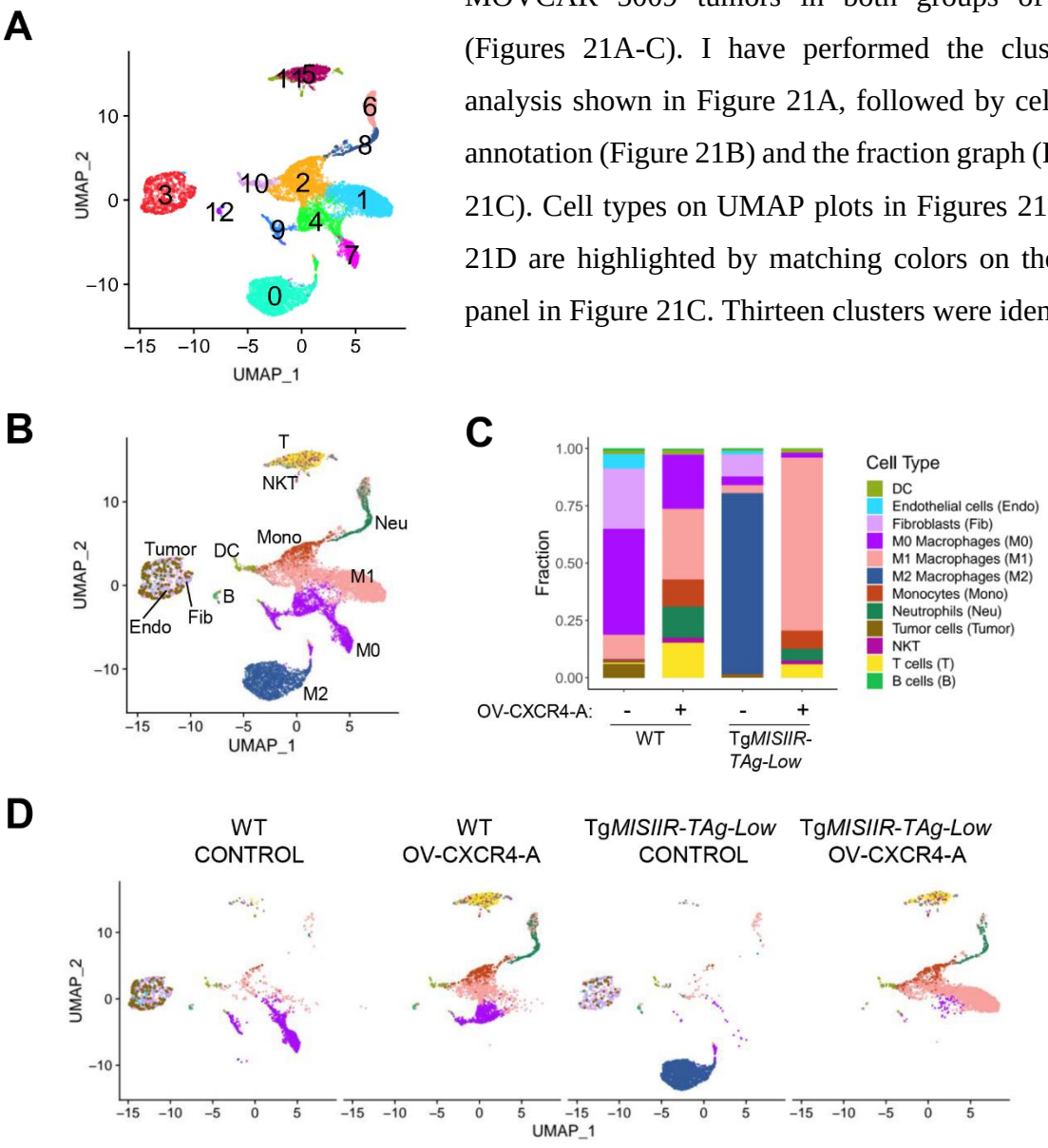

Figure 21. *OV-CXCR4-A-mediated changes in the immune profile of myeloid populations. (A) Clustering all single cells isolated from the peritoneal fluids of MOVCAR 5009 ovarian tumor-bearing untreated and OV-CXCR4-A-treated WT and TgMISIIR-TAg-Low mice. (B) UMAP plot of the peritoneal TME with cell-type annotation and (C) fraction graph. (D) Distribution of cell type populations in control and OV-CXCR4-A treated tumors in WT and TgMISIIR-TAg-Low mice.*

and the majority of macrophages or monocytes were organized in clusters: C0 (M2 TAMs), C1 and C6 (M1 TAMs), C2 (M1 TAMs and monocytes), C4, C7 and C9 (M0 TAMs). Other clusters contained neutrophils (C6, C8), DCs (C10), T cell/NKT cells (C5 and C11), B cells (C12), and $CD45^-$ fibroblasts, tumor and endothelial cells (C3). In Figure 21D we can observe differences in cluster distribution between cells isolated from the peritoneal TME of untreated and OV-CXCR4-A-treated mice based on the mouse background. Most prominent dissimilarity is presence of M2 macrophages cluster only in the untreated group of Tg*MISIIR-TAg-Low* mice. Additionally, cluster depicting tumor cells, fibroblasts and endothelial cells is notable in control tumor-bearing mice but not detected in the OV-CXCR4-A-treated tumors in mice of both genetic backgrounds. This is opposite to the lymphoid clusters (T cell/NKT cells) which are prominent in the OV-CXCR4-A-treated tumors of WT and Tg*MISIIR-TAg-Low* mice, but underrepresented in untreated tumor-bearing mice. These differences in cluster distribution between cells are consistent with the distinctly heterogeneous transcriptomic profile of individual clusters presented in Figure 22. Within the TAM subsets we could distinguish different transcriptomic profiles associated with anti-tumor activity M1-like macrophages and pro-tumorigenic M2-like phenotypes. Expression of M1 markers such as *H2-Aa, Irf8, Irf1, Stat1*, that are essential for type 1 response generation, was significantly lower in the tolerogenic TME of control tumors of Tg*MISIIR-TAg-Low* mice compared to their WT counterparts (Figure 23A). Concomitantly, expression of key M2 macrophages and MDSCs markers, such as *Arg1*, *Retnla*, *Chil3*, *Cd209a* and *Spp1*, was upregulated (Figure 23C). *Arg1*, *Retnla* and *Chil3* can mediate T cell suppression [103-105], *Cd209a* promotes $CD4^+Foxp3^+$ Treg cell expansion [106] and *Spp1* foster angiogenesis and modify tumor-associated inflammatory cell migration and function [107,108]. After OV-CXCR4-A treatment the transcriptomic M2 signature detected in the control tumors of Tg*MISIIR-TAg-Low* mice was no longer observed, and this resulted in similar M1-to-M2 scores in both groups of mice (Figures 23B and 23D).

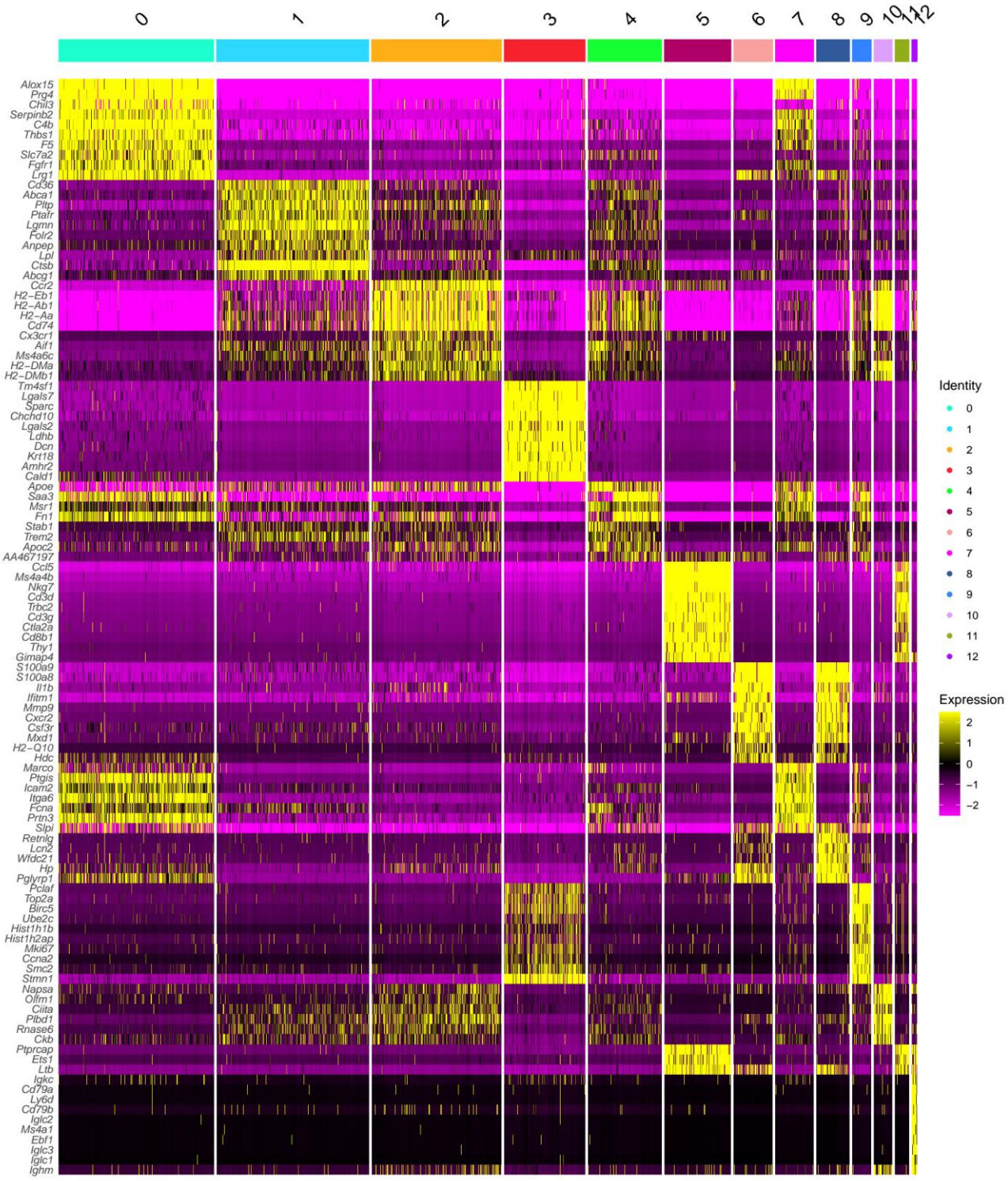

Figure 22. *Heatmap of genes of lymphoid and non-lymphoid TME cells. Thirteen clusters (0 to 12) were identified as: C0 - M2 TAMs; C1 - M1 TAMs; C2 - monocytes/M1 TAMs; C3 - tumor cells/endothelial cells/fibroblasts; C4 - M0 TAMs; C5 - T cells/NKT; C6 - M1 TAMs/neutrophils; C7 - M0 TAMs; C8 - neutrophils, C9 - M0 TAMs; C10 - DC; C11 - T cells; C12 - B cells.*

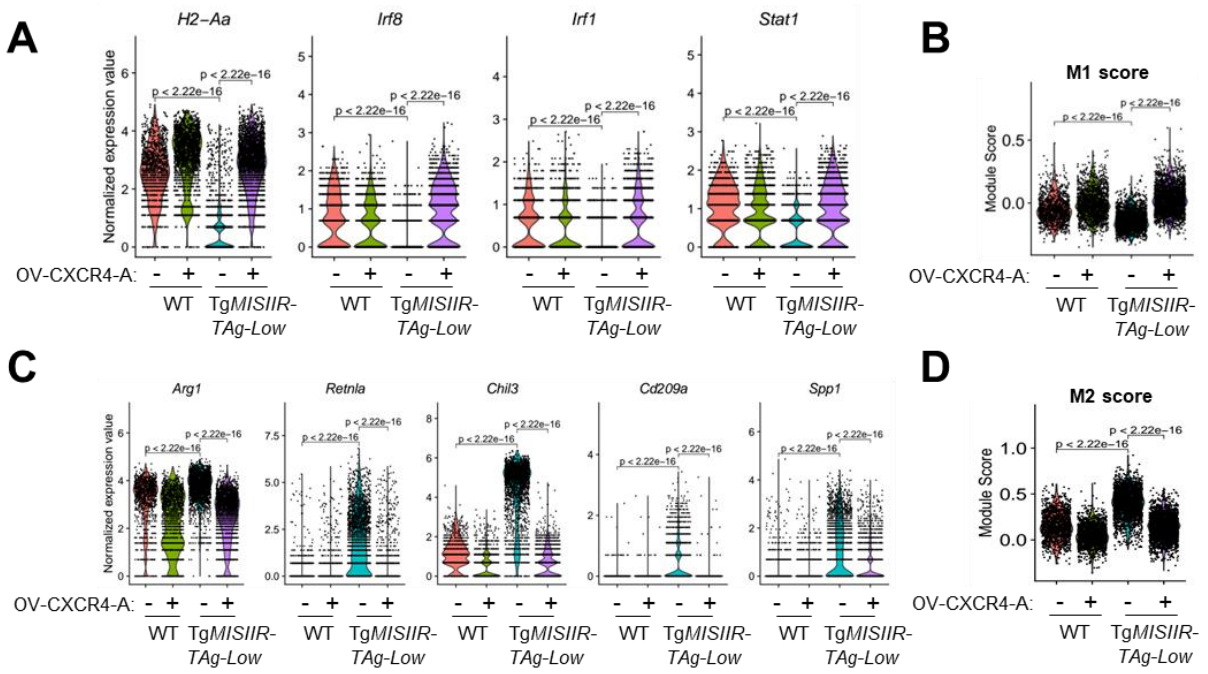

Figure 23. *M1 and M2 signature genes. (A) Violin plots showing expression of selected M1 genes (H2-Aa, Irf8, Irf1, and Stat1) in TAMs with significant changes in gene expression. (B) M1 score with significant changes in gene expression between indicated groups. (C) Violin plots showing expression of selected M2 genes (Arg1, Retnla, Chil3, Cd209a, and Spp1) in TAMs with significant changes in gene expression. (D) M2 scores with significant changes in gene expression between indicated groups.*

To further analyze and understand TAMs high heterogeneity I selected and re-clustered the macrophage populations. Nine separate clusters were identified (Figure 24A), where C4 was detected only in control tumor-bearing WT mice and C0 was unique for untreated tumors in transgenic mice (Figure 24B). Treatment with OV-CXCR4-A enriched TAM populations with cells assembled in cluster 5 for WT mice and cluster 1 for Tg*MISIIR-TAg-Low* mice. The transcriptomic differences between TAMs across the treatment conditions were analyzed by UMAP plots showing the expression of selected M1 (*H2-Aa, Irf8, Irf1, and Stat1*) and M2 (*Arg1, Spp1, Retnla, Chil3, and Cd209a*) genes (Figures 24C and 24D, respectively), and a normalized expression of selected genes in each myeloid cluster shown in Figure 24E. Macrophages from cluster 4, derived from untreated MOVCAR 5009-bearing WT mice, had elevated expression of M1 markers (*H2-Aa, Irf8, Irf1, Stat1, H2-DMb1*) and low levels of some M2 markers (such as *Spp1, Retnla, Cd209a*) except for *Arg1*, *Chil3*, and *Cd274*.

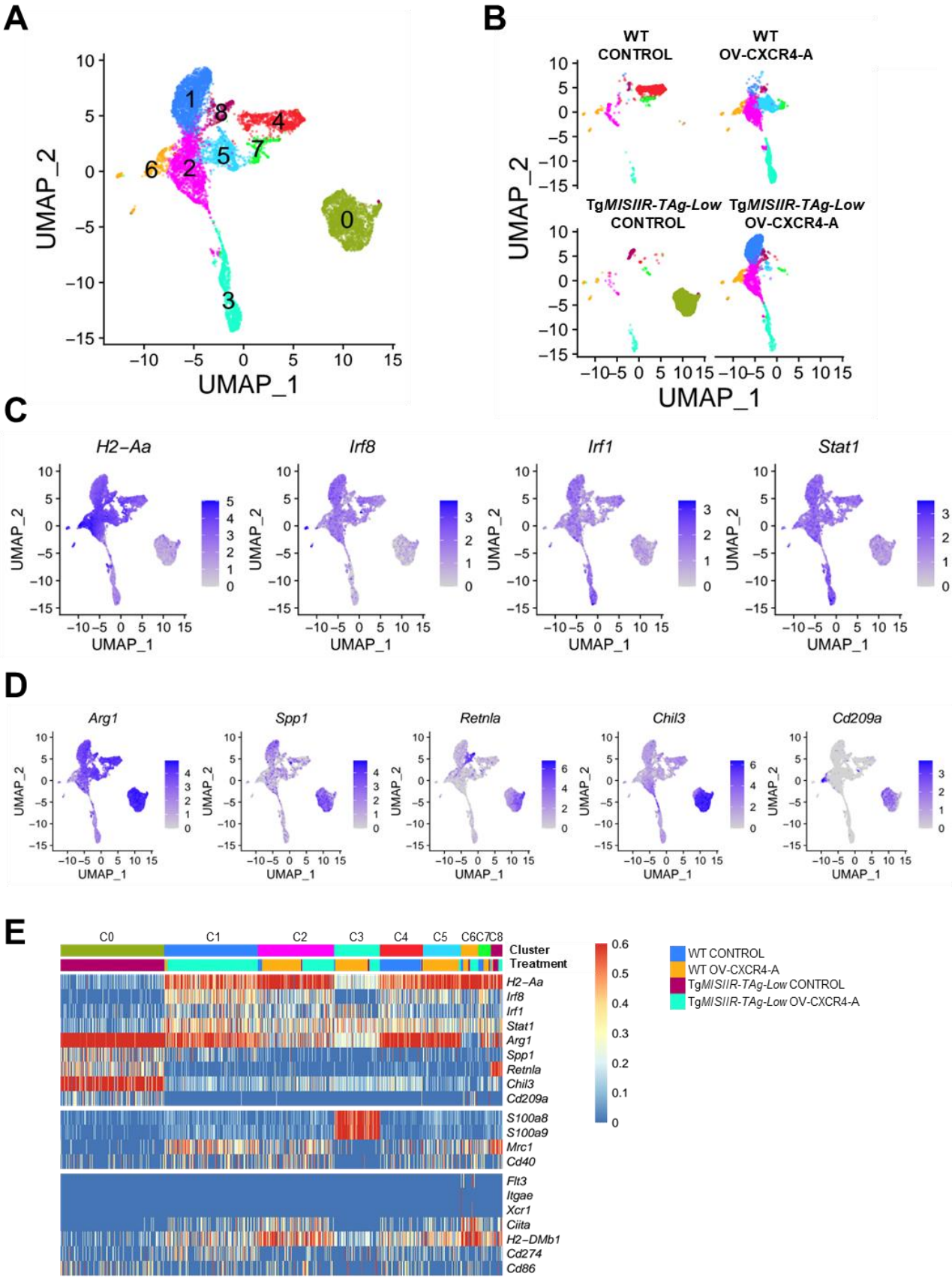
A
B
C
D
E
UMAP_1
UMAP_2
WT CONTROL
WT OV-CXCR4-A
TgMISIIR-TAg-Low CONTROL
TgMISIIR-TAg-Low OV-CXCR4-A
H2−Aa
Irf8
Irf1
Stat1
Arg1
Spp1
Retnla
Chil3
Cd209a
C0 C1 C2 C3 C4 C5 C6 C7 C8
Cluster
Treatment
S100a8
S100a9
Mrc1
Cd40
Flt3
Itgae
Xcr1
Ciita
H2−DMb1
Cd274
Cd86
WT CONTROL
WT OV-CXCR4-A
TgMISIIR-TAg-Low CONTROL
TgMISIIR-TAg-Low OV-CXCR4-A

Figure 24. *Transcriptional analyses of re-clustered TAMs. UMAP plots of re-clustered TAM subsets in the peritoneal TME of (A) all tumors and (B) individual control and treated MOVCAR 5009 tumors in WT and TgMISIIR-TAg-Low mice. TAM subsets were analyzed for expression of (C) H2-Aa, Irf8, Irf1, Stat1 and (D) Ag1, Spp1, Retnla, Chil3, and Cd209a. (E) Heatmap displaying a normalized expression of selected genes in each myeloid cluster in control and OV-CXCR4-A-treated tumors in syngeneic WT and TgMISIIR-TAg-Low mice.*

In contrast, TAMs in cluster 0 of control tumors in tolerogenic mice, exhibited a highly pro-tumorigenic immunosuppressive (M2-like) transcriptional profile with strongly elevated *Arg1* and *Chil3*, and other M2 markers such as *Spp1, Retnla,* and *Cd209a*. M1 markers (*H2-Aa, Irf8, Irf1, Stat1, and H2-DMb1*) had a uniformly low expression in this cluster. OV-CXCR4-A treatment in Tg*MISIIR-TAg-Low* mice sufficiently ablated this highly immunosuppressive cluster 0, and enriched TAMs with genes encoding M1 markers (*H2-Aa, Irf8, Irf1, Stat1, and H2-DMb1*), except of *Arg1* and *Mrc1*, in clusters 1 and 2. Armed virotherapy treatment enriched also population in cluster 3 with cells that highly express *S100A8/9* genes of low-molecular-weight intracellular calcium-binding proteins, which are the markers used to distinguish monocytic (M)-MDSCs from monocytes [109]. Cluster 5, uniquely presented in OV-CXCR4-A-treated WT mice, had a high expression of genes encoding M1 markers (*H2-Aa, Irf8, Irf1, Stat1, and H2-DMb1*), similarly to cluster 1, but also elevated levels of immunosuppressive *Arg1* and *Mrc1* genes (Figure 24E).

After transcriptional analysis, I wanted to determine if there are any functional changes in TAMs of untreated and OV-CXCR4-A-treated Tg*MISIIR-TAg-Low* mice. I performed a gene set enrichment analysis (GSEA) showing normalized enrichment score (NES) as shown in Figure 25. OV-CXCR4-A treatment in tolerogenic mice increased expression of genes that are involved with MHC class I and MHC class II antigen processing and presentation and co-stimulation of lymphoid cells compared to untreated tumors. Those processes were largely downregulated in the untreated tumors of Tg*MISIIR-TAg-Low* mice. These results suggest that OV-CXCR4-A treatment overcomes the immunosuppressive landscape of TAMs in tolerogenic tumors.

Although OV-CXCR4-A treatment increased DC numbers, they represented a minor portion of myeloid cells among the other subsets examined. DCs were mainly concentrated in the cluster 6 with unique expression of *Flt3, Itgae,* and *Xcr1*. The *Flt3* gene was mostly

expressed in OV-CXCR4-A-treated tumors, and *Itgae, Xcr1* were expressed predominantly in DCs from virus-treated WT mice (Figure 24E). Similar to TAMs, the DC population in the control tolerogenic tumors had reduced expression of *H2-Aa* (Figure 26), which was increased by OV-CXCR4-A treatment to levels comparable to those measured in the WT mice. In tumor-bearing Tg*MISIIR-TAg-Low* mice after the OV-CXCR4-A treatment I also observed a higher expression of the inhibitory leukocyte immunoglobulin-like receptor Lilrb4a [110] and Epstein-Barr virus-induced gene (*Ebi3*) involved in the regulation of Th17 and Treg cells [111] (Figure 26).

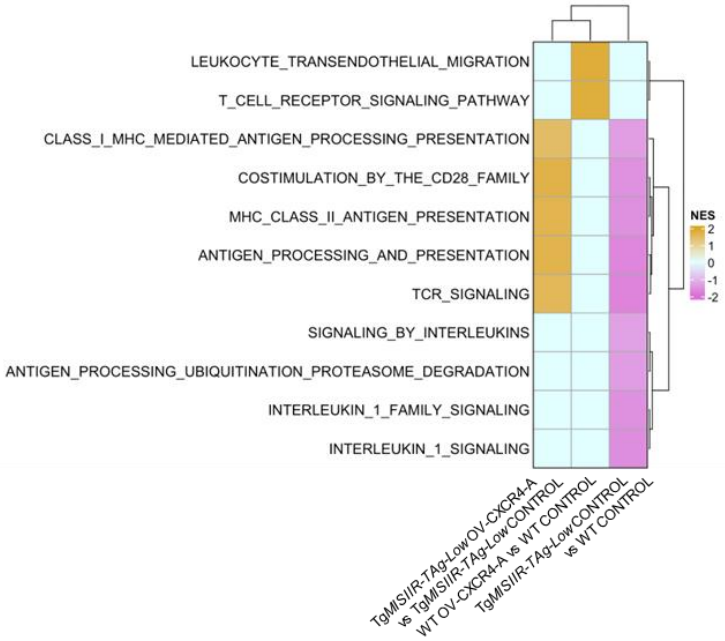

Figure 25. *Functional analysis of re-clustered TAMs. Heatmap of gene set enrichment analysis of TgMISIIR-TAg-Low OV-CXCR4-A vs TgMISIIR-TAg-Low CONTROL, WT OV-CXCR4-A vs WT CONTROL, and TgMISIIR-TAg-Low CONTROL vs WT CONTROL in TAMs showing normalized enrichment score (NES).*

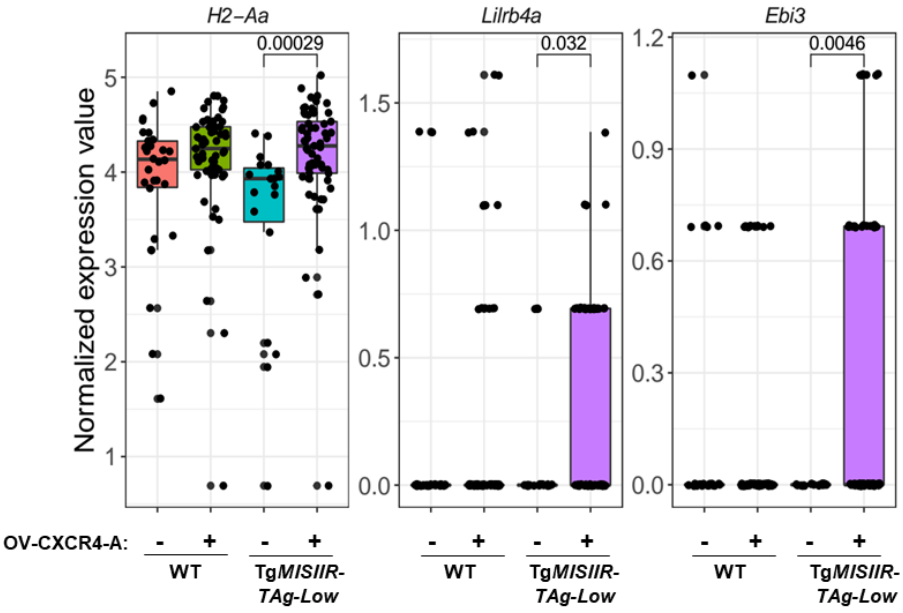

Figure 26. *Analysis of DCs in the peritoneal TME. Bar plots displaying a normalized expression of selected genes in tumor-infiltrating DCs in control and OV-CXCR4-A-treated WT and TgMISIIR-TAg-Low mice.*

scRNAseq data suggests that TAMs in control transgenic mice have an increased ability of immunosuppressive responses in comparison to the same cells in mice with WT background. To test how the differences in phenotypes and transcriptional signatures of TAMs relate to their functional activities, I performed adoptive cell transfer experiment to tumor-bearing WT mice. As shown in Figure 27A, $CD45^+CD11b^+F4/80^+$ TAMs were isolated from single-cell suspensions of peritoneal fluids of tumor-bearing WT or Tg*MISIIR-TAg-Low* mice by cell sorting. Isolated cells were injected intraperitoneally ($1x10^6$ cells/mouse) into tumor-challenged control and OV-CXCR4-A-treated WT mice 12 hours before the OV-CXCR4-A treatment. Tumor-bearing mice treated with PBS served as controls.

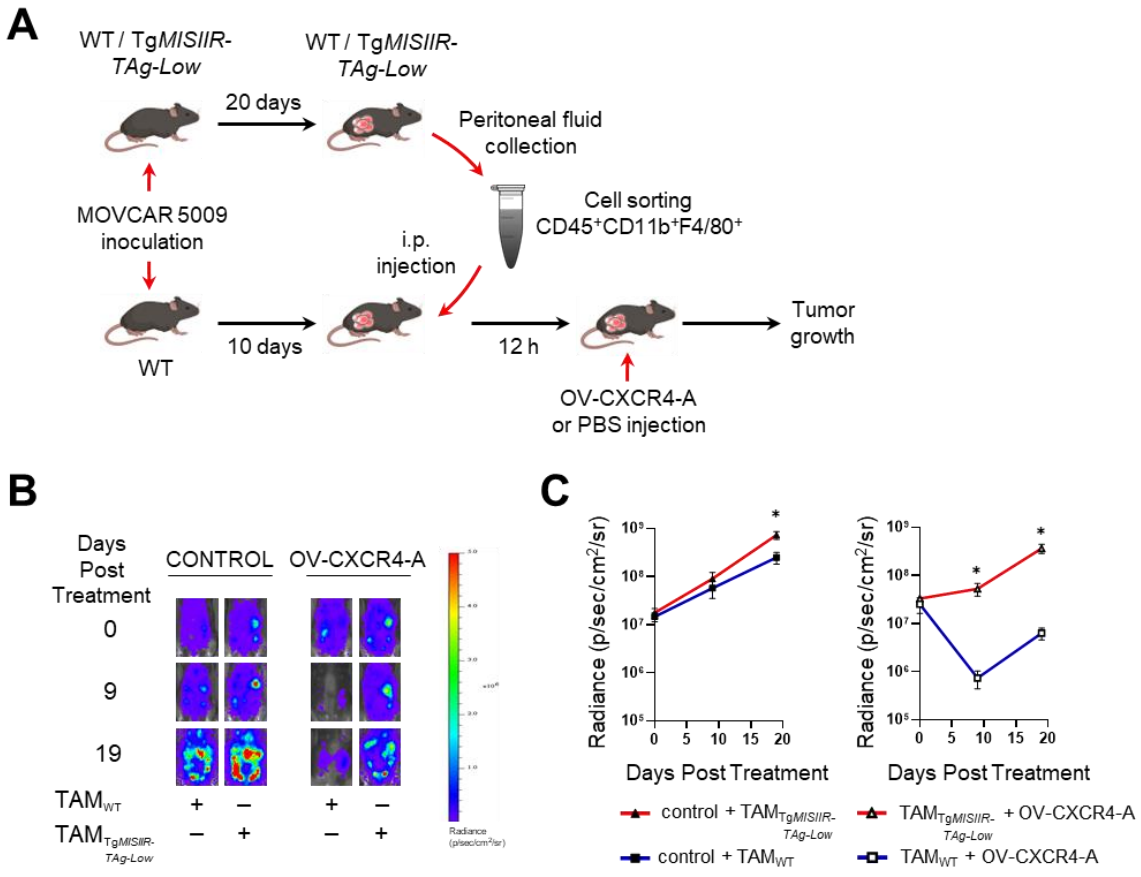

Figure 27. *TAMs adoptive cell transfer. (A) Graphical summary of immunosuppressive activity assay of TAMs ($CD45^+CD11b^+F4/80^+$) isolated from peritoneal fluids of MOVCAR 5009 tumors in control WT and TgMISIIR-TAg-Low mice (n = 10). (B) Representative bioluminescence images of mice from different treatment groups. Presented signals were measured on day 0, 9 and 19. (C) Tumor progression was monitored by bioluminescence and presented as the mean ± SEM. *p < 0.05*

Progression of tumor growth was quantified by bioluminescence imaging and representative results are presented in Figure 27B. Data showed that adoptively-transferred TAMs derived from Tg*MISIIR-TAg-Low* mice have stronger pro-tumorigenic properties than their WT counterparts, resulting in a little elevated signal 19 days after the adoptive cell transfer in untreated mice. TAMs isolated from Tg*MISIIR-TAg-Low* mice significantly augmented tumor growth in the untreated group of mice (Figure 27C, *left panel*, day 19: $p = 0.03$), and the effect was even stronger in OV-CXCR4-A-treated mice (Figure 27C, *right panel*; days 9 and 19: $p = 0.03$ and $p = 0.01$, respectively).

3.7 Expression profiling of heterogeneous and functionally divergent CAFs in MOVCAR 5009-challenged WT and Tg*MISIIR-TAg-Low* mice

As shown previously, delivery of OV-CXCR4-A led to depletion of CAF populations (Figure 14C). This prompted me to investigate their heterogeneity in the composition and function in MOVCAR 5009-challenged WT and Tg*MISIIR-TAg-Low* mice. Using CAFs isolated from tumor-bearing untreated or OV-CXCR4-A-treated WT and transgenic mice, I have performed differential gene expression and GSEA analyses. In Figure 28A and 28B we can see some differences in the transcriptional profiles of genes involved in immune responses and cell cycle pathways. Differential gene expression study underlined an enrichment in WT mice for expression of genes characteristic for transcriptionally unique population of ilCAFs (interferon-licensed CAFs) that are interferon (IFN)-responsive, including members of the guanylate-binding protein (Gbp) family, genes encoding for MHC proteins and MHC-related molecules (*i.a. H2-K1*, *H2-D1*, *B2m*, *Tap1*) and chemoattractants for antigen-experienced T cells, indicating that ilCAFs may have essential roles in directing T cell trafficking within tumors [112] (Figure 28A). This data also pointed to the upregulation of IFN signaling responses, including antigen processing and presentation (Figure 28B). On the contrary, CAFs in Tg*MISIIR-TAg-Low* mice had upregulated gene expression of *S100a6* and its target, Anx2 that are positively correlated with the progress of ovarian cancer by regulating the dynamics of cytoskeletal constituents and other membrane-associated cellular processes [113-115]. Also, Wnt signaling pathway, known to regulate stemness in a broad spectrum of stem cell niches including the ovary, was activated (upregulation of *Wnt4* expression). It is worth mentioning that Wnt activity was previously shown to correlate with grade, epithelial to mesenchymal

transition, chemotherapy resistance, and poor prognosis in ovarian cancer [116]. Lastly, observed high expression of an early growth response protein 1 (*Egr1*) correlates with an increase in proliferation of specific types of tumor cells by affecting the cell cycle, tumor invasion and metastasis [117,118]. Gene set enrichment analysis, presented in Figure 28B, correlates with differential gene analysis in CAFs isolated from untreated transgenic mice showing upregulated signaling pathways related to cell cycle, transcriptional regulation by *TP53*, pyrimidine metabolism, and tricarboxylic acid (TCA).

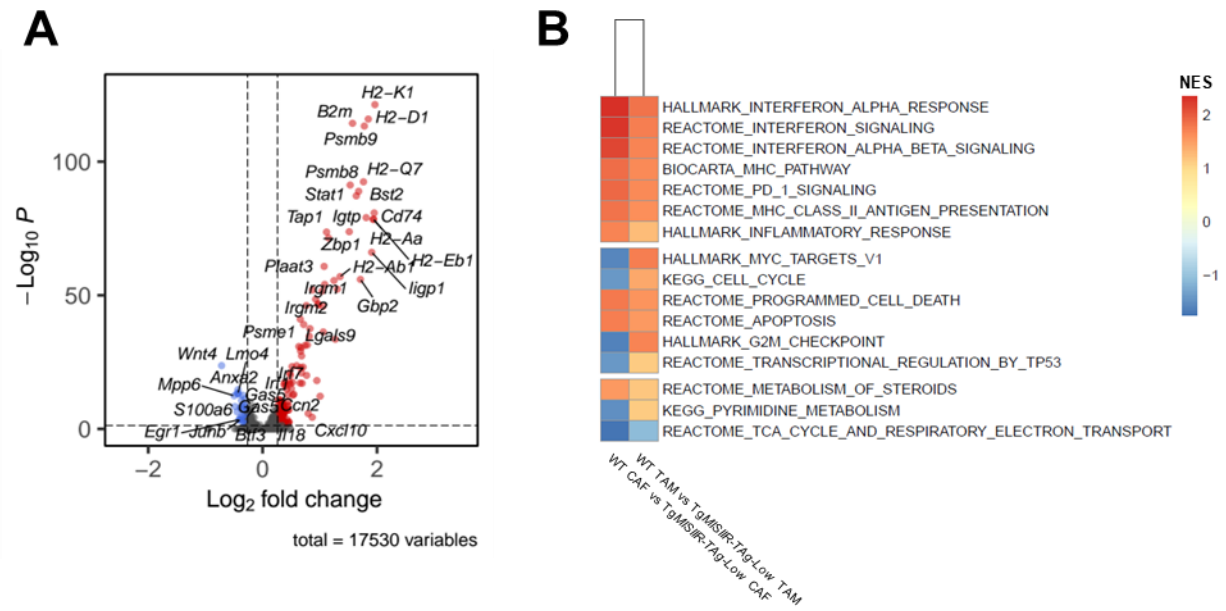

Figure 28. *Transcriptional and functional differences of CAFs. (A) Volcano plot showing enrichment of differentially expressed genes in CAF clusters between control tumors of WT and TgMISIIR-TAg-Low mice. Each red and blue dot denotes an individual gene with a Benjamini-Hochberg-adjusted p-value < 0.05 and fold change > 1.2. (B) Heatmap of gene set enrichment analysis of WT CAF vs TgMISIIR-TAg-Low CAF and WT TAM vs TgMISIIR-TAg-Low TAM showing NES.*

Next, I have examined if the differences in CAF transcriptomes may translate also to their function. To measure their immunosuppressive activity I have performed the adoptive cell transfer experiment to MOVCAR 5009-challenged WT mice. CAFs were isolated by negative selection from single-cell suspensions obtained from peritoneal fluids of WT or Tg*MISIIR-TAg-Low* tumor-bearing mice using the $CD45^+$ column. Over 88% $CD49e^+$ FAP^+ enriched CAF populations, as shown in Figure 29A, were injected intraperitoneally to MOVCAR 5009-bearing WT mice one day after tumor inoculation. Progression of tumor growth, measured by

bioluminescence activity (Figure 29B), revealed that CAFs derived from the tumor-challenged transgenic mice generated a significant increase in tumor load on days 9 and 10 in control (Figure 29C, *left panel*, p = 0.02 and p = 0.03, respectively) as well as OV-CXCR4-A-treated mice (p = 0.007 and p = 0.02, respectively). This data confirmed that Tg*MISIIR-TAg-Low*-derived CAFs exhibited higher pro-tumorigenic activities compared to their WT counterparts.

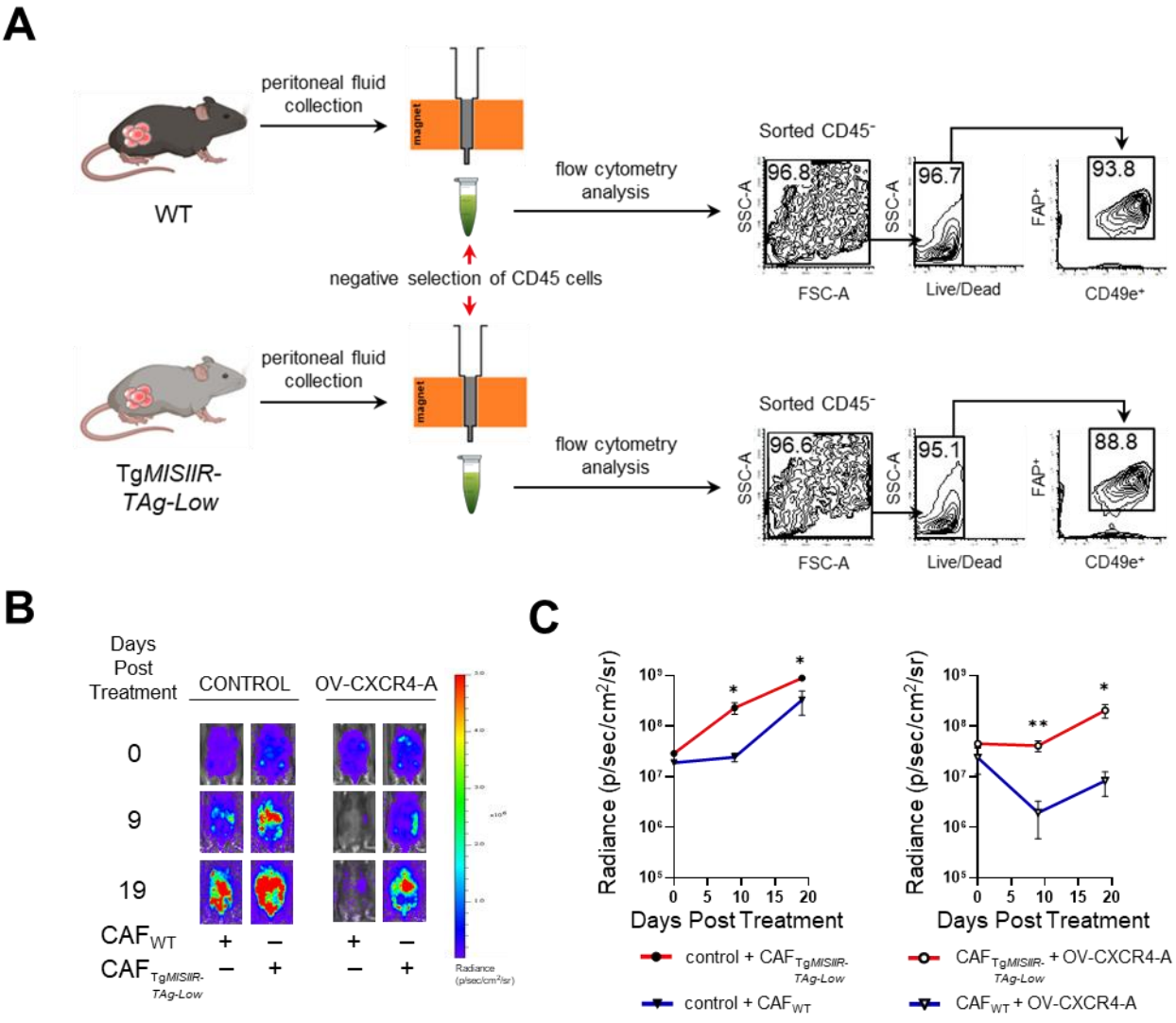

Figure 29. *CAFs adoptive cell transfer. (A) Graphical summary of CAFs isolation. CD45-negative cells were isolated from peritoneal fluids of MOVCAR 5009 tumor-bearing control WT and TgMISIIR-TAg-Low mice 20 days after tumor challenge by negative selection using CD45 MicroBeads. The expression of FAP and CD49e antigens on the isolated cells was analyzed by flow cytometry. (B) Representative bioluminescence images of mice from different treatment groups. Presented signals were measured on day 0, 9 and 19. (C) Tumor volume curves were generated with data points representing mean ± SEM of five mice per group (right panel). *p < 0.05, **p < 0.01.*

3.8 Expression profiling and cytotoxic activities of CD8$^+$ TALs in TME.

Prompted by the flow cytometry findings demonstrating that OV-CXCR4-A treatment induces rapid accumulation of cytotoxic CD4$^+$ and CD8$^+$ TALs, I have performed scRNAseq profiling analysis on these cell populations. Results shown in Figure 30A-D confirmed the low numbers of infiltrating both CD4$^+$ and CD8$^+$ TALs in the control tumors, and their increase after the OV-CXCR4-A treatment. CD8$^+$ TALs were organized in four main clusters 0, 1, 2, and 5, CD4$^+$ TALs were concentrated in cluster 3, whereas the cluster 4 consisted of NK/innate lymphoid cells (ILC) cells. In OV-CXCR4-A-treated tumors CD8$^+$ TALs exhibited upregulated expression of *Zap70* (Figure 30E) and *Lck* (Figure 30F) genes, indicating that they have been in contact with antigens, as T cell antigen receptor (TCR) signaling requires the sequential activities of the Lck and Zap70 kinases. Upon TCR stimulation, Lck phosphorylates the TCR, leading to the recruitment, phosphorylation, and activation of Zap70. The consequences of these early signaling events lead to T-cell activation, proliferation, and differentiation [119,120].

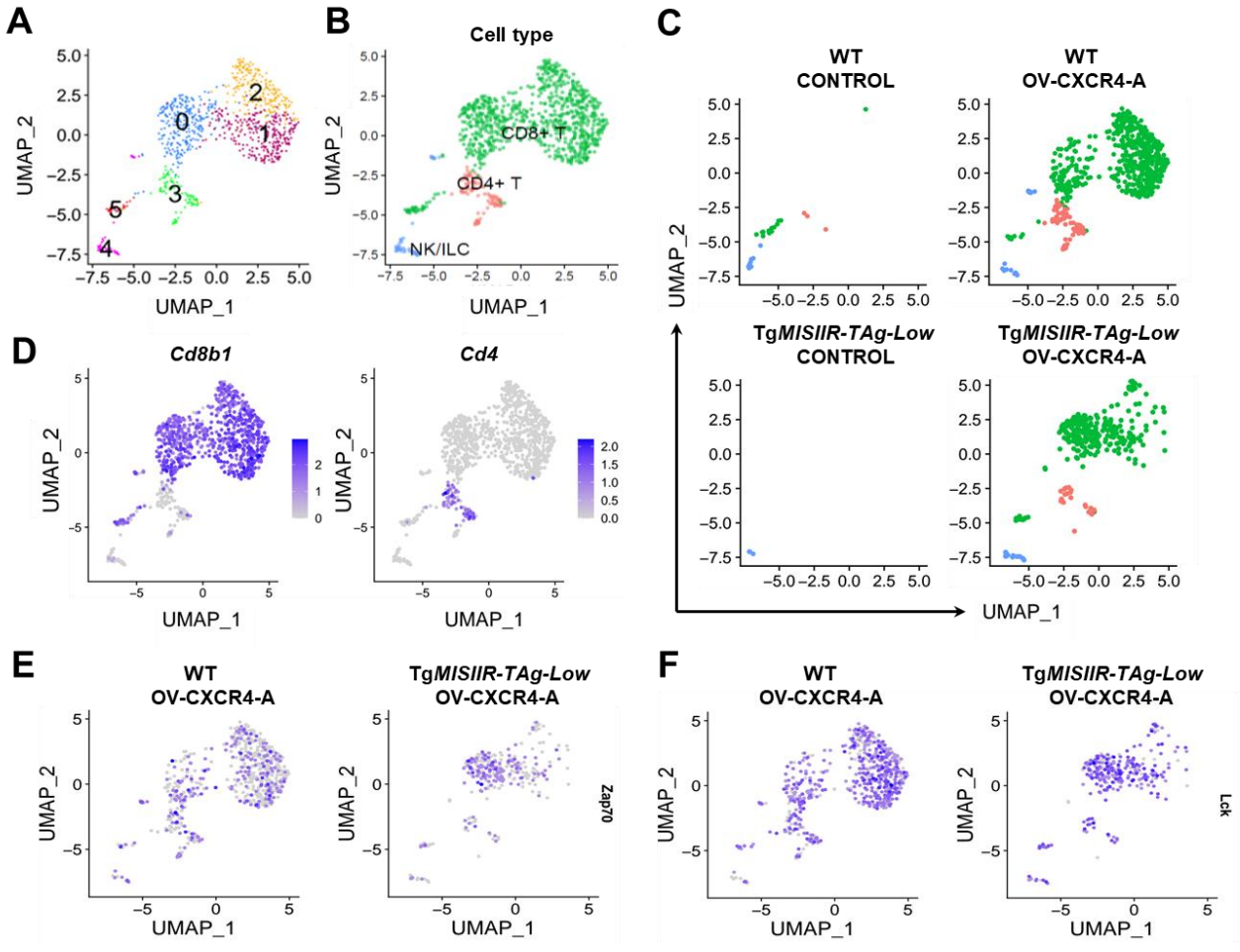

Figure 30. *Analyses of re-clustered TALs in the peritoneal TME. UMAP plots of TAL clusters with cell-type annotation in all (A-B) and untreated or OV-CXCR4-A-treated tumors in WT and TgMISIIR-TAg-Low mice (C). (D) UMAP plots of re-clustered CD8$^+$ T cells (left panel) and CD4$^+$ T cells (right panel). UMAP plots denote the expression of Zap70 (E) and Lck (F) genes in tumor-infiltrating CD8$^+$ T cell clusters in WT and transgenic OVCXCR4-A-treated mice.*

Expression profiling was performed only on CD8$^+$ T cells in OV-CXCR4-treated tumors, because of very low numbers of CD4$^+$ TALs and NK/ILC cells. Results are depicted as individual clusters of the heatmap in Figure 31A. In tumor microenvironment of OV-CXCR4-A-treated WT mice CD8$^+$ T cells were mostly concentrated in cluster 1 and 2 (Figure 30C) with elevated expression of genes important in regulating T cell development, differentiation, or survival (*Tcf7*) [121], genes involved in the regulation of T cell homeostasis (*Klf2, Il7r* and *Itgb1*) [122,123], activation and maintenance of effector cells (*Ifitm1*) [124], and effector function of cytotoxic T lymphocytes (*Gzma*) [125]. Expression of these genes was relatively lower in CD8$^+$ T cells of OV-CXCR4-A-treated transgenic mice, concentrated mostly in cluster 0. However, higher co-expression of *Gzmb, Eomes* and PD-1 protein encoded by the *Pdcd1* gene could indicate their exhaustion status [126]. This hypothesis seems to be confirmed by higher expression of genes associated with tumor-induced exhaustion (*Eomes*, *Gzmk, Pdcd1, Tox, and Lag3*) in cluster 0 [127-130] as well as upregulation of *Klre1* – a lectin-like receptor gene, that by cross-linking forms functional noncovalent heterodimers with killer-cell lectin-like receptor (KLRI1) and inhibits natural killer (NK) cell cytotoxicity [131,132]. Differential gene expression (DGE) analysis, demonstrated in Figure 31B, in line with previous results showed increases in *Gzmk, Gzmb, Pdcd1, Tox,* and *Klre1* gene expression aligned with downregulation of *Tcf7*, *Klf2*, *Il7r*, *Itgb1*, *Ifitm1* and *Gzma* in CD8$^+$ T cells of the OV-CXCR4-A-treated transgenic mice. In parallel, I performed gene set enrichment analysis to compare different conditions such as OV-CXCR4-A treatment vs untreated transgenic or WT mice, and the same treatment in WT mice vs their transgenic counterparts (Figure 31C). The analysis revealed that OV-CXCR4-A treatment activated CD8/TCR signaling pathways, interleukin-1 and mTOR signaling in CD8$^+$ T cells derived from the Tg*MISIIR-TAg-Low* mice. In mice with WT background, armed virotherapy increased the expression of genes that are known to be involved in cell migration pathways, such as *Runx3* [133].

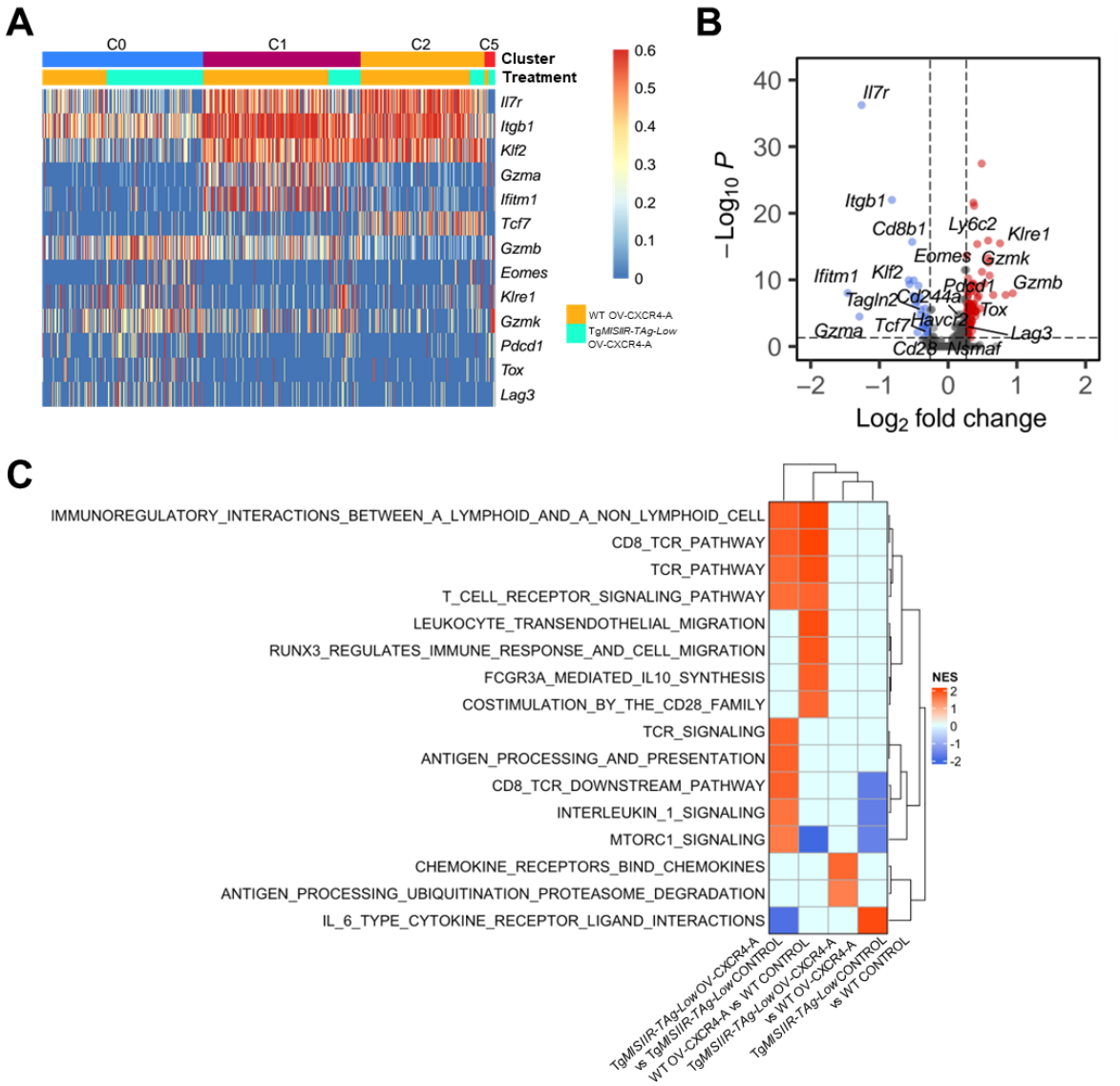

Figure 31. *Transcriptional analyses of CD8$^+$ TALs. (A) Heatmap displays a normalized expression of selected genes in each CD8$^+$ T cell cluster in OV-CXCR4-A-treated tumors in WT and TgMISIIR-TAg-Low mice. (B) Volcano plot showing enrichment of differentially expressed genes in CD8$^+$ T cell clusters between OV-CXCR4-A-treated tumors in TgMISIIR-TAg-Low and WT mice. Each red and blue dot denotes an individual gene with a Benjamini-Hochberg-adjusted p-value < 0.05 and fold change > 1.2. (C) Heatmap of gene set enrichment analysis in CD8$^+$ TALs of TgMISIIR-TAg-Low OV-CXCR4-A vs TgMISIIR-TAg-Low CONTROL, WT OV-CXCR4-A vs WT CONTROL, TgMISIIR-TAg-Low OV-CXCR4-A vs WT OV-CXCR4-A, and TgMISIIR-TAg-Low CONTROL vs WT CONTROL showing NES.*

Lastly, I performed cytotoxic assay to investigate whether transcriptomic differences of CD8$^+$ TALs correlate with their functional activities. Effector cells were isolated from single-cell suspensions of peritoneal fluids of control and OV-CXCR4-A-treated WT or Tg*MISIIR-*

TAg-Low mice and target MOVCAR 5009 tumor cells were stained with fluorescent dye to determine a number of live cells by flow cytometry after 17 hours of incubation. In Figure 32A we can see reduced lysis of tumor cells by $CD8^+$ TALs isolated from OV-CXCR4-A-treated transgenic mice, which confirms lower cytotoxic activity of those cells compared to their WT counterparts ($p = 0.03$). This data is consistent with previous results showing that those cells have an increased expression of genes associated with tumor-induced exhaustion and a reduced level of the $TCR_{Tag\text{-}I}$ tetramer binding compared to TALs from WT mice. Additionally, about 4% of OV-CXCR4-A-treated transgenic mice-derived $CD8^+$ T cells are positive for CD101 and CD38 markers (Figure 32B,C). Elevated expression of aforementioned proteins is correlated with a fixed dysfunctional state, described as terminal exhaustion, in which the cells are resistant to reprogramming [134,135] indicating that immune responses to the viral treatment in tolerogenic mice were less sustainable compared to those in WT mice.

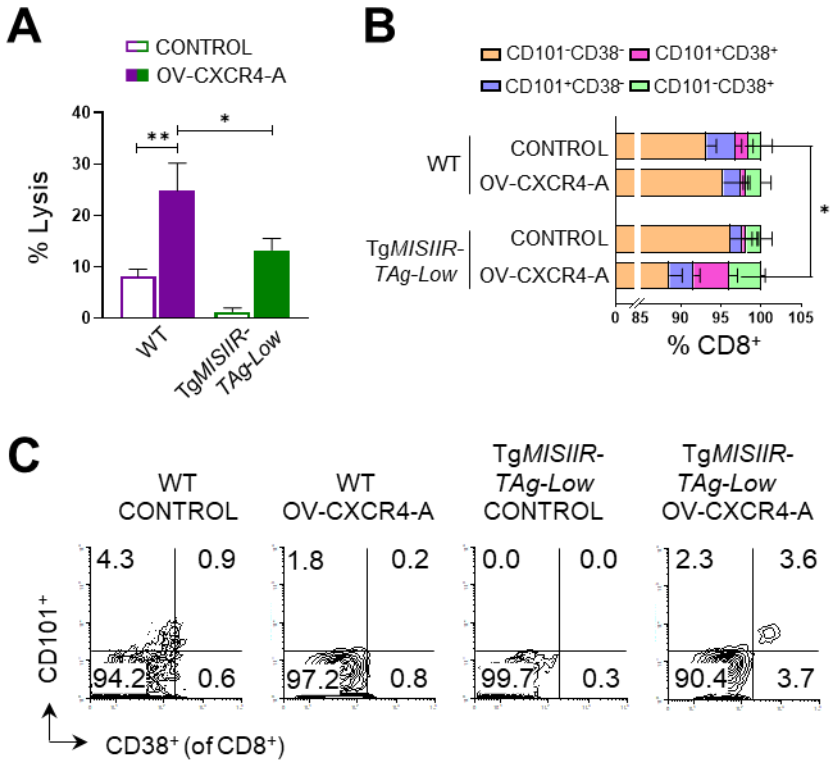

Figure 32. *$CD8^+$ TALs functional activity. (A) Cytotoxic activity presented as the percent of lysis of target MOVCAR 5009 cells in control and OV-CXCR4-A-treated WT and TgMISIIR-TAg-Low mice. Results are presented as mean ± SD of five mice per group. *p < 0.05, **p < 0.01. (B) Graphical depiction of CD101 and CD38 expression by CD8+ TALs in peritoneal cavities of tumor-bearing mice. Data presented as mean ± SD. *p < 0.05. (C) Representative flow cytometric plot of CD101 and CD38 expression on $CD8^+$ TALs in control and OV-CXCR4-A-treated tumors of WT and transgenic mice.*

4. DISCUSSION

In this study, I demonstrated that induction of tumor/self-specific $CD8^+$ T cell responses involved in tumor control was possible by targeting the interaction between immunosuppressive TAMs and CAFs in the tolerogenic tumor microenvironment using armed oncolytic virotherapy. The results of transcriptomic studies showed that $CD8^+$ TALs in Tg*MISIIR-TAg-Low* mice expressed genes characteristic of dysfunctional tumor-specific T cells despite maintaining some of the effector cell gene expression patterns. Moreover, functional assays showed that they were less effective in managing tumor growth compared to $CD8^+$ T cell in non-tolerogenic WT mice. The study also revealed distinctions in the tumorigenicity of TAg-expressing MOVCAR 5009 ovarian tumor and the effectiveness of antitumor $CD8^+$ T cell responses induced by OV-CXCR4-A in presenting TAg either as a neoantigen in syngeneic WT mice or as a tumor/self-antigen in Tg*MISIIR-TAg-Low* transgenic mice. The obtained data demonstrates that OV-CXCR4-A-induced epitope spreading, and TAg-specific antigen activation can reprogram unresponsive tumor-specific $CD8^+$ TALs in MOVCAR 5009-challenged transgenic mice. However, transcriptomic analysis of reprogrammed cells showed upregulation of *Tox* (thymocyte selection-associated HMG BOX) gene and inhibitory receptors genes, such as *Lag3* and *Pdcd1*, which indicates exhaustion state of those T cells. It is known that the immune co-inhibitory receptors: lymphocyte activation gene-3 (LAG3) and programmed cell death 1 (PD1) collaborate and interact to regulate T cell function and synergistically contribute to autoimmunity and tumor evasion [128,136]. These findings are consistent with the literature demonstrating that robust and systemic stimulation with self-antigens overcomes $CD8^+$ T cell tolerance to self- and tumor antigens, by altering previously fixed transcriptional signature. Targeted expansion of both self- and tumor neoantigen-specific T cells acts synergistically to boost anti-tumor immunity and elicits protection against tumor [101,137-139]. My study highlights the role of TAM-CAF crosstalk in tumor growth regulation and efficient induction of antitumor immunity in the context of immune tolerance to tumor/self-antigens. My results showed that the TME in transgenic mice is not only influenced by M2 TAMs, though, this data is consistent with the meta-analysis study performed on OC patients indicating that M2 macrophage infiltration in tumors was associated with poor prognosis and low overall survival [140]. However, TME is also largely influenced by CAFs. Adoptive cell transfer to MOVCAR 5009-challeneged WT mice of immunosuppressive CAFs accelerated tumor growth and

targeting CAFs by OV-CXCR4-A was essential in reversing their immunosuppressive properties. These findings emphasize the pivotal role of M2 TAMs and CAFs in maintaining a pro-tumoral niche and regulating tumor-stroma interactions [141]. It seems that the transcriptional and functional dichotomies of CAFs in MOVCAR 5009-bearingWT and Tg*MISIIR-TAg-Low* mice were less dependent on FAP and PDPN antigen expression because both markers were detected on pro-inflammatory and protumorigenic CAFs.

M2 macrophages undoubtedly dominated the landscape of peritoneal MOVCAR 5009 tumor microenvironment in Tg*MISIIR-TAg-Low* mice. I reason that highly immunosuppressive CAFs influenced the generation and maintenance of those M2 TAMs, which, in turn, suppressed the recruitment of $CD8^+$ T cells to TME, inhibited their proliferation and activation in a cell to cell contact-dependent manner [142]. It is possible that the therapeutic effect of OV-CXCR4-A treatment is based on M2 TAMs depletion, confirmed by scRNAseq analysis, in MOVCAR 5009-bearing Tg*MISIIR-TAg-Low* mice. This resulted in proinflammatory repolarization of M2-like TAMs and activation of TAg-specific $CD8^+$ T cells. A similar effect of M2-like macrophage repolarization was reported by Freedman *et al*. [143]. The research group modified oncolytic group B adenovirus enadenotucirev to express a stroma-targeted bispecific T-cell engager (BiTE), which binds to CAFs leading to T-cell activation and fibroblast death. It also caused upregulation of proinflammatory cytokines, increased gene expression of markers of antigen presentation, T cell function, trafficking and proinflammatory repolarization of M2-like ascites macrophages [143]. However, on the other hand, the mechanism behind the nearly complete depletion of CAFs by OV-CXCR4-A in my research is not clear. It can be speculated that binding of virally-delivered CXCR4 antagonist to CXCR4-expressing CAFs can result in apoptosis, as previously reported [144]. It would be of special interest to perform additional epigenomic profiling studies to better understand changes in CAFs from the tumor-bearing WT and Tg*MISIIR-TAg-Low* mice. It would help us to identify potential ways to reprogram CAFs to support immune activation and design effective combination therapy regimens. Current treatments for gynecologic cancers in the advanced stage are not sufficiently effective for good outcome in most patients. Especially, immune checkpoint blockade-based therapies, like PD-1/PD-L1 inhibitors, alone have limited efficacy for OC treatment. Combination with other therapeutics might be a promising treatment option [145,146]. This lack of effective anti-tumor

therapy stresses the need for new therapeutic approaches combined with an improved understanding of T cell biology in the context of the tolerogenic tumor microenvironment.

In 2021 research group Lal *et al*. [147] compared syngeneic and autochthonous models of breast cancer and tested their response to anti-CTLA4 and anti-PD-L1 therapy. They have revealed that TME of tumors from syngeneic models were vastly different from the autochthonous models [147]. Results obtained in the course of my study were consistent with aforementioned findings. MOVCAR 5009 cancer cells implanted in WT mice do not repeat the tolerogenic model of the same tumor-bearing Tg*MISIIR-TAg-Low* mice. Establishing WT and tolerogenic OC syngeneic murine models allowed us to study and explain some mechanisms underlaying the CAFs and TAMs interaction. Orthotopic implantation of MOVCAR 5009 cells resulted in spreading of tumor cells through the abdominal cavity. Both groups of mice developed a malignant, bloody ascites. However, tumor/self-antigen expressing transgenic Tg*MISIIR-TAg-Low* mice had increased tumorigenicity, which could be explained by a defective ability to generate effective antitumor immune responses due to tolerance. It is also possible that generated niche after tumor implantation is more or less favorable for tumor initiation process. Oncogenic SV40 TAg is not directly associated with human cancer development, but its expression at the tumor site results in functional inactivation of the critical tumor suppressors p53 and retinoblastoma protein (Rb), generating various tumor-derived factors that accelerate accumulation of immunosuppressive CAFs. Mutation of *TP53* is, by far, the most common genetic alteration observed in EOC, particularly the serous subtype. When p53 protein is mutated, the cell cycle is unrestricted and the damaged DNA is replicated, resulting in uncontrolled cell proliferation and tumorigenesis. Disruption of Rb signaling pathway is also a frequent event in development of human malignancies, resulting either from loss of function of negative regulators or from events leading to overexpression of proto-oncogenes [78,148]. In addition, SV40 TAg binds to and inhibits the activity of the protein phosphatase 2A (PP2A) family of serine-threonine phosphatases, which regulates multiple signaling pathways including phosphoinositide-3 kinase/protein kinase B (PI3K/AKT), mitogen-activated protein kinase (MAPK), Wnt, NF-kB, PKC, and Ca^{2+}-calmodulin-dependent signaling pathways as well as downstream targets of these and other pathways. Activation of the PI3K/AKT pathway may contribute to tumorigenesis, as AKT mediates survival signals that protect cells from apoptosis. Aforementioned signaling pathways are also frequently activated

in human OC [149,150]. Altogether, murine model where non-tumor prone Tg*MISIIR-TAg-Low* mice with the TAg antigen expression at the tumor site and murine ovarian carcinoma MOVCAR 5009 cells manifesting relevant for human OC genetic alterations is the exemplary research tool for the *in vivo* studies on the effects of oncogenic changes in the tumorigenic niche and dynamic interactions between cancer cells, immune cells and other components of tumor microenvironment in immunocompetent host.

My study explored the mechanisms of how the tumor microenvironment within the peritoneal cavity plays a pivotal role in the progression of ovarian cancer due to a wide range of different cellular components that have distinct functions and could be targeted or boosted by different immunotherapeutic strategies. For example, in 2019 my research that was focused on intratumoral $CD103^+$ dendritic cells revealed an important role of these cells in stimulating cytotoxic T cells and driving antitumor immunity. I demonstrated that local delivery of the CXCR4-A-armed virus augmented tumor infiltration of $CD103^+$ dendritic cells that were capable of phagocytic clearance of cellular debris from virally infected cancer cells and generating protective antitumor immunity. Thus, increased overall survival of tumor-bearing mice indicated that expansion of intratumoral $CD103^+$ dendritic cells by CXCR4-A-armed oncovirotherapy treatment could potentiate *in situ* cancer vaccine boosting [151]. Further study of tumor microenvironment and its interactions with ovarian cancer during oncolytic virotherapy treatment inspired the present investigation. My research has been focused on how these effects influence the tumor microenvironment itself and the activation of tumor/self-antigen- and neoantigen-specific $CD8^+$ T lymphocytes in tolerogenic and antigen-naïve wild-type murine ovarian cancer models, respectively. The findings of this study were published in 2023 [152] and are briefly summarized in Figure 33. Performed analyses revealed that in the tolerogenic murine ovarian cancer model, OV-CXCR4-A treatment led to a profound reduction in tumor load, the generation of TAg-specific CD8+ T cells, nearly complete depletion of immunosuppressive CAFs, and M2 to M1 repolarization of macrophages. In conclusion, this study showed that reprogramming the tumor microenvironment can significantly improve the efficacy of immunotherapy and highlighted the importance of targeting the immunosuppressive interaction between TAMs and CAFs by the CXCR4-antagonist-armed oncolytic virotherapy.

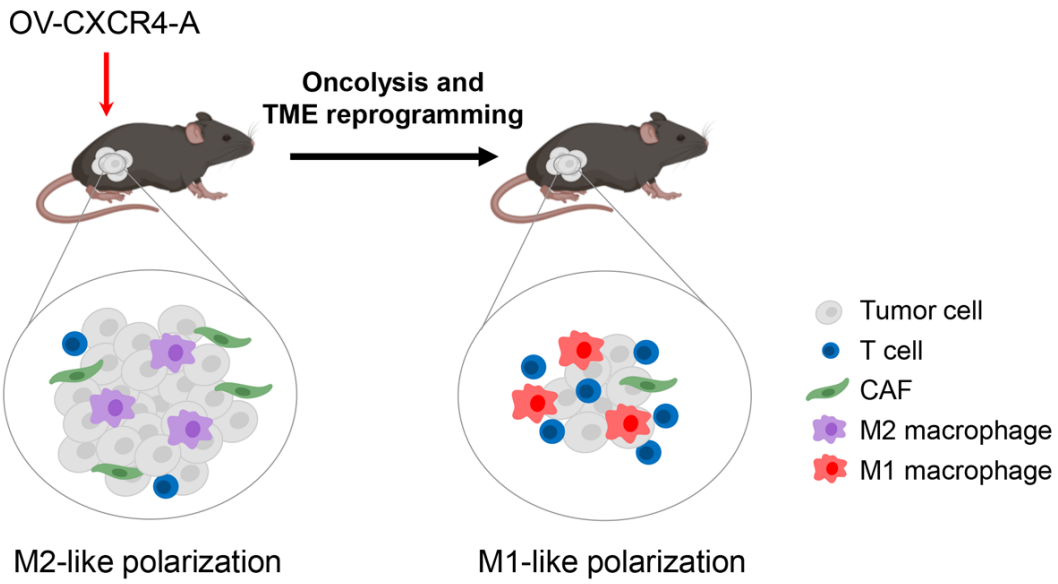

Figure 33. *Graphical summary of tumor microenvironment reprogramming by oncolytic virotherapy in tolerogenic mice.*

The great heterogeneity and complexity of ovarian carcinoma represents a challenge in the search for new treatments that are effective, especially at an advanced and metastatic stage. Common knowledge about ovarian cancer has made remarkable progress over the last years, yet still, there are many limitations and challenges related to disease complexity and current experimental techniques. Future studies are expected to employ clinically relevant models. My observations emphasize the potential of Tg*MISIIR-TAg-Low* murine model in preclinical evaluation of OC therapeutic agents. The current literature suggests that the collaboration of TAMs with CAFs plays a crucial role in tumor progression, yet it is not fully understood and a better recognition of the multidimensional interactions of CAFs, TAMs and cancer cells in tumor microenvironment will help in identification of novel therapeutic agents in order to better target the crucial mechanisms of carcinogenesis. There is a shortage of comprehensive studies describing the interplay between these cells as well as variable results with efforts to target CAFs or TAMs individually. Therefore, targeting TAM-CAF interactions by CXCR4-A-armed oncolytic virotherapy may hold significant potential to improve the outcome of cancer treatment when rationally combined with other treatment approaches. Oncolytic viruses are one of the most promising tumor-selective methods for targeting and remodeling the TME into an antitumor environment by enhancement of the infiltration, activation and effector function of

other components of the immune system. A major challenge to progress in cancer immunotherapy is the availability of reliable preclinical mouse models that reflect the complexity of human malignancy and immune responses within the tumor microenvironment. These models, such as one presented here, are urgently needed not only in OC but also across all malignancies to interrogate and predict antitumor immune responses and therapeutic efficacy in clinical trials. Therefore, to develop new effective immunotherapeutic approaches for patients with poor prognosis, it is essential to conduct further mechanistic interrogation that helps to explain molecular mechanisms that maintain tumor antigen-driven, dysfunctional differentiation of tumor/self- and neoantigen-specific T cells.

5. BIBLIOGRAPHY

1. Webb, P.M., and Jordan, S.J. (2017). Epidemiology of epithelial ovarian cancer. Best Pract Res Clin Obstet Gynaecol *41*, 3-14.

2. Gaona-Luviano, P., Medina-Gaona, L.A., and Magaña-Pérez, K. (2020). Epidemiology of ovarian cancer. Chin Clin Oncol *9*, 47.

3. Huang, J., Chan, W.C., Ngai, C.H., Lok, V., Zhang, L., Lucero-Prisno, D.E., 3rd, Xu, W., Zheng, Z.J., Elcarte, E., Withers, M., Wong, M.C.S., et al. (2022). Worldwide Burden, Risk Factors, and Temporal Trends of Ovarian Cancer: A Global Study. Cancers (Basel) *14*, 2230.

4. An, Y., and Yang, Q. (2021). Tumor-associated macrophage-targeted therapeutics in ovarian cancer. Int J Cancer *149*, 21-30.

5. Karam, A., Ledermann, J.A., Kim, J.W., Sehouli, J., Lu, K., Gourley, C., Katsumata, N., Burger, R.A., Nam, B.H., Bacon, M., Ng, C., et al. (2017). Fifth Ovarian Cancer Consensus Conference of the Gynecologic Cancer InterGroup: first-line interventions. Ann Oncol *28*, 711-717.

6. Gogineni, V., Morand, S., Staats, H., Royfman, R., Devanaboyina, M., Einloth, K., Dever, D., Stanbery, L., Aaron, P., Manning, L., Walter, A., et al. (2021). Current Ovarian Cancer Maintenance Strategies and Promising New Developments. J Cancer *12*, 38-53.

7. Morand, S., Devanaboyina, M., Staats, H., Stanbery, L., and Nemunaitis, J. (2021). Ovarian Cancer Immunotherapy and Personalized Medicine. Int J Mol Sci *22*, 6532.

8. Moss, B. (1996). Genetically engineered poxviruses for recombinant gene expression, vaccination, and safety. Proc Natl Acad Sci U S A *93*, 11341-11348.

9. Shen, Y., and Nemunaitis, J. (2005). Fighting cancer with vaccinia virus: teaching new tricks to an old dog. Mol Ther *11*, 180-195.

10. de Freitas, L.F.D., Oliveira, R.P., Miranda, M.C.G., Rocha, R.P., Barbosa-Stancioli, E.F., Faria, A.M.C., and da Fonseca, F.G. (2019). The Virulence of Different Vaccinia

Virus Strains Is Directly Proportional to Their Ability To Downmodulate Specific Cell-Mediated Immune Compartments In Vivo. J Virol *93*, e02191-18.

11. Kirn, D.H., and Thorne, S.H. (2009). Targeted and armed oncolytic poxviruses: a novel multi-mechanistic therapeutic class for cancer. Nat Rev Cancer *9*, 64-71.

12. Haddad, D. (2017). Genetically Engineered Vaccinia Viruses As Agents for Cancer Treatment, Imaging, and Transgene Delivery. Front Oncol *7*, 96.

13. Kirn, D., Martuza, R.L., and Zwiebel, J. (2001). Replication-selective virotherapy for cancer: Biological principles, risk management and future directions. Nat Med *7*, 781-787.

14. Guse, K., Cerullo, V., and Hemminki, A. (2011). Oncolytic vaccinia virus for the treatment of cancer. Expert Opin Biol Ther *11*, 595-608.

15. Downs-Canner, S., Guo, Z.S., Ravindranathan, R., Breitbach, C.J., O'Malley, M.E., Jones, H.L., Moon, A., McCart, J.A., Shuai, Y., Zeh, H.J., and Bartlett, D.L. (2016). Phase 1 Study of Intravenous Oncolytic Poxvirus (vvDD) in Patients With Advanced Solid Cancers. Mol Ther *24*, 1492-1501.

16. Miller, M.C., and Mayo, K.H. (2017). Chemokines from a Structural Perspective. Int J Mol Sci *18*, 2088.

17. Lai, W.Y., and Mueller, A. (2021). Latest update on chemokine receptors as therapeutic targets. Biochem Soc Trans *49*, 1385-1395.

18. Mousavi, A. (2020). CXCL12/CXCR4 signal transduction in diseases and its molecular approaches in targeted-therapy. Immunol Lett *217*, 91-115.

19. Braga, M., Leow, C.H., Gil, J.H., Teh, J.H., Carroll, L., Long, N.J., Tang, M.X., and Aboagye, E.O. (2021). Investigating CXCR4 expression of tumor cells and the vascular compartment: A multimodal approach. PLoS One *16*, e0260186.

20. Hall, J.M., and Korach, K.S. (2003). Stromal cell-derived factor 1, a novel target of estrogen receptor action, mediates the mitogenic effects of estradiol in ovarian and breast cancer cells. Mol Endocrinol *17*, 792-803.

21. Kaifi, J.T., Yekebas, E.F., Schurr, P., Obonyo, D., Wachowiak, R., Busch, P., Heinecke, A., Pantel, K., and Izbicki, J.R. (2005). Tumor-cell homing to lymph nodes and bone marrow and CXCR4 expression in esophageal cancer. J Natl Cancer Inst *97*, 1840-1847.

22. Taichman, R.S., Cooper, C., Keller, E.T., Pienta, K.J., Taichman, N.S., and McCauley, L.K. (2002). Use of the stromal cell-derived factor-1/CXCR4 pathway in prostate cancer metastasis to bone. Cancer Res *62*, 1832-1837.

23. Rubin, J.B., Kung, A.L., Klein, R.S., Chan, J.A., Sun, Y., Schmidt, K., Kieran, M.W., Luster, A.D., and Segal, R.A. (2003). A small-molecule antagonist of CXCR4 inhibits intracranial growth of primary brain tumors. Proc Natl Acad Sci U S A *100*, 13513-13518.

24. Jiang, Y.P., Wu, X.H., Shi, B., Wu, W.X., and Yin, G.R. (2006). Expression of chemokine CXCL12 and its receptor CXCR4 in human epithelial ovarian cancer: an independent prognostic factor for tumor progression. Gynecol Oncol *103*, 226-233.

25. Saur, D., Seidler, B., Schneider, G., Algül, H., Beck, R., Senekowitsch-Schmidtke, R., Schwaiger, M., and Schmid, R.M. (2005). CXCR4 expression increases liver and lung metastasis in a mouse model of pancreatic cancer. Gastroenterology *129*, 1237-1250.

26. Salvucci, O., Bouchard, A., Baccarelli, A., Deschênes, J., Sauter, G., Simon, R., Bianchi, R., and Basik, M. (2006). The role of CXCR4 receptor expression in breast cancer: a large tissue microarray study. Breast Cancer Res Treat *97*, 275-283.

27. Teicher, B.A., and Fricker, S.P. (2010). CXCL12 (SDF-1)/CXCR4 pathway in cancer. Clin Cancer Res *16*, 2927-2931.

28. Britton, C., Poznansky, M.C., and Reeves, P. (2021). Polyfunctionality of the CXCR4/CXCL12 axis in health and disease: Implications for therapeutic interventions in cancer and immune-mediated diseases. Faseb j *35*, e21260.

29. Magnaldo, I., Pouysségur, and Paris, S. (1989). Cyclic AMP inhibits mitogen-induced DNA synthesis in hamster fibroblasts, regardless of the signalling pathway involved. FEBS Lett *245*, 65-69.

30. Insel, P.A., Zhang, L., Murray, F., Yokouchi, H., and Zambon, A.C. (2012). Cyclic AMP is both a pro-apoptotic and anti-apoptotic second messenger. Acta Physiol (Oxf) *204*, 277-287.

31. Yang, L., Jackson, E., Woerner, B.M., Perry, A., Piwnica-Worms, D., and Rubin, J.B. (2007). Blocking CXCR4-mediated cyclic AMP suppression inhibits brain tumor growth in vivo. Cancer Res *67*, 651-658.

32. Liang, Z., Brooks, J., Willard, M., Liang, K., Yoon, Y., Kang, S., and Shim, H. (2007). CXCR4/CXCL12 axis promotes VEGF-mediated tumor angiogenesis through Akt signaling pathway. Biochem Biophys Res Commun *359*, 716-722.

33. Iwasa, S., Yanagawa, T., Fan, J., and Katoh, R. (2009). Expression of CXCR4 and its ligand SDF-1 in intestinal-type gastric cancer is associated with lymph node and liver metastasis. Anticancer Res *29*, 4751-4758.

34. Guo, L., Cui, Z.M., Zhang, J., and Huang, Y. (2011). Chemokine axes CXCL12/CXCR4 and CXCL16/CXCR6 correlate with lymph node metastasis in epithelial ovarian carcinoma. Chin J Cancer *30*, 336-343.

35. Barbolina, M.V., Kim, M., Liu, Y., Shepard, J., Belmadani, A., Miller, R.J., Shea, L.D., and Stack, M.S. (2010). Microenvironmental regulation of chemokine (C-X-C-motif) receptor 4 in ovarian carcinoma. Mol Cancer Res *8*, 653-664.

36. Popple, A., Durrant, L.G., Spendlove, I., Rolland, P., Scott, I.V., Deen, S., and Ramage, J.M. (2012). The chemokine, CXCL12, is an independent predictor of poor survival in ovarian cancer. Br J Cancer *106*, 1306-1313.

37. Hanahan, D., and Weinberg, R.A. (2011). Hallmarks of cancer: the next generation. Cell *144*, 646-674.

38. Kondo, M. (2010). Lymphoid and myeloid lineage commitment in multipotent hematopoietic progenitors. Immunol Rev *238*, 37-46.

39. Lebegge, E., Arnouk, S.M., Bardet, P.M.R., Kiss, M., Raes, G., and Van Ginderachter, J.A. (2020). Innate Immune Defense Mechanisms by Myeloid Cells That Hamper Cancer Immunotherapy. Front Immunol *11*, 1395.

40. Woo, S.R., Corrales, L., and Gajewski, T.F. (2015). Innate immune recognition of cancer. Annu Rev Immunol *33*, 445-474.

41. Yang, R., Cai, Z., Zhang, Y., Yutzy, W.H.t., Roby, K.F., and Roden, R.B. (2006). CD80 in immune suppression by mouse ovarian carcinoma-associated Gr-1+CD11b+ myeloid cells. Cancer Res *66*, 6807-6815.

42. Gabrilovich, D.I., Bronte, V., Chen, S.H., Colombo, M.P., Ochoa, A., Ostrand-Rosenberg, S., and Schreiber, H. (2007). The terminology issue for myeloid-derived suppressor cells. Cancer Res *67*, 425; author reply 426.

43. Lv, M., Wang, K., and Huang, X.J. (2019). Myeloid-derived suppressor cells in hematological malignancies: friends or foes. J Hematol Oncol *12*, 105.

44. Mantovani, A., Savino, B., Locati, M., Zammataro, L., Allavena, P., and Bonecchi, R. (2010). The chemokine system in cancer biology and therapy. Cytokine Growth Factor Rev *21*, 27-39.

45. Hamilton, T.A., Zhao, C., Pavicic, P.G., Jr., and Datta, S. (2014). Myeloid colony-stimulating factors as regulators of macrophage polarization. Front Immunol *5*, 554.

46. Wang, H.W., and Joyce, J.A. (2010). Alternative activation of tumor-associated macrophages by IL-4: priming for protumoral functions. Cell Cycle *9*, 4824-4835.

47. Cassetta, L., Noy, R., Swierczak, A., Sugano, G., Smith, H., Wiechmann, L., and Pollard, J.W. (2016). Isolation of Mouse and Human Tumor-Associated Macrophages. Adv Exp Med Biol *899*, 211-229.

48. Wang, B., Li, Q., Qin, L., Zhao, S., Wang, J., and Chen, X. (2011). Transition of tumor-associated macrophages from MHC class II(hi) to MHC class II(low) mediates tumor progression in mice. BMC Immunol *12*, 43.

49. Yin, M., Li, X., Tan, S., Zhou, H.J., Ji, W., Bellone, S., Xu, X., Zhang, H., Santin, A.D., Lou, G., and Min, W. (2016). Tumor-associated macrophages drive spheroid formation during early transcoelomic metastasis of ovarian cancer. J Clin Invest *126*, 4157-4173.

50. Ohri, C.M., Shikotra, A., Green, R.H., Waller, D.A., and Bradding, P. (2009). Macrophages within NSCLC tumour islets are predominantly of a cytotoxic M1 phenotype associated with extended survival. Eur Respir J *33*, 118-126.

51. Nowak, M., and Klink, M. (2020). The Role of Tumor-Associated Macrophages in the Progression and Chemoresistance of Ovarian Cancer. Cells *9*, 1299.

52. Zúñiga-Pflücker, J.C. (2004). T-cell development made simple. Nat Rev Immunol *4*, 67-72.

53. Rosenberg, S.A., Sherry, R.M., Morton, K.E., Scharfman, W.J., Yang, J.C., Topalian, S.L., Royal, R.E., Kammula, U., Restifo, N.P., Hughes, M.S., Schwartzentruber, D., et al. (2005). Tumor progression can occur despite the induction of very high levels of self/tumor antigen-specific CD8+ T cells in patients with melanoma. J Immunol *175*, 6169-6176.

54. Gordon, S., and Martinez, F.O. (2010). Alternative activation of macrophages: mechanism and functions. Immunity *32*, 593-604.

55. Borst, J., Ahrends, T., Bąbała, N., Melief, C.J.M., and Kastenmüller, W. (2018). CD4(+) T cell help in cancer immunology and immunotherapy. Nat Rev Immunol *18*, 635-647.

56. Wang, W., Zou, W., and Liu, J.R. (2018). Tumor-infiltrating T cells in epithelial ovarian cancer: predictors of prognosis and biological basis of immunotherapy. Gynecol Oncol *151*, 1-3.

57. Cassar, E., Kartikasari, A.E.R., and Plebanski, M. (2022). Regulatory T Cells in Ovarian Carcinogenesis and Future Therapeutic Opportunities. Cancers (Basel) *14*, 5488.

58. Ping, Q., Yan, R., Cheng, X., Wang, W., Zhong, Y., Hou, Z., Shi, Y., Wang, C., and Li, R. (2021). Cancer-associated fibroblasts: overview, progress, challenges, and directions. Cancer Gene Ther *28*, 984-999.

59. Sun, Q., Zhang, B., Hu, Q., Qin, Y., Xu, W., Liu, W., Yu, X., and Xu, J. (2018). The impact of cancer-associated fibroblasts on major hallmarks of pancreatic cancer. Theranostics *8*, 5072-5087.

60. Liu, Q., Liao, Q., and Zhao, Y. (2017). Chemotherapy and tumor microenvironment of pancreatic cancer. Cancer Cell Int *17*, 68.

61. Han, C., Liu, T., and Yin, R. (2020). Biomarkers for cancer-associated fibroblasts. Biomark Res *8*, 64.

62. Wong, P.F., Wei, W., Gupta, S., Smithy, J.W., Zelterman, D., Kluger, H.M., and Rimm, D.L. (2019). Multiplex quantitative analysis of cancer-associated fibroblasts and immunotherapy outcome in metastatic melanoma. J Immunother Cancer *7*, 194.

63. Mei, S., Chen, X., Wang, K., and Chen, Y. (2023). Tumor microenvironment in ovarian cancer peritoneal metastasis. Cancer Cell Int *23*, 11.

64. Gunaydin, G. (2021). CAFs Interacting With TAMs in Tumor Microenvironment to Enhance Tumorigenesis and Immune Evasion. Front Oncol *11*, 668349.

65. Comito, G., Giannoni, E., Segura, C.P., Barcellos-de-Souza, P., Raspollini, M.R., Baroni, G., Lanciotti, M., Serni, S., and Chiarugi, P. (2014). Cancer-associated fibroblasts and M2-polarized macrophages synergize during prostate carcinoma progression. Oncogene *33*, 2423-2431.

66. Augsten, M., Sjöberg, E., Frings, O., Vorrink, S.U., Frijhoff, J., Olsson, E., Borg, Å., and Östman, A. (2014). Cancer-associated fibroblasts expressing CXCL14 rely upon NOS1-derived nitric oxide signaling for their tumor-supporting properties. Cancer Res *74*, 2999-3010.

67. Pugliese, A. (2004). Central and peripheral autoantigen presentation in immune tolerance. Immunology *111*, 138-146.

68. Waldmann, H. (2016). Mechanisms of immunological tolerance. Clin Biochem *49*, 324-328.

69. Hogquist, K.A., Baldwin, T.A., and Jameson, S.C. (2005). Central tolerance: learning self-control in the thymus. Nat Rev Immunol *5*, 772-782.

70. Xing, Y., and Hogquist, K.A. (2012). T-cell tolerance: central and peripheral. Cold Spring Harb Perspect Biol *4*, a006957.

71. Schumacher, T.N., and Schreiber, R.D. (2015). Neoantigens in cancer immunotherapy. Science *348*, 69-74.

72. Xie, N., Shen, G., Gao, W., Huang, Z., Huang, C., and Fu, L. (2023). Neoantigens: promising targets for cancer therapy. Signal Transduct Target Ther *8*, 9.

73. Obeng, E.A., Stewart, C., and Abdel-Wahab, O. (2019). Altered RNA Processing in Cancer Pathogenesis and Therapy. Cancer Discov *9*, 1493-1510.

74. Method of the year 2013. (2014). Nat Methods *11*, 1.

75. Tang, F., Barbacioru, C., Wang, Y., Nordman, E., Lee, C., Xu, N., Wang, X., Bodeau, J., Tuch, B.B., Siddiqui, A., Lao, K., et al. (2009). mRNA-Seq whole-transcriptome analysis of a single cell. Nat Methods *6*, 377-382.

76. Choi, J.R., Yong, K.W., Choi, J.Y., and Cowie, A.C. (2020). Single-Cell RNA Sequencing and Its Combination with Protein and DNA Analyses. Cells *9*, 1130.

77. Danielski, K. (2023). Guidance on Processing the 10x Genomics Single Cell Gene Expression Assay. Methods Mol Biol *2584*, 1-28.

78. Quinn, B.A., Xiao, F., Bickel, L., Martin, L., Hua, X., Klein-Szanto, A., and Connolly, D.C. (2010). Development of a syngeneic mouse model of epithelial ovarian cancer. J Ovarian Res *3*, 24.

79. Connolly, D.C., and Hensley, H.H. (2009). Xenograft and Transgenic Mouse Models of Epithelial Ovarian Cancer and Non Invasive Imaging Modalities to Monitor Ovarian Tumor Growth In situ -Applications in Evaluating Novel Therapeutic Agents. Curr Protoc Pharmacol *45*, 14.12.11-14.12.26.

80. Wang, D., Gu, X., Liu, X., Liu, X., Wang, B., Lao, F., and Fang, M. (2019). "Acquired" NKG2D Ligand Stimulates NK Cell-mediated Tumor Immunosurveillance. J Immunother *42*, 189-196.

81. Gil, M., Seshadri, M., Komorowski, M.P., Abrams, S.I., and Kozbor, D. (2013). Targeting CXCL12/CXCR4 signaling with oncolytic virotherapy disrupts tumor vasculature and inhibits breast cancer metastases. Proc Natl Acad Sci U S A *110*, E1291-1300.

82. McCart, J.A., Ward, J.M., Lee, J., Hu, Y., Alexander, H.R., Libutti, S.K., Moss, B., and Bartlett, D.L. (2001). Systemic cancer therapy with a tumor-selective vaccinia virus mutant lacking thymidine kinase and vaccinia growth factor genes. Cancer Res *61*, 8751-8757.

83. Gil, M., Bieniasz, M., Wierzbicki, A., Bambach, B.J., Rokita, H., and Kozbor, D. (2009). Targeting a mimotope vaccine to activating Fcgamma receptors empowers dendritic cells to prime specific CD8+ T cell responses in tumor-bearing mice. J Immunol *183*, 6808-6818.

84. Cell Ranger Single-Cell Software Suite. http://software.10xgenomics.com/single-cell/overview/welcome.

85. Satija, R., Farrell, J.A., Gennert, D., Schier, A.F., and Regev, A. (2015). Spatial reconstruction of single-cell gene expression data. Nature Biotechnology *33*, 495-502.

86. Aran, D., Looney, A.P., Liu, L., Wu, E., Fong, V., Hsu, A., Chak, S., Naikawadi, R.P., Wolters, P.J., Abate, A.R., Butte, A.J., et al. (2019). Reference-based analysis of lung single-cell sequencing reveals a transitional profibrotic macrophage. Nature immunology *20*, 163-172.

87. Korotkevich, G., Sukhov, V., and Sergushichev, A. (2019). Fast gene set enrichment analysis. http://bioconductor.org/packages/release/bioc/html/fgsea.html.

88. Blighe, K., Rana, S., and Lewis, M. (2021). EnhancedVolcano: Publication-ready volcano plots with enhanced colouring and labeling. R package version 1.12.0. https://bioconductor.org/packages/release/bioc/html/EnhancedVolcano.html.

89. pheatmap R package. https://cran.r-project.org/package=pheatmap.

90. Aibar, S., González-Blas, C.B., Moerman, T., Huynh-Thu, V.A., Imrichova, H., Hulselmans, G., Rambow, F., Marine, J.-C., Geurts, P., Aerts, J., van den Oord, J., et al. (2017). SCENIC: single-cell regulatory network inference and clustering. Nat Methods *14*, 1083-1086.

91. Liberzon, A., Subramanian, A., Pinchback, R., Thorvaldsdóttir, H., Tamayo, P., and Mesirov, J.P. (2011). Molecular signatures database (MSigDB) 3.0. Bioinformatics *27*, 1739-1740.

92. Gil, M., Komorowski, M.P., Seshadri, M., Rokita, H., McGray, A.J., Opyrchal, M., Odunsi, K.O., and Kozbor, D. (2014). CXCL12/CXCR4 blockade by oncolytic virotherapy inhibits ovarian cancer growth by decreasing immunosuppression and targeting cancer-initiating cells. J Immunol *193*, 5327-5337.

93. Hussain, A., Voisin, V., Poon, S., Karamboulas, C., Bui, N.H.B., Meens, J., Dmytryshyn, J., Ho, V.W., Tang, K.H., Paterson, J., Clarke, B.A., et al. (2020). Distinct fibroblast functional states drive clinical outcomes in ovarian cancer and are regulated by TCF21. J Exp Med *217*, e20191094.

94. Altmann, A., Haberkorn, U., and Siveke, J. (2021). The Latest Developments in Imaging of Fibroblast Activation Protein. J Nucl Med *62*, 160-167.

95. Cremasco, V., Astarita, J.L., Grauel, A.L., Keerthivasan, S., MacIsaac, K., Woodruff, M.C., Wu, M., Spel, L., Santoro, S., Amoozgar, Z., Laszewski, T., et al. (2018). FAP Delineates Heterogeneous and Functionally Divergent Stromal Cells in Immune-Excluded Breast Tumors. Cancer Immunol Res *6*, 1472-1485.

96. Everts, A., Bergeman, M., McFadden, G., and Kemp, V. (2020). Simultaneous Tumor and Stroma Targeting by Oncolytic Viruses. Biomedicines *8*, 474.

97. Wang, L., Chard Dunmall, L.S., Cheng, Z., and Wang, Y. (2022). Remodeling the tumor microenvironment by oncolytic viruses: beyond oncolysis of tumor cells for cancer treatment. J Immunother Cancer *10*, e004167.

98. Fearon, D.T. (2014). The carcinoma-associated fibroblast expressing fibroblast activation protein and escape from immune surveillance. Cancer Immunol Res *2*, 187-193.

99. Righi, E., Kashiwagi, S., Yuan, J., Santosuosso, M., Leblanc, P., Ingraham, R., Forbes, B., Edelblute, B., Collette, B., Xing, D., Kowalski, M., et al. (2011). CXCL12/CXCR4 blockade induces multimodal antitumor effects that prolong survival in an immunocompetent mouse model of ovarian cancer. Cancer Res *71*, 5522-5534.

100. Wan, P.K., Ryan, A.J., and Seymour, L.W. (2021). Beyond cancer cells: Targeting the tumor microenvironment with gene therapy and armed oncolytic virus. Mol Ther *29*, 1668-1682.

101. Nelson, C.E., Mills, L.J., McCurtain, J.L., Thompson, E.A., Seelig, D.M., Bhela, S., Quarnstrom, C.F., Fife, B.T., and Vezys, V. (2019). Reprogramming responsiveness to checkpoint blockade in dysfunctional CD8 T cells. Proc Natl Acad Sci U S A *116*, 2640-2645.

102. Burrack, K.S., Tan, J.J., McCarthy, M.K., Her, Z., Berger, J.N., Ng, L.F., and Morrison, T.E. (2015). Myeloid Cell Arg1 Inhibits Control of Arthritogenic Alphavirus Infection by Suppressing Antiviral T Cells. PLoS Pathog *11*, e1005191.

103. Jablonski, K.A., Amici, S.A., Webb, L.M., Ruiz-Rosado Jde, D., Popovich, P.G., Partida-Sanchez, S., and Guerau-de-Arellano, M. (2015). Novel Markers to Delineate Murine M1 and M2 Macrophages. PLoS One *10*, e0145342.

104. Yang, Z., and Ming, X.F. (2014). Functions of arginase isoforms in macrophage inflammatory responses: impact on cardiovascular diseases and metabolic disorders. Front Immunol *5*, 533.

105. Yu, T., Gan, S., Zhu, Q., Dai, D., Li, N., Wang, H., Chen, X., Hou, D., Wang, Y., Pan, Q., Xu, J., et al. (2019). Modulation of M2 macrophage polarization by the crosstalk between Stat6 and Trim24. Nat Commun *10*, 4353.

106. Conde, P., Rodriguez, M., van der Touw, W., Jimenez, A., Burns, M., Miller, J., Brahmachary, M., Chen, H.M., Boros, P., Rausell-Palamos, F., Yun, T.J., et al. (2015). DC-SIGN(+) Macrophages Control the Induction of Transplantation Tolerance. Immunity *42*, 1143-1158.

107. Psallidas, I., Stathopoulos, G.T., Maniatis, N.A., Magkouta, S., Moschos, C., Karabela, S.P., Kollintza, A., Simoes, D.C., Kardara, M., Vassiliou, S., Papiris, S.A., et al. (2013). Secreted phosphoprotein-1 directly provokes vascular leakage to foster malignant pleural effusion. Oncogene *32*, 528-535.

108. Wei, T., Bi, G., Bian, Y., Ruan, S., Yuan, G., Xie, H., Zhao, M., Shen, R., Zhu, Y., Wang, Q., Yang, Y., et al. (2020). The Significance of Secreted Phosphoprotein 1 in Multiple Human Cancers. Front Mol Biosci *7*, 565383.

109. Kwak, T., Wang, F., Deng, H., Condamine, T., Kumar, V., Perego, M., Kossenkov, A., Montaner, L.J., Xu, X., Xu, W., Zheng, C., et al. (2020). Distinct Populations of

Immune-Suppressive Macrophages Differentiate from Monocytic Myeloid-Derived Suppressor Cells in Cancer. Cell Rep *33*, 108571.

110. Sharma, N., Atolagbe, O.T., Ge, Z., and Allison, J.P. (2021). LILRB4 suppresses immunity in solid tumors and is a potential target for immunotherapy. J Exp Med *218*, e20201811.

111. Lee, S.Y., Moon, S.J., Moon, Y.M., Seo, H.B., Ryu, J.G., Lee, A.R., Lee, C.R., Kim, D.S., Her, Y.M., Choi, J.W., Kwok, S.K., et al. (2022). A novel cytokine consisting of the p40 and EBI3 subunits suppresses experimental autoimmune arthritis via reciprocal regulation of Th17 and Treg cells. Cell Mol Immunol *19*, 79-91.

112. Grauel, A.L., Nguyen, B., Ruddy, D., Laszewski, T., Schwartz, S., Chang, J., Chen, J., Piquet, M., Pelletier, M., Yan, Z., Kirkpatrick, N.D., et al. (2020). TGFbeta-blockade uncovers stromal plasticity in tumors by revealing the existence of a subset of interferon-licensed fibroblasts. Nat Commun *11*, 6315.

113. Wang, X.H., Du, H., Li, L., Shao, D.F., Zhong, X.Y., Hu, Y., Liu, Y.Q., Xing, X.F., Cheng, X.J., Guo, T., Li, S., et al. (2017). Increased expression of S100A6 promotes cell proliferation in gastric cancer cells. Oncol Lett *13*, 222-230.

114. Nedjadi, T., Kitteringham, N., Campbell, F., Jenkins, R.E., Park, B.K., Navarro, P., Ashcroft, F., Tepikin, A., Neoptolemos, J.P., and Costello, E. (2009). S100A6 binds to annexin 2 in pancreatic cancer cells and promotes pancreatic cancer cell motility. Br J Cancer *101*, 1145-1154.

115. Leśniak, W., and Filipek, A. (2023). S100A6 Protein-Expression and Function in Norm and Pathology. Int J Mol Sci *24*, 1341.

116. Teeuwssen, M., and Fodde, R. (2019). Wnt Signaling in Ovarian Cancer Stemness, EMT, and Therapy Resistance. J Clin Med *8*, 1658.

117. Wang, B., Guo, H., Yu, H., Chen, Y., Xu, H., and Zhao, G. (2021). The Role of the Transcription Factor EGR1 in Cancer. Front Oncol *11*, 642547.

118. Cheng, J.C., Chang, H.M., and Leung, P.C. (2013). Egr-1 mediates epidermal growth factor-induced downregulation of E-cadherin expression via Slug in human ovarian cancer cells. Oncogene *32*, 1041-1049.

119. Wang, H., Kadlecek, T.A., Au-Yeung, B.B., Goodfellow, H.E., Hsu, L.Y., Freedman, T.S., and Weiss, A. (2010). ZAP-70: an essential kinase in T-cell signaling. Cold Spring Harb Perspect Biol *2*, a002279.

120. Lo, W.L., Shah, N.H., Ahsan, N., Horkova, V., Stepanek, O., Salomon, A.R., Kuriyan, J., and Weiss, A. (2018). Lck promotes Zap70-dependent LAT phosphorylation by bridging Zap70 to LAT. Nat Immunol *19*, 733-741.

121. Zhu, Y., Wang, W., and Wang, X. (2015). Roles of transcriptional factor 7 in production of inflammatory factors for lung diseases. J Transl Med *13*, 273.

122. Jha, P., and Das, H. (2017). KLF2 in Regulation of NF-κB-Mediated Immune Cell Function and Inflammation. Int J Mol Sci *18*, 2383.

123. Lu, Y.C., Jia, L., Zheng, Z., Tran, E., Robbins, P.F., and Rosenberg, S.A. (2019). Single-Cell Transcriptome Analysis Reveals Gene Signatures Associated with T-cell Persistence Following Adoptive Cell Therapy. Cancer Immunol Res *7*, 1824-1836.

124. Yánez, D.C., Ross, S., and Crompton, T. (2020). The IFITM protein family in adaptive immunity. Immunology *159*, 365-372.

125. Lieberman, J. (2010). Granzyme A activates another way to die. Immunol Rev *235*, 93-104.

126. Schietinger, A., Philip, M., Krisnawan, V.E., Chiu, E.Y., Delrow, J.J., Basom, R.S., Lauer, P., Brockstedt, D.G., Knoblaugh, S.E., Hammerling, G.J., Schell, T.D., et al. (2016). Tumor-Specific T Cell Dysfunction Is a Dynamic Antigen-Driven Differentiation Program Initiated Early during Tumorigenesis. Immunity *45*, 389-401.

127. Chen, Z., Ji, Z., Ngiow, S.F., Manne, S., Cai, Z., Huang, A.C., Johnson, J., Staupe, R.P., Bengsch, B., Xu, C., Yu, S., et al. (2019). TCF-1-Centered Transcriptional Network Drives an Effector versus Exhausted CD8 T Cell-Fate Decision. Immunity *51*, 840-855 e845.

128. Chu, T., Berner, J., and Zehn, D. (2020). Two parallel worlds of memory T cells. Nat Immunol *21*, 1484-1485.

129. Siddiqui, I., Schaeuble, K., Chennupati, V., Fuertes Marraco, S.A., Calderon-Copete, S., Pais Ferreira, D., Carmona, S.J., Scarpellino, L., Gfeller, D., Pradervand, S., Luther, S.A., et al. (2019). Intratumoral Tcf1(+)PD-1(+)CD8(+) T Cells with Stem-like Properties Promote Tumor Control in Response to Vaccination and Checkpoint Blockade Immunotherapy. Immunity *50*, 195-211 e110.

130. Wu, T., Ji, Y., Moseman, E.A., Xu, H.C., Manglani, M., Kirby, M., Anderson, S.M., Handon, R., Kenyon, E., Elkahloun, A., Wu, W., et al. (2016). The TCF1-Bcl6 axis counteracts type I interferon to repress exhaustion and maintain T cell stemness. Sci Immunol *1*, eaai8593.

131. Westgaard, I.H., Dissen, E., Torgersen, K.M., Lazetic, S., Lanier, L.L., Phillips, J.H., and Fossum, S. (2003). The lectin-like receptor KLRE1 inhibits natural killer cell cytotoxicity. J Exp Med *197*, 1551-1561.

132. Saether, P.C., Westgaard, I.H., Hoelsbrekken, S.E., Benjamin, J., Lanier, L.L., Fossum, S., and Dissen, E. (2008). KLRE/I1 and KLRE/I2: a novel pair of heterodimeric receptors that inversely regulate NK cell cytotoxicity. J Immunol *181*, 3177-3182.

133. Heinze, K., Hölzer, M., Ungelenk, M., Gerth, M., Thomale, J., Heller, R., Morden, C.R., McManus, K.J., Mosig, A.S., Dürst, M., Runnebaum, I.B., et al. (2021). RUNX3 Transcript Variants Have Distinct Roles in Ovarian Carcinoma and Differently Influence Platinum Sensitivity and Angiogenesis. Cancers (Basel) *13*, 476.

134. Philip, M., Fairchild, L., Sun, L., Horste, E.L., Camara, S., Shakiba, M., Scott, A.C., Viale, A., Lauer, P., Merghoub, T., Hellmann, M.D., et al. (2017). Chromatin states define tumour-specific T cell dysfunction and reprogramming. Nature *545*, 452-456.

135. Jiang, W., He, Y., He, W., Wu, G., Zhou, X., Sheng, Q., Zhong, W., Lu, Y., Ding, Y., Lu, Q., Ye, F., et al. (2020). Exhausted CD8+T Cells in the Tumor Immune Microenvironment: New Pathways to Therapy. Front Immunol *11*, 622509.

136. Huang, R.Y., Eppolito, C., Lele, S., Shrikant, P., Matsuzaki, J., and Odunsi, K. (2015). LAG3 and PD1 co-inhibitory molecules collaborate to limit CD8+ T cell signaling and dampen antitumor immunity in a murine ovarian cancer model. Oncotarget *6*, 27359-27377.

137. Nelson, C.E., Thompson, E.A., Quarnstrom, C.F., Fraser, K.A., Seelig, D.M., Bhela, S., Burbach, B.J., Masopust, D., and Vezys, V. (2019). Robust Iterative Stimulation with Self-Antigens Overcomes CD8(+) T Cell Tolerance to Self- and Tumor Antigens. Cell Rep *28*, 3092-3104.e3095.

138. Schietinger, A., Delrow, J.J., Basom, R.S., Blattman, J.N., and Greenberg, P.D. (2012). Rescued tolerant CD8 T cells are preprogrammed to reestablish the tolerant state. Science *335*, 723-727.

139. Enouz, S., Carrié, L., Merkler, D., Bevan, M.J., and Zehn, D. (2012). Autoreactive T cells bypass negative selection and respond to self-antigen stimulation during infection. J Exp Med *209*, 1769-1779.

140. Yuan, X., Zhang, J., Li, D., Mao, Y., Mo, F., Du, W., and Ma, X. (2017). Prognostic significance of tumor-associated macrophages in ovarian cancer: A meta-analysis. Gynecol Oncol *147*, 181-187.

141. Kalluri, R. (2016). The biology and function of fibroblasts in cancer. Nat Rev Cancer *16*, 582-598.

142. Pan, Y., Yu, Y., Wang, X., and Zhang, T. (2020). Tumor-Associated Macrophages in Tumor Immunity. Front Immunol *11*, 583084.

143. Freedman, J.D., Duffy, M.R., Lei-Rossmann, J., Muntzer, A., Scott, E.M., Hagel, J., Campo, L., Bryant, R.J., Verrill, C., Lambert, A., Miller, P., et al. (2018). An Oncolytic Virus Expressing a T-cell Engager Simultaneously Targets Cancer and Immunosuppressive Stromal Cells. Cancer Res *78*, 6852-6865.

144. Komorowski, M.P., McGray, A.R., Kolakowska, A., Eng, K., Gil, M., Opyrchal, M., Litwinska, B., Nemeth, M.J., Odunsi, K.O., and Kozbor, D. (2016). Reprogramming antitumor immunity against chemoresistant ovarian cancer by a CXCR4 antagonist-armed viral oncotherapy. Mol Ther Oncolytics *3*, 16034.

145. Zhu, J., Yan, L., and Wang, Q. (2021). Efficacy of PD-1/PD-L1 inhibitors in ovarian cancer: a single-arm meta-analysis. J Ovarian Res *14*, 112.

146. Drakes, M.L., Czerlanis, C.M., and Stiff, P.J. (2020). Immune Checkpoint Blockade in Gynecologic Cancers: State of Affairs. Cancers (Basel) *12*, 3301.

147. Lal, J.C., Townsend, M.G., Mehta, A.K., Oliwa, M., Miller, E., Sotayo, A., Cheney, E., Mittendorf, E.A., Letai, A., and Guerriero, J.L. (2021). Comparing syngeneic and autochthonous models of breast cancer to identify tumor immune components that correlate with response to immunotherapy in breast cancer. Breast Cancer Res *23*, 83.

148. Hashiguchi, Y., Tsuda, H., Yamamoto, K., Inoue, T., Ishiko, O., and Ogita, S. (2001). Combined analysis of p53 and RB pathways in epithelial ovarian cancer. Hum Pathol *32*, 988-996.

149. Arroyo, J.D., and Hahn, W.C. (2005). Involvement of PP2A in viral and cellular transformation. Oncogene *24*, 7746-7755.

150. Altomare, D.A., Wang, H.Q., Skele, K.L., De Rienzo, A., Klein-Szanto, A.J., Godwin, A.K., and Testa, J.R. (2004). AKT and mTOR phosphorylation is frequently detected in ovarian cancer and can be targeted to disrupt ovarian tumor cell growth. Oncogene *23*, 5853-5857.

151. Mistarz, A., Komorowski, M.P., Graczyk, M.A., Gil, M., Jiang, A., Opyrchal, M., Rokita, H., Odunsi, K.O., and Kozbor, D. (2019). Recruitment of Intratumoral CD103(+) Dendritic Cells by a CXCR4 Antagonist-Armed Virotherapy Enhances Antitumor Immunity. Mol Ther Oncolytics *14*, 233-245.

152. Mistarz, A., Winkler, M., Battaglia, S., Liu, S., Hutson, A., Rokita, H., Gambotto, A., Odunsi, K.O., Singh, P.K., McGray, A.J.R., Wang, J., et al. (2023). Reprogramming the tumor microenvironment leverages CD8(+) T cell responses to a shared tumor/self antigen in ovarian cancer. Mol Ther Oncolytics *28*, 230-248.

6. LIST OF PUBLICATIONS

1. **Mistarz, A.**, Winkler, M., Battaglia, S., Liu, S., Hutson, A., Rokita, H., Gambotto, A., Odunsi, K.O., Singh, P.K., McGray, A.J.R., Wang, J., Kozbor, D. (2023). Reprogramming the tumor microenvironment leverages CD8+ T cell responses to a shared tumor/self antigen in ovarian cancer. Mol. Ther. Oncolytics *28*, 230-248.
2. Mark, J., Fisher, D.T., Kim, M., Emmons, T., Khan, A.N.M.N., Alqassim, E., Singel, K., **Mistarz, A.**, Lugade, A., Zhan, H., Yu, H., Segal, B., Lele, S., Frederick, P., Kozbor, D., Skitzki, J., Odunsi, K. (2023). Carboplatin enhances lymphocyte-endothelial interactions to promote CD8+ T cell trafficking into the ovarian tumor microenvironment. Gynecol Oncol. *168*, 92-99.
3. **Mistarz, A.**, Graczyk, M., Winkler, M., Singh, P.K., Cortes, E., Miliotto, A., Liu, S., Long, M., Yan, L., Stablewski, A., O'Loughlin, K., Minderman, H., Odunsi, K., Rokita, H., McGray, A.J.R., Zsiros, E., Kozbor, D. (2021). Induction of cell death in ovarian cancer cells by doxorubicin and oncolytic vaccinia virus is associated with CREB3L1 activation. Mol. Ther. Oncolytics *23*, 38-50.
4. **Mistarz, A.**, Komorowski, M.P., Graczyk, M.A., Gil, M., Jiang, A., Opyrchal, M., Rokita, H., Odunsi, K.O., Kozbor, D. (2019). Recruitment of Intratumoral CD103+ Dendritic Cells by a CXCR4 Antagonist-Armed Virotherapy Enhances Antitumor Immunity. Mol. Ther. Oncolytics *14*, 233-245.
5. Boratyn, E., Nowak, I., Horwacik, I., Durbas, M., **Mistarz, A.**, Kukla, M., Kaczówka, P., Łastowska, M., Jura, J., Rokita, H. (2016). Monocyte chemoattractant protein-induced protein 1 overexpression modulates transcriptome, including miRNA, in human neuroblastoma cells. J. Cell. Biochem. *117*, 694-707.